Iterative Frequency-Domain Channel Equalisation and Estimation for Single-Carrier Multi-Input Multi-Output Wireless Communication Systems

Thesis submitted in accordance with the requirements
of the University of Liverpool for the
degree of Doctor in Philosophy

By

Ye Wu

August 2008

Declaration

The work in this thesis is based on research carried out at the University of Liverpool. No part of this thesis has been submitted elsewhere for any other degree or qualification and it is all my own work unless referenced to the contrary in the text.

Abstract

In the forthcoming broadband wireless communications, channel equalisation and estimation solutions are required to be robust against frequency selective fading channels and have a low signal processing complexity. This thesis investigates iterative frequency-domain channel equalisation and estimation for single-carrier (SC) multi-input multi-output (MIMO) wireless communication systems, aiming to outperform iterative time-domain channel equalisation and estimation with a low complexity. The thesis contains three main contributions described as follows.

First, a low complexity Turbo space-frequency equalisation (TSFE) structure is proposed, which combines the advantages of MIMO frequency-domain equalisation (FDE) and iterative (Turbo) equalisation, and is effective to combat frequency-selective fading channels. As a result, a new concise block-wise FDE structure is proposed. TSFE introduces a tremendous complexity reduction over the symbol-wise TSFE structure as well as the previously proposed Turbo time-domain equalisation (TTDE) and Turbo FDE (TFDE) structures. With a moderate code rate and the increase of the number of iterations, TSFE significantly outperforms its Turbo orthogonal frequency division multiplexing (TOFDM) counterpart, at a comparable complexity. The complexity of the proposed TSFE increases linearly with the number of subcarriers and the number of samples per symbol period, which is much lower than the complexities of the

previously proposed Turbo frequency-domain equalisation structures.

Second, adaptive iterative frequency-domain channel estimation is proposed to address unknown time-varying fading channels, which is categorised into hard-input iterative channel estimation and soft-input iterative (Turbo) channel estimation. The proposed iterative channel estimation is based on a variety of criteria. Under each criterion, unstructured channel estimation (UCE) and structured channel estimation (SCE) are investigated. Hard-input iterative channel estimation is first investigated. In particular, least mean squares (LMS) SCE tracks the channel variations effectively with a reasonably low complexity as well as the highest convergence speed among all the hard-input channel estimation methods. To combat the sensitivity to error propagation, soft-input iterative (Turbo) channel estimation is proposed. The simplified Turbo recursive least squares (RLS) SCE provides nearly the same performance as Turbo RLS (TRLS) SCE, with a tremendous complexity reduction. Turbo normalised RLS (NRLS) SCE outperforms Turbo Kalman SCE in terms of the steady-state mean squared error (MSE), with a wide range of signal-to-noise ratios (SNRs) and root mean squared (RMS) delay spreads, and a medium to high Doppler spread. An intensive performance analysis of Turbo Kalman channel estimation and Turbo NRLS channel estimation is provided.

Third, adaptive Turbo multiuser detection and co-channel interference (CCI) suppression are applied to the uplink MIMO single-carrier frequency division multiple access (SC-FDMA) system. The proposed Turbo SC-FDMA system significantly outperforms its Turbo orthogonal frequency division multiple access (OFDMA) counterpart. In the presence of unknown CCI, the simplified TRLS-SCE along with low-pass CCI suppression (LPCCIS) provides a performance very close to the case with perfect channel state information (CSI), and outperforms

the existing temporal CCI suppression (TCCIS) scheme.

Acknowledgement

I would like to thank the following people without any reservation, without whom this dissertation would not have been what it is:

My supervisors: Xu Zhu for motivating and helping me to commence this research and for giving valuable comments and suggestion all the way; Asoke. K. Nandi for supervising a doctoral work with his best.

ORSAS committee, UK: financial support of my Ph.D. research-It was ORSAS that allowed me all the way from China to study in the University of Liverpool, UK, which had always been my dream. As a Chinese student, I deeply felt the sincere help from the UK government, which truly made my dream of studying in UK come true.

ORSAS committee of The Liverpool University: The useful scholarship supplement to ORSAS symbolising the support from the university to encourage me to execute my study to perfection.

Signal Processing Group, the Department of Electrical Engineering and Electronics: L. Sarperi for Linux system using knowledge and S. Punnoose for early supporting knowledge of wireless communications and latter inter-communication in my project.

Fellow workmates in communications lab: J. B. Gao, N. Zhou, O. Nwamadi and M. Musbah for creating a family-like atmosphere in the office in which it is

my pleasure to have been working.

Last, but certainly not least, my family: My parents for supporting and encouraging me to pursue my academic goal in my life. Their unselfish support was, is and will always be the most precious gift I can receive in this world.

Contents

List of Figures

List of Tables

Acronyms

3GPP	Third Generation Partnership Project
AR	Autoregressive
AWGN	Additive White Gaussian Noise
BER	Bit Error Rate
BRAN	Broadband Radio Access Network
CCI	Co-Channel Interference
CCIS	Co-Channel Interference Suppression
CDMA	Code Division Multiple Access
CIR	Channel Impulse Response
CP	Cyclic Prefix
CP-CDMA	Cyclic Prefix Code Division Multiple Access
CSI	Channel State Information
DFE	Decision Feedback Equalisation
DFT	Discrete Fourier Transform

ECC	Error Control Code
ETSI	European Telecommunications Standards Institute
FDE	Frequency-Domain Equalisation
FD-TLE	Frequency-Domain Turbo Linear Equalisation
FFT	Fast Fourier Transform
HiperMAN	High-Performance Metropolitan Area Network
IBI	Inter Block Interference
IFFT	Inverse Fast Fourier Transform
LLR	Log-Likelihood Ratio
ISI	Inter Symbol Interference
LMS	Least Mean Squares
LMS-UCE	Least Mean Squares Unstructured Channel Estimation
LMS-SCE	Least Mean Squares Structured Channel Estimation
LPCCIS	Low-Pass Co-Channel Interference Suppression
LS	Least Squares
MAN	Metropolitan Area Network
MAP	Maximum *A Posteriori* Probability
MC	Multi-Carrier
MIMO	Multiple-Input Multiple-Output

MISO	Multiple-Input Single-Output
ML	Maximum Likelihood
MLSE	Maximum Likelihood Sequence Estimation
MMSE	Minimum Mean Squared Error
MSE	Mean Squared Error
NLOS	Non-Line-of-Sight
NRLS	Normalised Recursive Least Squares
OFDM	Orthogonal Frequency Division Multiplexing
OFDMA	Orthogonal Frequency Division Multiplexing Access
PAPR	Peak-to-Average Power Ratio
PD	Positive Definite
PDF	Probability Density Function
PSD	Power Spectral Density
PSK	Phase Shift Keying
RLS	Recursive Least Squares
RLS-UCE	Recursive Least Squares Unstructured Channel Estimation
RLS-SCE	Recursive Least Squares Structured Channel Estimation
RMS	Root Mean Squared
RSC	Recursive Systematic Convolutional

SC	Single-Carrier
SCE	Structured Channel Estimation
SC-FDE	Single-Carrier Frequency Domain Equalisation
SC-FDMA	Single-Carrier Frequency Division Multiple Access
SIMO	Single-Input Multiple-Output
SINR	Signal to Interference plus Noise Ratio
SIR	Signal to Interference Ratio
SISO	Single-Input Single-Output
SNR	Signal-to-Noise Ratio
SOHO	Small Office/Home Office
STBC	Space-Time Block Code
SVD	Singular Value Decomposition
TCCIS	Temporal Co-Channel Interference Suppression
TDE	Time-Domain Equalisation
TDMA	Time Division Multiple Access
TFDE	Turbo Frequency-Domain Equalisation
TK-SCE	Turbo Kalman Structured Channel Estimation
TK-UCE	Turbo Kalman Unstructured Channel Estimation
TLMS-SCE	Turbo Least Mean Squares Structured Channel Estimation

TNRLS-SCE Turbo Normalised Recursive Least Squares Structured Channel Estimation

TNRLS-UCE Turbo Normalised Recursive Least Squares Unstructured Channel Estimation

TRLS-SCE Turbo Recursive Least Squares Structured Channel Estimation

TOFDM Turbo Orthogonal Frequency Division Multiplexing

TSFE Turbo Space-Frequency Equalisation

TTDE Turbo Time-Domain Equalisation

UCE Unstructured Channel Estimation

US Uncorrelated Scattering

V-BLAST Vertical Bell Laboratories Layered Space-Time

WSS Wide-Sense Stationary

WSSUS Wide-Sense Stationary Uncorrelated Scattering

ZF Zero Forcing

Chapter 1

Introduction

1.1 Motivation

Over the past decades, wireless communications have continuously strived forward to tackle challenges, (*e.g.*, higher throughput on non-free frequency bandwidth, lower power consumption at mobile terminals and more seamless fusion of infrastructures). Recently, one of the most exciting breakthroughs has come from the multi-input multi-output (MIMO) technology [1, 2, 3], which has opened the new possibility of improving capacity and reliability with no need of increasing bandwidth and transmit power.

The next generation wireless communication systems will face highly dispersive channels relative to the increased symbol rate. It has triggered the use of orthogonal frequency division multiplexing (OFDM) [4] and frequency-domain equalisation (FDE) [5], both of which are capable of combating frequency selective fading channels and are consistent with low-complexity hardware solutions. The trend that OFDM and FDE will respectively take the roles of the downlink and uplink in the next generation wireless communications has emerged more

and more evidently due to their higher throughput and lower complexities than the conventional time-domain equalisation (TDE). Although OFDM is regarded as the maturer technique, FDE is less sensitive to carrier synchronisation with a lower peak-to-average power ratio (PAPR) [6].

Turbo equalisation is another state-of-the-art technology, which may reshape the future of signal processing at the physical layer. It can be extended as a low complexity iterative FDE solution, which makes FDE even more attractive. Although showing up after its ancestor, tremendous Turbo codes [7], Turbo equalisation has demonstrated its potential by providing a flexibility of tradeoff between performance and complexity.

To track unknown fading channels, channel estimation is traditionally incorporated with TDE, which operates symbol by symbol and is a complexity-demanding task, especially in highly dispersive channels. To reduce the complexity, frequency-domain channel estimation incorporated with FDE estimates channel state information (CSI) block by block. The other benefit of frequency-domain channel estimation is its fast convergence speed. Turbo channel estimation, also known as soft-input iterative channel estimation, exploits the soft estimates of signals from the decoder for channel estimation and has been shown to be more robust against channel variations than the hard estimation based iterative channel estimation [8].

This thesis presents iterative frequency-domain channel equalisation and estimation, which both operate at the receiver side and are incorporated with each other to combat frequency-selective fading channels in single-carrier (SC) MIMO systems. A low complexity Turbo space-frequency equalisation (TSFE) structure is proposed, which combines the advantages of MIMO frequency-domain equalisation (FDE) and iterative (Turbo) equalisation. Turbo frequency-domain channel

estimation is investigated, especially from a perspective of the complexity. The thesis reveals the application prospect of the proposed iterative frequency-domain channel equalisation and estimation in an uplink MIMO SC frequency division multiple access (SC-FDMA) system.

1.2 Research Contributions

The research conducted has produced the following main contributions.

- A low complexity Turbo space-frequency equalisation (TSFE) structure is proposed, which combines the advantages of MIMO FDE and iterative (Turbo) equalisation. It introduces a tremendous complexity reduction over the symbol-wise TSFE structure as well as the previously proposed Turbo time-domain equalisation (TTDE) and Turbo FDE (TFDE) structures and outperforms its Turbo orthogonal frequency division multiplexing (TOFDM) counterpart with a comparable complexity.

- An intensive investigation of hard-input iterative and soft-input iterative (Turbo) frequency-domain channel estimation is provided. Under each of the proposed criteria, unstructured channel estimation (UCE) and structured channel estimation (SCE) are investigated. Least mean squares (LMS) SCE tracks the channel variations effectively with a low complexity as well as a highest convergence speed. The simplified Turbo recursive least squares (RLS) SCE provides nearly the same performance as Turbo RLS (TRLS) SCE, with a tremendous complexity reduction. Turbo normalised RLS (NRLS) SCE outperforms Turbo Kalman SCE in terms of the steady-state mean squared error (MSE). An intensive performance analysis of Turbo

Kalman channel estimation and Turbo NRLS channel estimation is provided.

- Adaptive Turbo multiuser detection and co-channel interference (CCI) suppression are applied to the uplink MIMO SC-FDMA system. The proposed Turbo SC-FDMA system significantly outperforms its Turbo orthogonal frequency division multiple access (OFDMA) counterpart. In the presence of unknown CCI, the simplified Turbo RLS channel estimation along with low-pass CCI suppression (LPCCIS) provides a performance very close to the case with perfect channel state information CSI, and outperforms the existing temporal CCI suppression (TCCIS) scheme.

1.3 Thesis Organisation

The rest of the thesis is organised in five chapters. An overview of the techniques relative to the research is provided in Chapter 2. Chapter 3 proposes the TSFE structure, which is compared with TTDE, TFDE, and TOFDM. Incorporated with TSFE, adaptive iterative frequency-domain channel estimation schemes are investigated in Chapter 4. Chapter 5 presents an adaptive Turbo MIMO SC-FDMA system with CCI suppression (CCIS), which is demonstrated as a very useful application of TSFE and Turbo channel estimation. Conclusions and future work are discussed in the final chapter.

1.4 Publication List

A list of publications during the course of this research is provided below, which all contribute to the thesis.

- Journal Papers

  1. Y. Wu, X. Zhu, and A. K. Nandi, "Low complexity adaptive Turbo space-frequency equalization for single-carrier multi-input multi-output systems," *IEEE Trans. Wireless Commun.*, vol. 7, pp. 2050-2056, Jun. 2008.

  2. Y. Wu, X. Zhu, and A. K. Nandi, "Low complexity adaptive Turbo frequency-domain channel estimation for single-carrier multi-user detection," to appear in *IEEE Trans. Wireless Commun.*

  3. Y. Wu, X. Zhu, and A. K. Nandi, "Soft Input Turbo Channel Estimation for Single-Carrier Multiple-Input Multiple-Output Systems," submitted to *IEEE Trans. Veh. Technol.*

- Conference Papers

  1. Y. Wu, X. Zhu, and A. K. Nandi, "MIMO single-carrier FDMA with adaptive Turbo multiuser detection and co-channel interference suppression," in *Proc. IEEE ICC'08*, Beijing, China, Jun. 2008.

  2. Y. Wu, X. Zhu, and A. K. Nandi, "Soft input Turbo frequency-domain channel estimation for single-carrier multiuser detection," in *Proc. IEEE ICC'08*, Beijing, China, Jun. 2008.

  3. Y. Wu, X. Zhu, and A. K. Nandi, "Low complexity adaptive Turbo frequency-domain channel estimation for single-carrier multi-user detection with unknown co-channel interference," in *Proc. IEEE ICC'07*, Glasgow, U.K., Jun. 2007.

  4. Y. Wu, X. Zhu, A. K. Nandi, and Y. Huang, "Turbo Space-Frequency Equalization with Adaptive Channel Estimation," in *Proc. CODEC'06*,

Kolkata, India, Dec. 2006.

5. Y. Wu, X. Zhu, and A. K. Nandi, "Low complexity Turbo space-frequency equalization for single-carrier MIMO wireless communications," in *Proc. EUSIPCO'06*, Florence, Italy, Sep. 2006.

6. Y. Wu, X. Zhu, and A. K. Nandi, "Adaptive layered space-frequency equalization for MIMO frequency selective channels," in *Proc. EUSIPCO'05*, Antalya, Turkey, Sep. 2005.

7. X. Zhu, Y. Wu, and A. K. Nandi, "Adaptive iterative layered space-frequency equalization for single-carrier MIMO systems," in *Proc. EUSIPCO'05*, Antalya, Turkey, Sep. 2005.

8. Y. Wu, X. Zhu, Y. Gong and A. K. Nandi, "Adaptive layered space-frequency equalization for MIMO frequency selective channels," in *Proc. ICCCAS'05*, Hongkong, China, May 2005.

Chapter 2

Research Overview

Having been applied in this work, four relevant techniques are reviewed in this chapter: 1) MIMO; 2) FDE; 3) iterative (Turbo) equalisation; and 4) iterative channel estimation.

2.1 Multi-Input Multi-Output (MIMO) Technique

MIMO technology has attracted tremendous attention, since it offers significant increases in data throughput and link range without additional bandwidth or transmit power. Pioneering work by Winters [1], Foschini [2], and Telatar [3] ignited much interest in this area by predicting remarkable spectral efficiencies for wireless systems with multiple antennas when the channel exhibits rich scattering and its variations can be accurately tracked.

MIMO systems employ multiple antennas at the receiver and transmitter. Based on multipath effects, multiple spatial branches can be established between transmitter and receiver. Traditionally, this effect has been exploited in diversity

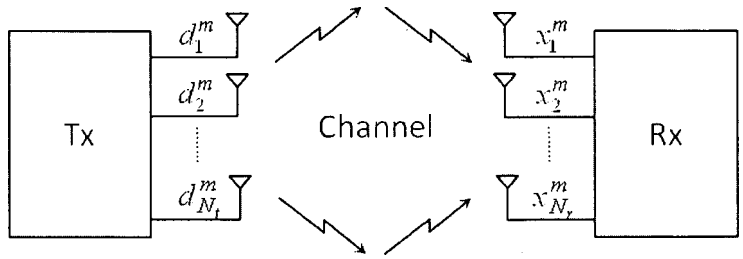

Figure 2.1: Diagram of a MIMO system with N_t transmit antennas and N_r receive antennas.

systems to improve the link quality by reducing the fading effects. When multiple antennas are employed in single user systems, the possible system configurations include: multiple-input single-output (MISO), single-input multiple-output (SIMO) and MIMO. A typical discrete time MIMO system with N_t transmit antennas and N_r receive antennas is depicted in Figure 2.1.

The overall channel memory is assumed to be N. Assuming symbol spaced sampling, the mth receive signal sample at the lth ($l = 1, \cdots, N_r$) receive antenna is given by

$$x_l^m = \sum_{n=1}^{N_t} \sum_{i=0}^{N} h_{ln}^{mi} d_n^{m-i} + n_l^m \tag{2.1}$$

where h_{ln}^{mi} denotes the ith ($i = 0, \cdots, N$) path gain between the nth transmit antenna and the lth receive antenna at time m, and n_l^m denotes the additive white Gaussian noise (AWGN) with the single-sided power spectral density (PSD) N_0.

2.1.1 Spatial Diversity

It has been found that an antenna spacing of at least $\lambda/2$ results in sufficiently uncorrelated branches, which can be exploited by a spatial diversity system or spatial multiplexing system, where λ is the wavelength. This corresponds to 16 cm at 900 MHz or 8 cm at 1800 MHz, which are typical operating frequencies of current mobile telephone networks. This makes the use of multiple antennas at

the mobile station feasible.

Space-Time Block Codes (STBCs) can obtain transmit diversity without knowledge of the channel at the receiver. This is particularly interesting in a mobile communications scenario, where it is not always possible to implement multiple antennas at the receiver. The Alamouti scheme can be regarded as a special case of STBCs [9]. It has a simple implementation and no channel knowledge is necessary at the transmitter. Other STBCs include the trellis space-time code, which uses a Viterbi maximum likelihood decoder. It obtains better performance than the Alamouti scheme but entails an increased computational burden at the receiver. There are also forms of indirect transmit diversity, which convert spatial diversity to time or frequency diversity using appropriate encoding at the transmitter.

At the receiver, the signals from the uncorrelated branches have to be combined in a suitable way to minimise fading of the combined signal. The following are some standard combining methods:

- Maximum ratio combining: Weighing of the branch signals according to signal-to-noise ratio (SNR), co-phasing and combining.
- Equal gain combining: Same weighing for all branch signals, co-phasing and combining.
- Selection combining: Selects the branch signal with the highest SNR.

2.1.2 Spatial Multiplexing

Spatial multiplexing uses the statistically uncorrelated branches between multiple transmit and receive antennas to increase the data rate by transmitting data in parallel. The large spectral efficiencies associated with MIMO channels are based

on the fact that a rich scattering environment is able to provide independent transmission paths from each transmit antenna to each receive antenna. Therefore, for single-user systems, a transmission and reception strategy that exploits this structure achieves capacity on approximately $min\,(N_t, N_r)$ separate channels, where N_t is the number of transmit antennas and N_r is the number of receive antennas. Thus, capacity scales linearly with $min\,(N_t, N_r)$ relative to a system with just one transmit and one receive antenna. This capacity increase requires a scattering environment such that the matrix of channel gains between transmit and receive antenna pairs has full rank and independent entries and that perfect estimates of these gains are available at the receiver. Much subsequent work has been aimed at characterising MIMO channel capacity under more realistic assumptions about the underlying channel model and the channel estimates available at the transmitter and receiver. MIMO channel capacity depends heavily on the statistical properties and antenna element correlations of the channel. Previous work has developed both analytical and measurement-based MIMO channel models along with the corresponding capacity calculations for typical indoor and outdoor environments [10]. Antenna correlation varies drastically as a function of the scattering environment, the distance between transmitter and receiver, the antenna configurations, and the Doppler spread [11, 12]. As shown in [13], the effect of channel correlation on capacity depends on what is known about the channel at the transmitter and receiver: correlation sometimes increases capacity and sometimes reduces it [14].

2.1.3 Reserach on MIMO

Many practical MIMO techniques have been developed to capitalise on the theoretical capacity gains predicted by Shannon theory. A major focus of such work

is space-time coding: recent work in this area is summarised in [15]. Other techniques for MIMO systems include space-time modulation [16, 17], adaptive modulation and coding [18], space-time equalisation [19, 20], space-time signal processing [21], space-time code division multiple access (CDMA) [22, 23], and space-time OFDM [24, 25, 26]. An overview of the recent advances in these areas and other practical techniques along with their performance can be found in [27].

2.2 Frequency-Domain Equalisation (FDE)

Since FDE was proposed as an alternative equalisation scheme to traditional SC systems [28], and frequency-domain adaptive filtering appeared in signal processing literature [29], it has almost fallen into disuse. FDE hasn't made itself a popular technique over the past three decades, since TDE has dominated the realm of adaptive SC equalisation. However, FDE has shown a strong comeback to earn itself a place in the next generation wireless communication systems due to its favorable tradeoff between performance in frequency selective fading channels and signal processing complexity.

In the next generation wireless communications, broadband wireless access technologies is required to offer bit rates of tens of megabits per second or more to residential and business subscribers. Air interface standards for such broadband wireless metropolitan area network (MAN) systems in licensed and unlicensed bands below 11 GHz have been developed by the IEEE 802.16 working group and also by the European Telecommunications Standards Institute (ETSI) Broadband Radio Access Network (BRAN) High-Performance MAN (HiperMAN) group. Such systems may serve residential and small office/home office (SOHO) subscribers, operating over non-line-of-sight (NLOS) links where multipath effect

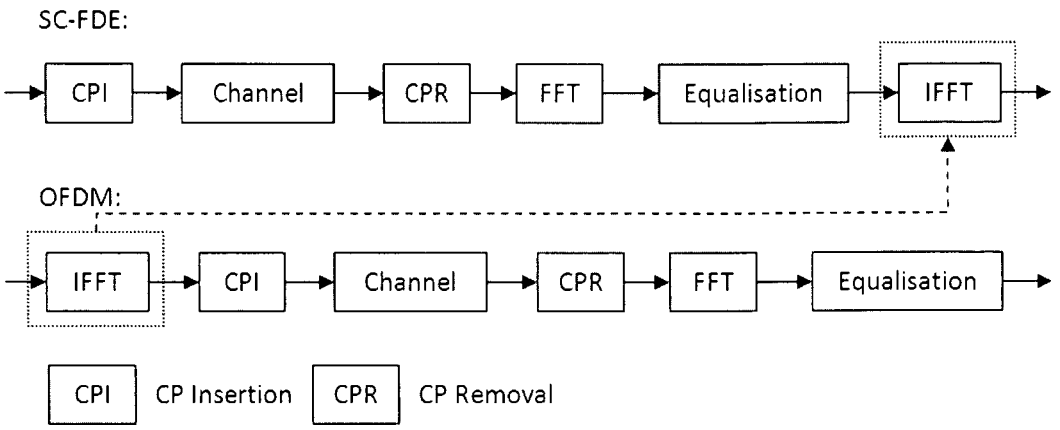

Figure 2.2: SC-FDE and OFDM - signal processing similarities and differences.

can be severe. This raises the question of what types of anti-multipath techniques are necessary, and consistent with low-cost solutions. Both SC-FDE and OFDM have been regarded the most promising techniques to be deployed in the next generation communications.

2.2.1 FDE vs. OFDM

As shown in Figure 2.2, SC-FDE has a similar structure to OFDM except that the inverse fast Fourier transform (IFFT) block is moved from the transmitter to the receiver [5, 30]. In a SC-FDE system, each block of M modulated symbols are transmitted after the cyclic prefix (CP) is inserted at the head of the block. At the receiver side, CP is removed and fast Fourier transform (FFT) transforms the time-domain signal into the frequency domain. Since CP makes the channel circulant, each frequency bin is simply linearly equalised by a equaliser coefficient. Finally, the equalised signal are transformed from the frequency domain back to the time domain by IFFT for detection or decoding.

Since SC-FDE systems are closely related to OFDM systems, only the modifications of the equalisation methods required for SC-FDE systems are discussed.

One of the main difference from OFDM is that although equalisation is performed in the frequency domain, the source data is in the time domain. The linear equalisation schemes (Zero Forcing (ZF), Minimum Mean Squared Error (MMSE)) are analogous to the OFDM case, however, equalisation needs to be performed in all frequency bins in order to recover the time-domain stream estimates. If maximum likelihood (ML) equalisation is applied to SC-FDE systems, a time-domain formulation is essential, compared to the frequency-domain one for OFDM system. In the case of MIMO FDE, vertical bell laboratories layered space-time (V-BLAST) equalisation is mostly used, where the optimal detection order should be determined all frequency bins for each antenna, while MIMO-OFDM employs the optimum ordering on each frequency bin for each antenna.

Low complexity of linear signal processing and robustness against dispersive channels are the common characteristics to both of the two techniques, but the use of SC modulation and FDE by processing the FFT of the received signal has several attractive features:

- SC modulation has reduced peak-to-average power ratio (PAPR) requirements from OFDM, thereby allowing the use of less costly power amplifiers.
- The performance of SC-FDE is similar to that of OFDM, even for very long channel delay spread.
- Frequency-domain receiver processing has a similar complexity reduction advantage to that of OFDM.
- Coding, while desirable, is not necessary for combating frequency selectivity, as it is in nonadaptive OFDM.
- SC modulation is a well-proven technology in many existing wireless and

wireline applications, and its linearity requirement for the amplifier is well known.

- From a carrier synchronisation point of view, FDE with SC modulation suffers from single unsynchronised carrier less than OFDM suffers from multi unsynchronised carriers.

2.2.2 Research on FDE

Compared to TDE such as decision feedback equalisation (DFE) [31] and maximum likelihood sequence estimation (MLSE) [32], FDE requires less complexity to achieve the same performance, especially in highly dispersive channels [33]. In [34], FDE was employed in MIMO systems, where all the signals are detected simultaneously. A layered space-frequency equalisation structure was proposed in [35] for MIMO systems, which provides enhanced performance over the single-stage MIMO FDE [34] by combining FDE and successive interference cancellation. However, [34] and [35] only assumed quasi-static channels.

Adaptive FDE structures were investigated in [33] and [36] for time-varying channels, where the equaliser coefficients are updated directly without explicit channel estimation. This however may introduce a relatively slow convergence speed in fast fading channels. Another type of adaptive FDE structures are based on separate adaptive channel estimation [37, 38] and equalisation. The work in [37] assumed single-input single-output (SISO) and SIMO systems, which was extended for the MIMO case in [38].

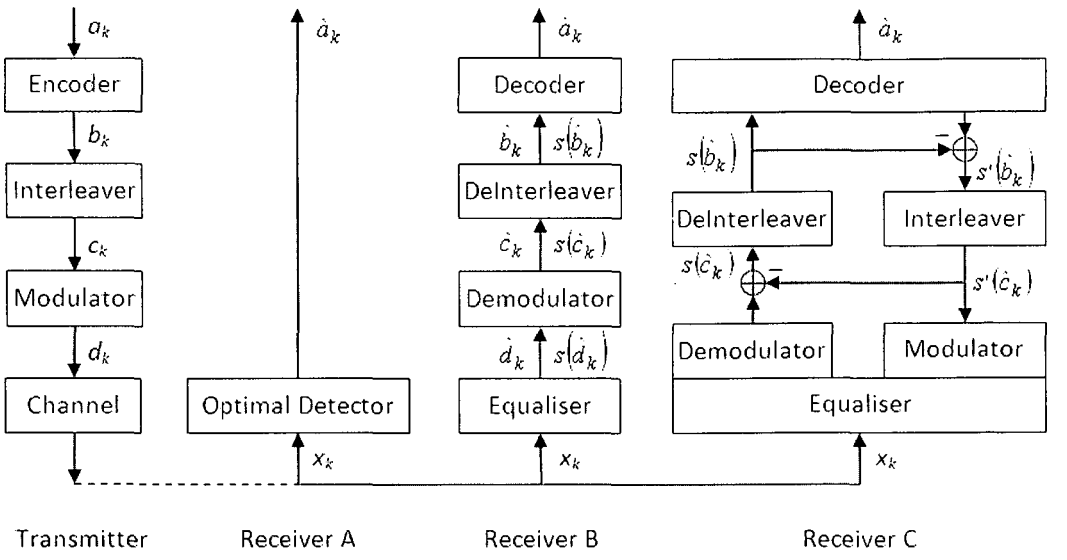

Figure 2.3: Transmitter and three receiver structures: the optimal detector (receiver A), one-time equalisation and decoding using hard or soft inputs (receiver B), and Turbo equalisation (receiver C).

2.3 Iterative (Turbo) Equalisation

Iterative (Turbo) equalisation is an iterative equalisation and decoding technique, which provides substantial insights into the significant performance improvement over the conventional equalisation techniques [39].

2.3.1 Iterative (Turbo) Receiver

Figure 2.3 contains a system configuration for a digital transmitter as part of a communication link. These basic elements are contained in most practical communication systems and are essential components of a transmitter such that Turbo equalisation can be used in the receiver.

The role of the encoder, usually for the error control code (ECC), is to take the binary data sequence to be transmitted as input and produce an output that contains not only this data but also additional redundant information that can be

used to protect the data of interest in the event of errors during transmission. To ensure that single-bit errors appear randomly and to avoid long error bursts, an interleaver is used to randomise the order of the code bits prior to transmission. Finally, the permuted code bits are then modulated at baseband and transmitted over a passband channel.

To estimate the transmitted data optimally, the receiver must find the set of transmitted bits that are most probable. Such a receiver, as depicted in Figure 2.3 as receiver A, takes into account the ECC, the interleaver, the symbol mapping, and knowledge of the channel. With so many factors involved, the resulting statistical relationship rapidly becomes difficult to manage in an efficient manner. As such, receiver A is simply infeasible, as it amounts to essentially trying to fit all possible sequences of transmitted bits to the received data, a task whose complexity grows exponentially.

The way that most practical receivers have been designed is to equalise the received observations to account for the effects of the channel, which is the first step in receiver B from Figure 2.3. Equaliser outputs can be demodulated into code bits, deinterleaved, and then decoded using a bit error rate (BER) optimal decoder for the ECC. The most straightforward way to implement this separate equalisation and decoding process is for the equaliser to make hard decisions as to which sequence of channel symbols were transmitted and for these hard decisions to be mapped into binary code bits. These binary code bits can then be processed with the decoder for the ECC. The process of making hard decisions on the channel symbols actually destroys information pertaining to how likely each of the possible channel symbols might have been, however. This additional soft information can be converted into probabilities that each of the received code bits takes on the value of zero or one that, after deinterleaving, is precisely the form

of information that can be exploited by a BER optimal decoding algorithm.

The remarkable performance of Turbo codes makes it clear that the soft information need not only flow in one direction. Once the error control decoding algorithm processes the soft information it can, in turn, generate its own soft information indicating the relative likelihood of each of the transmitted bits. This soft information from the decoder could then be properly interleaved and taken into account in the equalisation process, creating a feedback loop between the equaliser and decoder, through which each of the constituent algorithms communicates its beliefs about the relative likelihood that each given bit takes on a particular value. The feedback loop structure described here and depicted in receiver C in Figure 2.3 is essentially the process of Turbo equalisation.

Turbo equalisation systems were first proposed in [40] and developed further by a number of others [41]. In particular, the original system introduced by Douillard *et al.* can be viewed as an extension of the Turbo decoding algorithm by considering the effect of the inter symbol interference (ISI) channel as another form of error protection, *i.e.*, as a rate−1 convolutional code. In each of these Turbo equalisation systems, maximum *a posteriori* probability (MAP) based techniques, are used exclusively for both equalisation and decoding.

An information bit sequence $\mathbf{a}$ is encoded and interleaved into a code sequence $\mathbf{c} = [\mathbf{c}_1\mathbf{c}_2\cdots\mathbf{c}_M]$, where $\mathbf{c}_n = [c_{n,1}c_{n,2}\cdots c_{n,Q}]\,(n = 1,\cdots,M)$. The binary code sequence $\mathbf{c}$ is mapped to a data sequence of M data symbols according to the symbol alphabet $\boldsymbol{\alpha} = \{\alpha_1,\cdots,\alpha_S\}$, where $\alpha_s(s = 1,\cdots,S)$ has unit symbol energy and a bit patten $\mathbf{p}_s = [p_{s,1}p_{s,2}\cdots p_{s,Q}]$ with $p_{s,q} \in \{0,1\}(q = 1,\cdots,Q)$. Finally the data sequence is transmitted over the frequency selective fading channel.

Assuming the received sequence is $\mathbf{x}$, the *a posteriori* LLR $L\,(c_{n,q}|\mathbf{x})$ is com-

puted by the MAP equaliser as

$$L\left(c_{n,q}|\mathbf{x}\right) = ln\frac{P\left(c_{n,q}=1|\mathbf{x}\right)}{P\left(c_{n,q}=0|\mathbf{x}\right)}$$

$$= ln\frac{\sum_{\forall \mathbf{c}:c_{n,q}=1} p(\mathbf{x}|\mathbf{c})P(\mathbf{c})}{\sum_{\forall \mathbf{c}:c_{n,q}=0} p(\mathbf{x}|\mathbf{c})P(\mathbf{c})} \tag{2.2}$$

which can be broken into the sum

$$\underbrace{ln\frac{\sum_{\forall \mathbf{c}:c_{n,q}=1} p(\mathbf{x}|\mathbf{c}) \prod_{n'\neq n,q'\neq q} P(c_{n',q'})}{\sum_{\forall \mathbf{c}:c_{n,q}=1} p(\mathbf{x}|\mathbf{c}) \prod_{n'\neq n,q'\neq q} P(c_{n',q'})}}_{L_e(c_{n,q})} + L\left(c_{n,q}\right) \tag{2.3}$$

The first term $L_e\left(c_{n,q}\right)$ represents the information about $c_{n,q}$ contained in $\mathbf{x}$ and in the bit $c_{n,q}$ $(n'\neq n, q'\neq q)$, which is interleaved and conveyed to the decoder. The decoder generates its new LLRs, which are interleaved and fed back to the equaliser. The loop continues until LLRs converge.

2.3.2 Research on Iterative (Turbo) Equalisation

MAP based Turbo equalisation suffers from impractically high computational complexity, especially for highly dispersive channels, due to the need to perform equalisation and decoding several times for each block of data. One of the research focuses of Turbo equalisation is the development of low complexity alternatives to MAP based Turbo equalisation. Wang and Poor [42] proposed a Turbo equalisation-like system for multi-user detection in CDMA systems, where the MAP equaliser is replaced by a linear equaliser based on the MMSE criterion. In [43, 44, 45], another MMSE based suboptimum Turbo equaliser was proposed using the so-called 'average variance' technique (*i.e.*, the variance of each symbol is replaced by the time average of all the variances), whose coefficients remain

unchanged within a data block. Another common technique to decrease the complexity of the MAP equaliser is to reduce the number of states in the underlying trellis, which was applied to Turbo equalisation in [46]. However, most previous work on Turbo equalisation assumed time-domain processing, which still introduces a high complexity with a large number of antennas and a high channel delay spread.

Turbo equalisation was incorporated with FDE for SC MIMO systems in [47], which is referred to as TFDE here. TFDE is an easy extension of TTDE [47] to MIMO systems, based on the work in [43]. However, the equaliser coefficients of TFDE (as well as TTDE) are mainly derived in the time domain, which involves the inverse of a big matrix. Hence, TFDE requires a much higher complexity than its TOFDM counterpart [47], which operates on each subcarrier independently.

2.4 Iterative Channel Estimation

In practice, channels are time-varying and unknown to receivers. Therefore, adaptive channel estimation is desirable. Under the principle of Turbo equalisation, channel estimation is also iterative. To be coupled with Turbo equalisation, two categories of iterative channel estimation are available: 1) joint iterative channel estimation with Turbo equalisation; 2) separate iterative channel estimation.

The first category operates channel estimation by adaptively compute equaliser coefficients, which takes channel uncertainty into account for trellis based Turbo equalisation. However, joint channel estimation based on trellis based Turbo equalisation requires a huge complexity in implementation.

The second category regards the channel estimation task as an independent signal processing task. In this case, the channel estimates are used to generate the

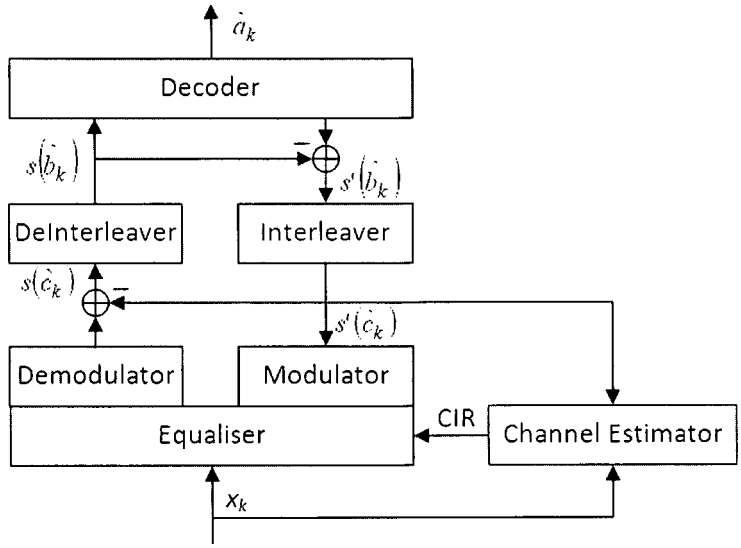

Figure 2.4: Separate Iterative channel estimation incorporated with Turbo equalisation.

equaliser coefficients iteratively. This allows combination of a wide range of channel estimation algorithms [48] and Turbo equalisation algorithms [40, 43, 49], to make a good tradeoff between the performance and complexity. This advantage over joint iterative channel estimation makes the separate iterative channel estimation much more popular, since it can significantly reduce the implementation difficulties on hardware.

There are two different types of separate iterative channel estimation. The difference lies in whether hard inputs or soft inputs are utlised during channel estimation. Compared with hard-input channel estimation, soft-input channel estimation requires a comparable complexity with improved estimation accuracy due to the reduction of error propagation. Figure 2.4 illustrates separate iterative channel estimation incorporated with Turbo equalisation. Although soft input from the decoder is employed to perform iterative channel estimation in the figure, iterative channel estimation also can operate based on hard inputs from the decoder. The received signal and soft input from the decoder for each

iteration are fed to the iterative channel estimator, which generates and passes the channel impulse response (CIR) to the next iteration of equalisation.

There has been some work on iterative joint equalisation and channel estimation, in which hard inputs from the decoder are used to refine a channel estimate, in the context of OFDM transmission [50, 51]. However, the updates of channel estimation in these systems were based on hard inputs of signals, which introduce significant error propagation. In [52] and [53], adaptive trellis based Turbo equalisation was proposed to perform joint iterative channel estimation and equalisation, which, however, requires a high computational complexity.

Separate soft-input iterative (Turbo) channel estimation was applied to flat fading channels in [54], and frequency selective fading channels in [55], both based on the MMSE criterion. In [8], a Kalman filtering based Turbo channel estimation and a weighted Turbo RLS based channel estimation schemes were proposed. A Kalman smoothing based channel estimation scheme was proposed in [56] to improve the accuracy of the channel estimate. In [57], Turbo RLS based channel estimation reduces to Turbo LMS channel estimation nearly with no performance loss given phase shift keying (PSK) modulation. However, most previous work on Turbo channel estimation was symbol wise and was incorporated with TDE, which requires a prohibitive complexity for highly dispersive channels [58].

Compared to OFDM, SC-FDE has a lower PAPR and less sensitivity to carrier synchronisation. Turbo channel estimation incorporated with FDE performs on blocks, which saves a substantial complexity over the symbol-wise Turbo channel estimation incorporated with TDE [8, 54, 55, 56, 57]. In [59], a least squares (LS) based Turbo channel estimation scheme was proposed for SC-FDE systems. A simplified Turbo frequency-domain RLS channel estimation scheme was proposed for SC MIMO systems, which provides nearly the same performance as its full

complexity counterpart with a tremendous complexity reduction [58]. To the best of the knowledge, however, no work has been reported on the Kalman based Turbo channel estimation for SC-FDE systems.

Chapter 3

Turbo Equalisation Techniques

This chapter proposes an MMSE based low complexity adaptive TSFE structure for SC MIMO systems with block transmission, combining the advantages of MIMO Turbo equalisation and block processing for SC-FDE. This work is different in that the equaliser coefficients are derived in the frequency domain, using the 'average variance' technique [43, 44, 45]. This is a novel and effective application of the 'average variance' technique in SC MIMO FDE, which allows channel equalisation on each independent frequency bin. As a result, a new concise block-wise FDE structure is proposed and computational complexity is significantly reduced.

It is shown that the proposed block-wise low complexity TSFE introduces a tremendous complexity reduction over the symbol-wise TSFE as well as TTDE and TFDE for SC MIMO systems. In terms of performance, the low complexity TSFE is close to the symbol-wise TSFE, equivalent to TFDE and superior over TTDE over highly dispersive channels, achieving the same bandwidth efficiency. With a moderate code rate and the increase of the number of iterations, SC TSFE also significantly outperforms its TOFDM counterpart [47] for multi-carrier

(MC) block transmission, at a comparable complexity. An intensive performance analysis is provided for the low complexity TSFE, compared to TOFDM. The effects of the channel delay spread and the numbers of antennas on performance are also shown.

The symbol-spaced TSFE is extended to the case with oversampling, which avoids an information loss in discretising the received signals. The complexity of the oversampled TSFE increases linearly with the number of samples per block, and is much lower than the complexities of TTDE [47] and FD-TLE [60], which increase nonlinearly with the number of samples per block.

3.1 System Model

This section introduces the SC MIMO system model, on which the proposed TSFE and iterative channel estimation are based.

3.1.1 Notations

$\lfloor . \rfloor$ and $\lceil . \rceil$ are reserved for integer flooring and integer ceiling, respectively, and % for *mod* operation. $J_0(.)$ denotes the 0th order Bessel function. $(.)^*$ denotes the complex conjugate of a complex number. Let $(.)^T$ and $(.)^H$ denote the transpose and complex-conjugate transpose of a matrix/vector, respectively. The trace of a square matrix is given by $tr(.)$. $E(\mathbf{X})$ and $Cov(\mathbf{X}, \mathbf{Y}) = E(\mathbf{X}\mathbf{Y}^H) - E(\mathbf{X})E(\mathbf{Y}^H)$ respectively denote the expectation and covariance operators. The element in the ith row and kth column of the matrix $\mathbf{X}$ is denoted by $[\mathbf{X}]_{i,k}$. Diagonal and block diagonal matrices are denoted by $diag(.)$ and $DIAG(.)$, respectively, with elements/matrices on the diagonal listed in the parentheses. $\mathbf{I}_N$ is an $N \times N$

identity matrix. Also define operators *vec* and *mat* as:

$$vec(\mathbf{a}_1 \cdots \mathbf{a}_Q) = \left[\mathbf{a}_1^T \cdots \mathbf{a}_Q^T\right]^T$$

$$mat(\mathbf{a}_1 \cdots \mathbf{a}_Q) = \begin{bmatrix} \mathbf{a}_1 & \mathbf{0} & \cdots & \mathbf{0} \\ \mathbf{0} & \mathbf{a}_2 & \cdots & \mathbf{0} \\ \vdots & \vdots & \ddots & \vdots \\ \mathbf{0} & \mathbf{0} & \cdots & \mathbf{a}_Q \end{bmatrix}$$

where $\mathbf{a}_q (q = 1, \cdots, Q)$ denotes a column vector.

3.1.2 SC MIMO System Model

A MIMO system with N_t transmit antennas and N_r receive antennas employed in this chapter and Chapter 4 is depicted in Figure 3.1. An information bit sequence $\mathbf{b}$ is encoded into a terminated recursive systematic convolutional (RSC) code sequence $\mathbf{c} = [\mathbf{c}_1 \mathbf{c}_2 \cdots \mathbf{c}_{N_t M}]$, where $\mathbf{c}_t = [c_{t,1} c_{t,2} \cdots c_{t,Q}] (t = 1, \cdots, N_t M)$ with $c_{t,q} \in \{0, 1\} (q = 1, \cdots, Q)$ denoting the qth coded bit in $\mathbf{c}_t$. The encoder has a memory of M_c (M_c bits are tailed to the information bit sequence $\mathbf{b}$ which forces the encoder to the all-zero state using the encoder circuit). The binary code sequence $\mathbf{c}$ is interleaved and mapped to a data sequence of $N_t M$ S-ary data symbols according to the symbol alphabet $\boldsymbol{\alpha} = \{\alpha_1, \cdots, \alpha_S\}$, where $\alpha_s (s = 1, \cdots, S)$ has unit symbol energy and a bit patten $\mathbf{p}_s = [p_{s,1} p_{s,2} \cdots p_{s,Q}]$ with $p_{s,q} \in \{0, 1\} (q = 1, \cdots, Q)$. Finally the data sequence is multiplexed into N_t transmission blocks, each containing M symbols. Let $d_n^i (i = 0, \cdots, M-1)$ denote the ith data symbol of a symbol period of T in a block transmitted by the nth $(n = 1, \cdots, N_t)$ antenna, and $\mathbf{c}_n^i = \left[c_{n,1}^i c_{n,2}^i \cdots c_{n,Q}^i\right]$ the bit patten d_n^i.

The overall channel memory is assumed to be N, lumping the effects of the

transmit filter, receive filter and physical channel. The channel is assumed to be block fading, i.e., the CSI is constant over a block. To implement the SC-FDE block transmission, each data block is prepended with a CP, which is the replica of the last N symbols in the block, and is discarded at the receiver to prevent inter-block interference (IBI). The received signals are sampled at the symbol rate. Within each block, the mth ($m = 0, \cdots, M-1$) sample at the lth receive antenna is given by

$$x_l^m = \sum_{n=1}^{N_t} \sum_{i=0}^{N} h_{ln}^i d_n^{m-i} + n_l^m \tag{3.1}$$

where h_{ln}^i denotes the ith ($i = 0, \cdots, N$) path gain between the nth transmit antenna and the lth receive antenna. n_l^m is the AWGN with the single-sided PSD N_0. Define $\mathbf{x}^m = \left[x_1^m \cdots x_{N_r}^m\right]$ as the received signal vector at the mth sampling time within a block, which is given by

$$\mathbf{x}^m = \sum_{n=1}^{N_t} \sum_{i=0}^{N} \mathbf{h}_n^i d_n^{m-i} + \mathbf{n}^m \tag{3.2}$$

The received signals are transferred into the frequency domain by FFT. The signal on the mth ($m = 0, \cdots, M-1$) frequency bin at the lth receive antenna is given by

$$X_l^m = \sum_{n=1}^{N_t} H_{ln}^m D_n^m + N_l^m \tag{3.3}$$

where

$$X_l^m = \sum_{i=0}^{M-1} x_l^i e^{-j2\pi mi/M} \tag{3.4}$$

$$H_{ln}^m = \sum_{i=0}^{N} h_{ln}^i e^{-j2\pi mi/M} \tag{3.5}$$

$$D_n^m = \sum_{i=0}^{M-1} d_n^i e^{-j2\pi mi/M} \tag{3.6}$$

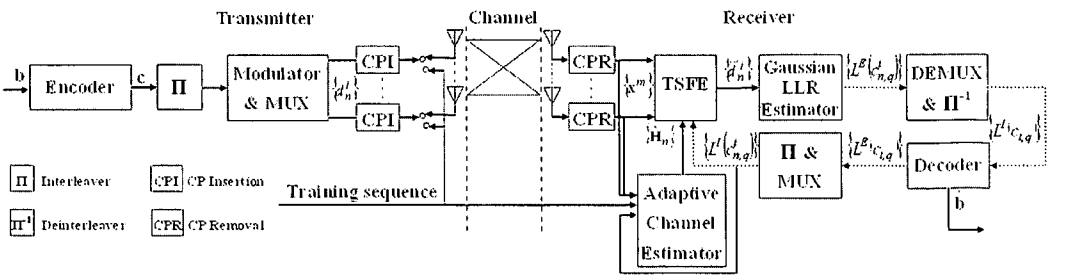

Figure 3.1: Block diagram of the SC MIMO system with adaptive TSFE at the receiver.

$$N_l^m = \sum_{i=0}^{M-1} n_l^i e^{-j2\pi mi/M} \tag{3.7}$$

respectively denote the discrete Fourier transforms (DFTs) of x_l^i, h_{ln}^i, d_n^i and n_l^i. Furthermore, let

$$\mathbf{X}^m = \sum_{n=1}^{N_t} \mathbf{H}_n^m D_n^m + \mathbf{N}^m \tag{3.8}$$

where $\mathbf{X}^m = \left[X_1^m \cdots X_{N_r}^m\right]^T$, $\mathbf{H}_n^m = \left[H_{1n}^m \cdots H_{N_r n}^m\right]^T$, $\mathbf{N}^m = \left[N_1^m \cdots N_{N_r}^m\right]^T$.

At the receiver, the mean μ_n^i and variance v_n^i of d_n^i are computed before equalisation:

$$\mu_n^i = E(d_n^i) = \sum_{\alpha_s \in \boldsymbol{\alpha}} \alpha_s P(d_n^i = \alpha_s) \tag{3.9}$$

$$v_n^i = Cov(d_n^i, d_n^i) = \sum_{\alpha_s \in \boldsymbol{\alpha}} |\alpha_s|^2 P(d_n^i = \alpha_s) - |\mu_n^i|^2 \tag{3.10}$$

using the *a priori* information $P(d_n^i = \alpha_s)$:

$$P(d_n^i = \alpha_s) = \prod_{q=1}^{Q} \frac{1 + \hat{p}_{s,q} tanh\left(L^I\left(c_{n,q}^i\right)/2\right)}{2} \tag{3.11}$$

where

$$\hat{p}_{s,q} = \begin{cases} 1 & p_{s,q} = 1 \\ -1 & p_{s,q} = 0 \end{cases} \tag{3.12}$$

and $L^I\left(c^i_{n,q}\right)$ is the LLR defined as

$$L^I\left(c^i_{n,q}\right) = ln\frac{P\left(c^i_{n,q}=1\right)}{P\left(c^i_{n,q}=0\right)} \tag{3.13}$$

3.2 Turbo TDE (TTDE), Turbo FDE (TFDE) and Turbo OFDM (TOFDM)

Before proposing the low complexity TSFE structure, TTDE, TFDE and TOFDM [47] are reviewed as good references due to their structural similarities to TSFE. TTDE and TFDE are easy extensions of [43] to MIMO systems with SC block transmission, and TOFDM for MC block transmission performs Turbo equalisation on each flat fading subcarrier independently.

3.2.1 TTDE and TFDE

TTDE is a direction extension of the work in [43] to the MIMO systems, which employs the same block transmission structure shown in Section 3.1 except that no CP is used in each block. With TTDE, the received signals are passed through a filter which spans F symbol periods. During the ith sampling period, the signals spanned by the linear filter are denoted by $\bar{\mathbf{x}}^i = vec\left(\mathbf{x}^{i+N_d}\cdots\mathbf{x}^{i+N_d-F+1}\right)$, where N_d is the decision delay of the filter. $\bar{\mathbf{x}}^i$ can be expressed in matrix notation as

$$\bar{\mathbf{x}}^i = \sum_{n=1}^{N_t}\bar{\mathbf{h}}_n\bar{\mathbf{d}}^i_n + \bar{\mathbf{n}}^i \tag{3.14}$$

where $\bar{\mathbf{d}}_n^i = \left[d_n^{i+N_d} \cdots d_n^{i+N_d-N-F+1}\right]^T$, $\bar{\mathbf{n}}^i = vec\left(\mathbf{n}^{i+N_d} \cdots \mathbf{n}^{i+N_d-F+1}\right)$, and

$$\bar{\mathbf{h}}_n = \begin{bmatrix} \tilde{\mathbf{h}}_n & \cdots & \mathbf{0} \\ \vdots & \ddots & \vdots \\ \mathbf{0} & \cdots & \tilde{\mathbf{h}}_n \end{bmatrix} \tag{3.15}$$

which is an $N_r F \times (N+F)$ block Toeplitz matrix, with $\tilde{\mathbf{h}}_n = \left[\mathbf{h}_n^0 \cdots \mathbf{h}_n^N\right]$.

Let $\mathbf{w}_k^i$ and b_k^i respectively denote the linear filter weight vector and feedback coefficient with respect to $d_k^i (k = 1, \cdots, N_t; i = 0, \cdots, M-1)$. The corresponding equaliser output signal is given by

$$\tilde{d}_k^i = \mathbf{w}_k^{iH} \bar{\mathbf{x}}^i + b_k^i \tag{3.16}$$

By minimising the mean squared error (MSE) cost function

$$J_k^i = E\left|\tilde{d}_k^i - d_k^i\right|^2 \tag{3.17}$$

The optimum linear filter weight vector $\mathbf{w}_k^i$ is obtained, which is expressed as

$$\mathbf{w}_k^i = v_k^i \left(\sum_{n=1}^{N_t} \hat{\bar{\mathbf{h}}}_n Cov(\bar{\mathbf{d}}_n^i, \bar{\mathbf{d}}_n^i) \hat{\bar{\mathbf{h}}}_n^H + N_0 \mathbf{I}_{N_r F}\right)^{-1} \hat{\bar{\mathbf{h}}}_k^{N_d+1} \tag{3.18}$$

where $\hat{\bar{\mathbf{h}}}_n$ denotes the estimate of $\bar{\mathbf{h}}_n$, $\hat{\bar{\mathbf{h}}}_k^{N_d+1}$ denotes the (N_d+1)th column of $\hat{\bar{\mathbf{h}}}_k$, and

$$Cov(\bar{\mathbf{d}}_n^i, \bar{\mathbf{d}}_n^i) = diag\left(v_n^{i+N_d} \cdots v_n^{i+N_d-N-F+1}\right) \tag{3.19}$$

To reduce the computational complexity, $v_n^m (m = i+N_d, \cdots, i+N_d-N-F+1)$

in (3.19) can be approximated by its average $\bar{v}_n$ for all m within the block, *i.e.*,

$$\bar{v}_n = \frac{1}{M} \sum_{i=0}^{M-1} v_n^i \tag{3.20}$$

Thus, (3.18) becomes

$$\mathbf{w}_k^i = v_k^i \left(\sum_{n=1}^{N_t} \bar{v}_n \hat{\mathbf{h}}_n \hat{\mathbf{h}}_n^H + N_0 \mathbf{I}_{N_r F} \right)^{-1} \hat{\mathbf{h}}_k^{N_d+1} \tag{3.21}$$

The corresponding optimum feedback coefficient b_k^i is given by

$$b_k^i = \mu_k^i - \mathbf{w}_k^{iH} \sum_{n=1}^{N_t} \hat{\mathbf{h}}_n E\left(\bar{\mathbf{d}}_n^i\right) \tag{3.22}$$

where $E\left(\bar{\mathbf{d}}_n^i\right) = \left[\mu_n^{i+N_d} \cdots \mu_n^{i+N_d-N-F+1}\right]^T$.

TFDE [47] is similar to TTDE, except that a CP is introduced in the transmission block as shown in Section 3.1. The linear filter of TFDE is implemented in the frequency domain, and its coefficients are obtained by simply transferring the time-domain weight vector $\mathbf{w}_k^i$ in (3.21) into the frequency domain by FFT, with $F = M$ and $N_d = M - 1$. After the frequency-domain equalised symbol is transferred back into the time domain, a feedback coefficient b_k^i defined in (3.22) is added to it to remove the residue inter-symbol interference and inter-channel interference.

3.2.2 TOFDM

OFDM has a similar structure to SC-FDE except that the IFFT block is moved from the receiver to the transmitter [5, 30]. The frequency-domain received

TOFDM signal vector $\mathbf{X}^m$ on the mth subcarrier is given by

$$\mathbf{X}^m = \sqrt{M} \sum_{n=1}^{N_t} \mathbf{H}_n^m d_n^m + \mathbf{N}^m \tag{3.23}$$

where d_n^m denotes the mth OFDM symbol within a block transmitted by the nth antenna.

Letting $\mathbf{W}_k^m$ and b_k^m respectively denote the linear frequency-domain filter weight vector and feedback coefficient with respect to d_k^m, the equalised symbol $\tilde{d}_k^m$ for TOFDM is given by

$$\tilde{d}_k = \mathbf{W}_k^{m^H} \mathbf{X}^m + b_k^m \tag{3.24}$$

$\mathbf{W}_k^m$ and b_k^m are determined to minimise the MSE cost function defined in (3.17). It can be derived that the optimum linear filter weight vector $\mathbf{W}_k^m$ is expressed as

$$\mathbf{W}_k^m = \frac{1}{\sqrt{M}} v_k^m \mathbf{R}^{m^{-1}} \hat{\mathbf{H}}_k^m \tag{3.25}$$

where

$$\mathbf{R}^m = \sum_{n=1}^{N_t} v_n^m \hat{\mathbf{H}}_n^m \hat{\mathbf{H}}_n^{m^H} + N_0 \mathbf{I}_{N_r} \tag{3.26}$$

and $\hat{\mathbf{H}}_n^m$ denotes the estimate of $\mathbf{H}_n^m$.

The corresponding optimum feedback coefficient is given by

$$b_k^m = \mu_k^m - \sqrt{M} \mathbf{W}_k^{m^H} \left(\sum_{n=1}^{N_t} \mu_n^m \hat{\mathbf{H}}_n^m \right) \tag{3.27}$$

The resulting MSE with respect to d_k^m is expressed as

$$J_k^m = 1 - \frac{1}{(1 - v_k^m) + \frac{1}{\hat{\mathbf{H}}_k^{m^H} \mathbf{R}^{m^{-1}} \hat{\mathbf{H}}_k^m}} \tag{3.28}$$

Remark: Calculating the equaliser coefficients plays a major part in the whole computational complexity, for which TTDE and TFDE need to find the inverse of a big matrix of dimensions $FN_r \times FN_r$ and $MN_r \times MN_r$, respectively, while TOFDM needs to compute the inverse of an $N_r \times N_r$ matrix $\mathbf{R}^m (m = 0, \cdots, M-1)$ in (3.26). Since the number of multiplications required for the inverse of a size $P \times P$ matrix is in the order of P^3, TTDE and TFDE with SC transmission require much higher complexity than TOFDM with MC transmission, using a large filter length F and a large block size M. Hence, a low complexity Turbo equaliser is desired for SC MIMO systems.

3.3 Turbo Space-Frequency Equalisation (TSFE)

The iterative receiver with TSFE is depicted in the right part of Figure 3.1, which consists of a soft-input soft-output equaliser using TSFE, a Gaussian LLR estimator [44], an ECC decoder and an iterative channel estimator. The hard input iterative channel estimation and soft input iterative (Turbo) channel estimation will be investigated in Chapter 4. The equaliser output signals $\left\{\tilde{d}_n^i\right\} (n = 1, \cdots, N_t; i = 0, \cdots, M-1)$ are passed to the Gaussian LLR estimator for estimation of the extrinsic LLRs $\left\{L^E(c_{n,q}^i)\right\}$, which are obtained as in [43]. $\left\{L^E(c_{n,q}^i)\right\}$ are demultiplexed and deinterleaved to the intrinsic LLRs $\left\{L^I(c_{t,q})\right\}$, and are then input to the decoder as its *a priori* information. Both the estimate of information bit sequence $\hat{\mathbf{b}}$ and the extrinsic LLRs $\left\{L^E(c_{t,q})\right\}$ are generated by the decoder. $\left\{L^E(c_{t,q})\right\}$ are interleaved and multiplexed to the intrinsic LLRs $\left\{L^I(c_{n,q}^i)\right\}$, and are then fed back to the equaliser and channel estimator for the next iteration.

3.3.1 Symbol-wise TSFE

To detect substream $\{d_k^i\}$ $(i = 0, \cdots, M-1)$ which is transmitted from the kth $(k = 1, \cdots, N_t)$ antenna, the symbol-wise MMSE TSFE employs a symbol-wise frequency-domain linear filter for each iteration. Let $\mathbf{W}_k^{i,m}(m = 0, \cdots, M-1)$ denote a size-$N_r \times 1$ frequency-domain weight vector with respect to d_k^i on the mth frequency bin, and b_k^i denote the corresponding time-domain feedback coefficient. Letting $\mathbf{U}_k^i = vec(\mathbf{W}_k^{i,0} \cdots \mathbf{W}_k^{i,M-1})$ and $\mathbf{X} = mat(\mathbf{X}^0 \cdots \mathbf{X}^{M-1})$, the equaliser output symbol $\tilde{d}_k^i$ is given by

$$\begin{aligned} \tilde{d}_k^i &= \frac{1}{M} \sum_{m=0}^{M-1} \mathbf{W}_k^{i,m} \mathbf{X}^m e^{j2\pi mi/M} + b_k^i \\ &= \frac{1}{M} \mathbf{U}_k^i \mathbf{X} \mathbf{f}^i + b_k^i \end{aligned} \tag{3.29}$$

where

$$\mathbf{f}^i = \left[e^{j2\pi 0i/M} \cdots e^{j2\pi(M-1)i/M} \right]^T \tag{3.30}$$

In particular, $\mathbf{f}^0$ is a vector of all unit elements. Furthermore, let $\mathbf{D}_n = diag(D_n^0 \cdots D_n^{M-1})$, and $\hat{\mathbf{H}}_n = mat(\hat{\mathbf{H}}_n^0 \cdots \hat{\mathbf{H}}_n^{M-1})$, where $\hat{\mathbf{H}}_n^m (m = 0, \cdots, M-1)$ denotes the estimate of $\mathbf{H}_n^m$. As shown in Appendix A, the equaliser coefficients are derived based on the MMSE criterion, which minimises the MSE cost function

$$J_k^i = E\left| \tilde{d}_k^i - d_k^i \right|^2 \tag{3.31}$$

It can be derived that the linear weight vector $\mathbf{U}_k^i$ is expressed as

$$\mathbf{U}_k^i = \frac{\mathbf{\Omega}^{i-1} \hat{\mathbf{H}}_k \mathbf{f}^0}{1 + \frac{1-v_k^i}{M} \mathbf{f}^{0H} \hat{\mathbf{H}}_k^H \mathbf{\Omega}^{i-1} \hat{\mathbf{H}}_k \mathbf{f}^0} \tag{3.32}$$

where

$$\mathbf{\Omega}^i = \frac{1}{M}\sum_{n=1}^{N_t}\sum_{m=0}^{M-1} v_n^m \hat{\mathbf{H}}_n \mathbf{f}^{i-m}\mathbf{f}^{i-m\,H}\hat{\mathbf{H}}_n^H + N_0\mathbf{I}_{N_r M} \tag{3.33}$$

The corresponding feedback coefficient is given by

$$b_k^i = \mu_k^i - \frac{1}{M}\mathbf{U}_k^{i\,H}\left(\sum_{n=1}^{N_t}\hat{\mathbf{H}}_n E(\mathbf{D}_n)\right)\mathbf{f}^i \tag{3.34}$$

where

$$E(\mathbf{D}_n) = diag\left(E(D_n^0)\cdots E(D_n^{M-1})\right) \tag{3.35}$$

with $E(D_n^m) = \sum_{i=0}^{M-1}\mu_n^i e^{-j2\pi mi/M}(m = 0,\cdots,M-1)$ denoting the DFT of μ_n^i. The resulting equaliser output $\tilde{d}_k^i$ is:

$$\tilde{d}_k^i = \frac{1}{M}\mathbf{U}_k^{i\,H}\left(\mathbf{X} - \sum_{n=1}^{N_t}\hat{\mathbf{H}}_n E(\mathbf{D}_n)\right)\mathbf{f}^i + \frac{1}{M}\mu_k^i\mathbf{U}_k^{i\,H}\hat{\mathbf{H}}_k\mathbf{f}^0 \tag{3.36}$$

which is illustrated by the equivalent block diagram in the upper part of Figure 3.2. To detect substream $\{d_k^i\}(i = 0,\cdots,M-1)$ from the kth antenna, at a particular iteration the frequency-domain received signals are passed through a linear filter with weight vector $\mathbf{U}_k^i$ corresponding to d_k^i. Channel equalisation and interference suppression are performed using $\left\{L^I(c_{n,q}^i)\right\}$ from the previous iteration ($L^I(c_{n,q}^i) = 0$ for all n, i, q for the first iteration). The frequency-domain equalised signals are then transferred into the time domain by multiplying the ith output signal vector $\mathbf{U}_k^{i\,H}\left(\mathbf{X} - \sum_{n=1}^{N_t}\hat{\mathbf{H}}_n E(\mathbf{D}_n)\right)$ by $\mathbf{f}^i/M$. Finally, a constant $\frac{1}{M}\mu_k^i\mathbf{U}_k^{i\,H}\hat{\mathbf{H}}_k\mathbf{f}^0$ is added to the ith output branch to remove the residual interference. The resulting MSE with respect to d_k^i is given by

$$J_k^i = 1 - \frac{1}{M}\mathbf{U}_k^{i\,H}\hat{\mathbf{H}}_k\mathbf{f}^0 \tag{3.37}$$

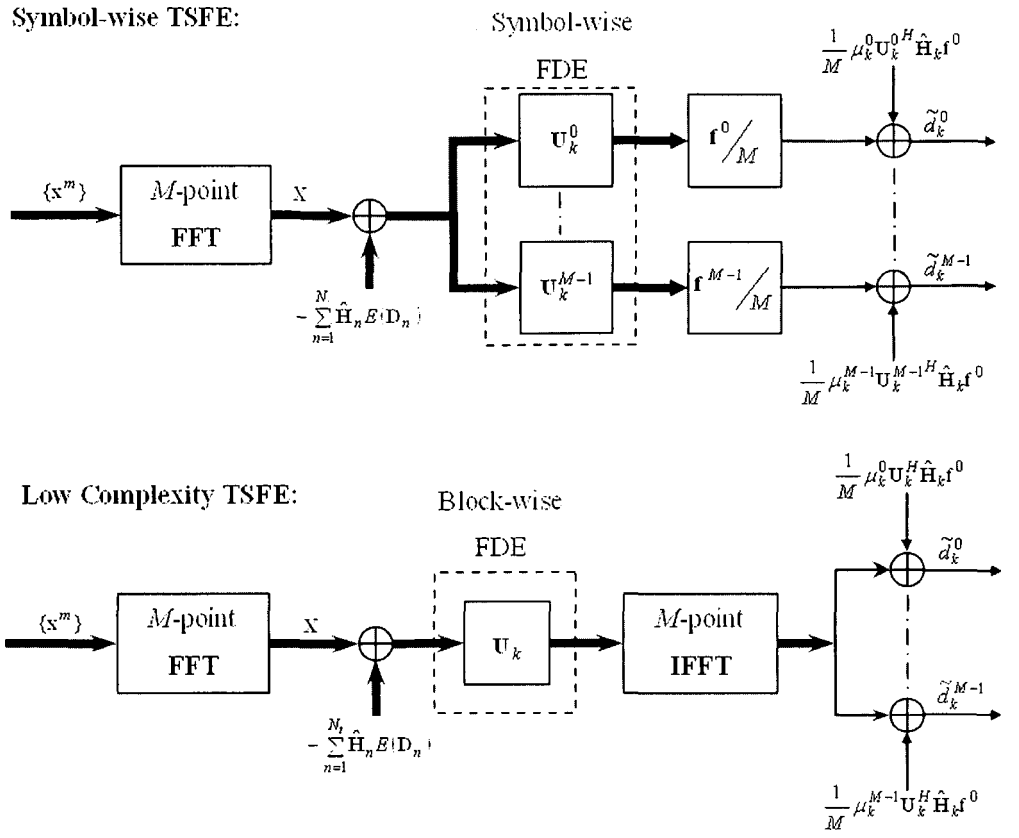

Figure 3.2: Block diagrams of the symbol-wise TSFE and block-wise low complexity TSFE at a particular iteration for detection of substream $\{d_k^i\}$ $(k = 1, \cdots, N_t; i = 0, \cdots, M-1)$.

The above procedure is repeated for substreams from different transmit antennas.

3.3.2 Low Complexity Block-wise TSFE

The frequency-domain linear filter weights of the symbol-wise TSFE in Subsection 3.3.1 are different for each symbol within a data block, and therefore requires a huge computational complexity. To reduce the computation burden, a direct and effective approach is to implement the block processing on each frequency bin independently, *i.e.*, to make $\mathbf{U}_k^i$ independent of the time index i. This can be achieved by simply replacing $v_n^i (n = 1, \cdots, N_t; i = 0, \cdots, M-1)$ in (3.32) by

$\bar{v}_n = \frac{1}{M}\sum_{i=0}^{M-1} v_n^i$, which is the average of v_n^i within a block [43]. Thus, $\mathbf{\Omega}^i$ in (3.32) reduces to a block diagonal matrix as

$$\mathbf{\Omega} = DIAG\left(\bar{\mathbf{R}}^0 \cdots \bar{\mathbf{R}}^{M-1}\right) \tag{3.38}$$

where

$$\bar{\mathbf{R}}^m = \sum_{n=1}^{N_t} \bar{v}_n \hat{\mathbf{H}}_n^m \hat{\mathbf{H}}_n^{m^H} + N_0 \mathbf{I}_{N_r} \tag{3.39}$$

As a result, $\mathbf{U}_k^i$ reduces to $\mathbf{U}_k = vec(\mathbf{W}_k^0 \cdots \mathbf{W}_k^{M-1})$, where

$$\mathbf{W}_k^m = \frac{\bar{\mathbf{R}}^{m^{-1}} \hat{\mathbf{H}}_k^m}{1 + \frac{1-\bar{v}_k}{M} \sum_{m=0}^{M-1} \hat{\mathbf{H}}_k^{m^H} \bar{\mathbf{R}}^{m^{-1}} \hat{\mathbf{H}}_k^m} \tag{3.40}$$

The resulting equaliser output $\tilde{d}_k^i$ in (3.36) can be expressed as

$$\tilde{d}_k^i = \frac{1}{M} \mathbf{U}_k^H \left(\mathbf{X} - \sum_{n=1}^{N_t} \hat{\mathbf{H}}_n E(\mathbf{D}_n) \right) \mathbf{f}^i + \frac{1}{M} \mu_k^i \mathbf{U}_k^H \hat{\mathbf{H}}_k \mathbf{f}^0 \tag{3.41}$$

This is depicted in the lower part of Figure 3.2, which proposes a new block-wise linear frequency-domain filter, rather than the symbol-wise filter for the symbol-wise TSFE, is employed, as $\mathbf{U}_k$ is independent of the time index i. The frequency-domain equalised signals are transferred back into the time domain by IFFT. Finally, a constant $\frac{1}{M}\mu_k^i \mathbf{U}_k^{i\,H} \hat{\mathbf{H}}_k \mathbf{f}^0$ is added to the ith output branch to remove the residual interference.

The resulting MSE with respect to d_k^i also becomes independent of the time index i, expressed as

$$J_k = 1 - \frac{\frac{1}{M} \sum_{m=0}^{M-1} \hat{\mathbf{H}}_k^{m^H} \bar{\mathbf{R}}^{m^{-1}} \hat{\mathbf{H}}_k^m}{1 + \frac{1-\bar{v}_k}{M} \sum_{m=0}^{M-1} \hat{\mathbf{H}}_k^{m^H} \bar{\mathbf{R}}^{m^{-1}} \hat{\mathbf{H}}_k^m} \tag{3.42}$$

Similar to TOFDM [47], the frequency-domain linear filter weights of the

block-wise TSFE are derived on each independent frequency bin. Thus, the block-wise TSFE requires a much lower complexity than the symbol-wise TSFE, as well as TTDE [47].

3.3.3 Gaussian LLR Estimation

The probability density function (PDF) of $p(\tilde{d}_n^i|d_n^i = \alpha_s) = p(\tilde{d}_n^i|\mathbf{c}_n^i = \mathbf{p}_s)(n = 1, \cdots, N_t; i = 0, \cdots, M-1)$ is assumed to be Gaussian with the mean $\mu_{n,s}^i = E(\tilde{d}_n^i|d_n^i = \alpha_s)$ and the variance $v_{n,s}^i = Cov(\tilde{d}_n^i, \tilde{d}_n^i|d_n^i = \alpha_s)$ [43], where $E(.|con)$ and $Cov(.|con)$ refer to the conditional expectation and covariance, respectively. With the symbol-wise TSFE, the statistics for d_n^i is computed as:

$$\mu_{n,s}^i = \frac{(1 - J_n^i)\,\alpha_s}{M} \tag{3.43}$$

$$v_{n,s}^i = J_n^i \left(1 - J_n^i\right) \tag{3.44}$$

For the low complexity TSFE proposed in Subsection 3.3.2, J_n^i in (3.43) and (3.44) is replaced by J_n in (3.42).

Letting $\rho_{n,s}^i = \left|\tilde{d}_n^i - \mu_{n,s}^i\right|^2 / v_{n,s}^i$, the extrinsic LLR $L^E\left(c_{n,q}^i\right)$ can be computed by the Gaussian LLR estimator as

$$\begin{aligned} L^E\left(c_{n,q}^i\right) &= ln\left[\frac{\sum_{\forall \mathbf{p}_s: p_{s,q}=1} p(\tilde{d}_n^i|\mathbf{c}_n^i = \mathbf{p}_s)\Pi_{q' \neq q} P(c_{n,q'}^i = p_{s,q'})}{\sum_{\forall \mathbf{p}_s: p_{s,q}=0} p(\tilde{d}_n^i|\mathbf{c}_n^i = \mathbf{p}_s)\Pi_{q' \neq q} P(c_{n,q'}^i = p_{s,q'})}\right] \\ &= ln\left[\frac{\sum_{\forall \mathbf{p}_s: p_{s,q}=1} exp\left(-\rho_{n,s}^i + \sum_{q' \neq q} \frac{\hat{p}_{s,q'} L^I\left(c_{n,q'}^i\right)}{2}\right)}{\sum_{\forall \mathbf{p}_s: p_{s,q}=0} exp\left(-\rho_{n,s}^i + \sum_{q' \neq q} \frac{\hat{p}_{s,q'} L^I\left(c_{n,q'}^i\right)}{2}\right)}\right] \end{aligned} \tag{3.45}$$

The extrinsic LLRs $\left\{L^E\left(c_{n,q}^i\right)\right\}$ are demultiplexed and deinterleaved to the

intrinsic LLRs $\left\{L^I\left(c_{t,q}\right)\right\}$, and are then input into the decoder as its *a priori* information, as illustrated in Figure 3.1.

3.3.4 Oversampled TSFE

Oversampling of the received signals is critical in practice, which is adopted to avoid an information loss in discretising the received signals. Assuming N_s samples per symbol period, the received signals at each receive antenna are arranged in blocks with each consisting of N_sM samples. Within each block, the mth $(m = 0, \cdots, N_sM - 1)$ sample at the lth receive antenna can be expressed as

$$x_l^m = \sum_{n=1}^{N_t} \sum_{i=0}^{N_s(N+1)-1} h_{ln}^i d_n^{m-\lfloor i/N_s \rfloor} + n_l^m \tag{3.46}$$

where h_{ln}^i denotes the ith $(i = 0, \cdots, N_s(N+1) - 1)$ sample of the continuous-time channel path gain at time instant iT/N_s between the nth transmit antenna and the lth receive antenna. The oversampled received signals are transferred into the frequency domain by FFT. The signal on the mth $(m = 0, \cdots, N_sM - 1)$ frequency bin at the lth receive antenna is still given by (3.3), where, however,

$$X_l^m = \sum_{i=0}^{N_sM-1} x_l^i e^{-j2\pi mi/(N_sM)} \tag{3.47}$$

$$H_{ln}^m = \sum_{i=0}^{N_s(N+1)-1} h_{ln}^i e^{-j2\pi mi/(N_sM)} \tag{3.48}$$

$$D_n^m = \sum_{i=0}^{M-1} d_n^i e^{-j2\pi mi/M} \tag{3.49}$$

$$N_l^m = \sum_{i=0}^{N_sM-1} n_l^i e^{-j2\pi mi/(N_sM)} \tag{3.50}$$

due to oversampling of the received signals. The frequency-domain received vector is still given by (3.8).

The symbol-spaced TSFE in Subsections 3.3.1 and 3.3.2 is extended to the oversampled TSFE, where the notations in Subsections 3.3.1 and 3.3.2 are redefined.

First define $\mathbf{X} = mat(\mathbf{X}^0 \cdots \mathbf{X}^{N_s M-1})$, $\mathbf{D}_n = diag(D_n^0 \cdots D_n^{N_s M-1})$, and $\hat{\mathbf{H}}_n = mat(\hat{\mathbf{H}}_n^0 \cdots \hat{\mathbf{H}}_n^{N_s M-1})$, where $\hat{\mathbf{H}}_n^m (m = 0, \cdots, N_s M - 1)$ denotes the estimate of $\mathbf{H}_n^m$. The frequency-domain equaliser weight vector with respect to d_k^i is denoted by $\mathbf{U}_k^i = vec(\mathbf{W}_k^{i,0} \cdots \mathbf{W}_k^{i,N_s M-1})$, where $\mathbf{W}_k^{i,m} (m = 0, \cdots, N_s M - 1)$ is a weight vector of size $N_r \times 1$ on the mth frequency bin. The equaliser output signal with respect to d_k^i is given by:

$$\tilde{d}_k^i = \frac{1}{N_s M} \mathbf{U}_k^{i\,H} \left(\mathbf{X} - \sum_{n=1}^{N_t} \hat{\mathbf{H}}_n E(\mathbf{D}_n) \right) \mathbf{f}^i \tag{3.51}$$

where $\mathbf{f}^i = \left[e^{j2\pi 0 i/(N_s M)} \cdots e^{j2\pi (N_s M-1) i/(N_s M)} \right]^T$, and $E(\mathbf{D}_n) = diag\left(E(D_n^0) \cdots E(D_n^{N_s M-1}) \right)$, with $E(D_n^m) = \sum_{i=0}^{M-1} \mu_n^i e^{-j2\pi mi/M}$ $(m = 0, \cdots, N_s M - 1)$ denoting the DFT of μ_n^i.

The equaliser coefficients are still derived based on the MMSE criterion, by minimising the MSE cost function in (3.31). The linear weight vector $\mathbf{U}_k^i$ is expressed as

$$\mathbf{U}_k^i = \frac{\mathbf{\Omega}^{i-1} \hat{\mathbf{H}}_k \mathbf{f}^0}{1 + \frac{1 - v_k^i}{N_s M} \mathbf{f}^{0H} \hat{\mathbf{H}}_k^H \mathbf{\Omega}^{i-1} \hat{\mathbf{H}}_k \mathbf{f}^0} \tag{3.52}$$

where

$$\mathbf{\Omega}^i = \frac{1}{N_s M} \sum_{n=1}^{N_t} \sum_{m=0}^{M-1} v_n^m \hat{\mathbf{H}}_n \mathbf{f}^{i-N_s m} \mathbf{f}^{i-N_s m\,H} \hat{\mathbf{H}}_n^H + N_0 \mathbf{I}_{N_s N_r M} \tag{3.53}$$

To reduce the computational burden, $\mathbf{U}_k^i$ is made independent of the time index i by replacing $v_n^i (n = 1, \cdots, N_t; i = 0, \cdots, M - 1)$ in (3.52) by $\bar{v}_n = \frac{1}{M} \sum_{i=0}^{M-1} v_n^i$,

which is the average of v_n^i within a block [43, 61]. Thus, $\mathbf{\Omega}^i$ in (3.53) reduces to a block diagonal matrix as $\mathbf{\Omega} = DIAG\left(\bar{\mathbf{R}}^0 \cdots \bar{\mathbf{R}}^{N_s M-1}\right)$, where

$$\bar{\mathbf{R}}^m = \sum_{n=1}^{N_t} \bar{v}_n \hat{\mathbf{H}}_n^m \hat{\mathbf{H}}_n^{mH} + N_0 \mathbf{I}_{N_r} \tag{3.54}$$

As a result, $\mathbf{U}_k^i$ reduces to $\mathbf{U}_k = vec(\mathbf{W}_k^0 \cdots \mathbf{W}_k^{N_s M-1})$, where

$$\mathbf{W}_k^m = \frac{\bar{\mathbf{R}}^{m-1} \hat{\mathbf{H}}_k^m}{1 + \frac{1-\bar{v}_k}{N_s M} \sum_{m=0}^{N_s M-1} \hat{\mathbf{H}}_k^{mH} \bar{\mathbf{R}}^{m-1} \hat{\mathbf{H}}_k^m} \tag{3.55}$$

It was shown in [61] that the above approximation has very little impact on performance. The resulting equaliser output $\tilde{d}_k^i$ in (3.51) can be expressed as

$$\tilde{d}_k^i = \frac{1}{N_s M} \mathbf{U}_k^H \left(\mathbf{X} - \sum_{n=1}^{N_t} \hat{\mathbf{H}}_n E(\mathbf{D}_n) \right) \mathbf{f}^i + \frac{1}{N_s M} \mu_k^i \mathbf{U}_k^H \hat{\mathbf{H}}_k \mathbf{f}^0 \tag{3.56}$$

3.4 Performance Analysis

This section provides intensive theoretical performance analysis of the symbol-spaced low complexity TSFE structure, whose performance approaches that of the symbol-wise TSFE, as can be shown in Section 3.6. As in [35, 62], appropriate analytical performance bounds are shown with given channel realisations. For simplicity, this section only investigates the BER performance before decoding, as the overall performance is dominated by Turbo equalisation instead of decoding with a relatively weak code such as the convolutional code (compared to the Turbo code). The block indexes are ignored for the simplicity of expression.

3.4.1 TSFE vs. TOFDM

Let γ_k denote the equaliser output signal to interference-and-noise ratio (SINR) with respect to the detected substream $\{d_k^i\}\,(i = 0, \cdots, M-1)$ from the kth $(k = 1, \cdots, N_t)$ transmit antenna at a particular iteration. For an unbiased MMSE filter [31], it can be shown that the output SINR is related to the MSE by $\gamma_k = 1/J_k - 1$. Without loss of generality, QPSK modulation is assumed here. Thus, the corresponding BER can be approximated by $BER_k = Q(\sqrt{\gamma_k})$ [63]. Using the Gaussian tail function and further approximations, the BER can be upperbounded by $BER_k \leq exp(-\gamma_k/2)/2$ at a high SNR [64]. Therefore, the BER for TSFE is given by

$$BER_k^{TSFE} \leq \frac{1}{2} exp\left(\frac{1}{2} \cdot \frac{\frac{1}{M}\sum_{m=0}^{M-1} \hat{\mathbf{H}}_k^{m^H} \bar{\mathbf{R}}^{m^{-1}} \hat{\mathbf{H}}_k^m}{\frac{\bar{v}_k}{M}\sum_{m=0}^{M-1} \hat{\mathbf{H}}_k^{m^H} \bar{\mathbf{R}}^{m^{-1}} \hat{\mathbf{H}}_k^m - 1}\right) \tag{3.57}$$

It is of interest to compare the performance of TSFE and its TOFDM counterpart [47], assuming the same number of iterations and the same channel estimates. At a particular iteration, the output SINR with respect to the mth OFDM symbol (or subcarrier) transmitted by the kth antenna is given by $\gamma_k^m = 1/J_k^m - 1$. The average BER of OFDM with given channel realisation is determined by averaging over all the symbols, which is bounded by:

$$\begin{aligned} BER_k^{TOFDM} &= \frac{1}{M}\sum_{m=0}^{M-1} BER_k^{m,TOFDM} \\ &\leq \frac{1}{2M}\sum_{m=0}^{M-1} exp\left(\frac{1}{2} \cdot \frac{\hat{\mathbf{H}}_k^{m^H} \mathbf{R}^{m^{-1}} \hat{\mathbf{H}}_k^m}{v_k^m \hat{\mathbf{H}}_k^{m^H} \mathbf{R}^{m^{-1}} \hat{\mathbf{H}}_k^m - 1}\right) \end{aligned} \tag{3.58}$$

Performance with a large number of iterations at a high SNR: With the increase of the number of iterations, μ_k^m approaches d_k^m, and therefore v_k^m in (3.58) approaches zero at a high SNR, *i.e.*, $v_k^0 \cong v_k^1 \cong \cdots v_k^{M-1} \cong 0$, as can be testified by

simulations. Thus, the BER of TOFDM can be approximated by

$$BER_k^{TOFDM} \cong \frac{1}{2M}\sum_{m=0}^{M-1} exp\left(-\frac{1}{2}\hat{\mathbf{H}}_k^{m^H}\mathbf{R}^{m^{-1}}\hat{\mathbf{H}}_k^m\right) \tag{3.59}$$

In this case, $v_n^0 \cong v_n^1 \cong \cdots v_n^{M-1} \cong \bar{v}_n \cong 0$, which leads to $\bar{\mathbf{R}}^m \cong \mathbf{R}^m$. Thus, the BER of TSFE can be approximated by

$$BER_k^{TSFE} \cong \frac{1}{2}exp\left(-\frac{1}{2M}\sum_{m=0}^{M-1}\left(\hat{\mathbf{H}}_k^{m^H}\mathbf{R}^{m^{-1}}\hat{\mathbf{H}}_k^m\right)\right) \tag{3.60}$$

Using $exp\left(\frac{1}{n}\sum_{i=1}^{n} x_i\right) \leq \frac{1}{n}\sum_{i=1}^{n} exp(x_i)(x_i \leq 0, \forall i)$, it can be shown that the BER of TSFE with given channel realisation is not higher than that of its TOFDM counterpart, with a large number of iterations. Thus, TSFE achieves a better average BER performance than TOFDM in frequency selective fading channels with the increase of the number of iterations. Comparing the output SINRs for TOFDM to that of TSFE, it suggests that less fluctuation of SINR is likely to yield a better average BER performance.

3.4.2 Special Case: Flat Fading Channels

In the flat fading environment (*i.e.*,N=0), the channel frequency response $\mathbf{H}_k^m (m = 0, \cdots, M-1)$ reduces to the CIR vector $\mathbf{h}_k$ of size $N_r \times 1$. Correspondingly, the BER for TOFDM is expressed as

$$BER_k^{TOFDM} \leq \frac{1}{2M}\sum_{m=0}^{M-1} exp\left(\frac{1}{2}\cdot\frac{\hat{\mathbf{h}}_k^H\mathbf{r}^{m^{-1}}\hat{\mathbf{h}}_k}{v_k^m\hat{\mathbf{h}}_k^H\mathbf{r}^{m^{-1}}\hat{\mathbf{h}}_k - 1}\right) \tag{3.61}$$

where $\hat{\mathbf{h}}_k$ denotes the estimate of $\mathbf{h}_k$, and $\mathbf{r}^m = \sum_{n=1}^{N_t} v_n^m \hat{\mathbf{h}}_n \hat{\mathbf{h}}_n^H + N_0 \mathbf{I}_{N_r}$. It can be derived that the BER of TSFE is given by

$$BER_k^{TSFE} \leq \frac{1}{2} exp\left(\frac{1}{2} \cdot \frac{\hat{\mathbf{h}}_k^H \mathbf{r}^{-1} \hat{\mathbf{h}}_k}{\bar{v}_k \hat{\mathbf{h}}_k^H \mathbf{r}^{-1} \hat{\mathbf{h}}_k - 1}\right) \tag{3.62}$$

where $\mathbf{r} = \sum_{n=1}^{N_t} \bar{v}_n \hat{\mathbf{h}}_n \hat{\mathbf{h}}_n^H + N_0 \mathbf{I}_{N_r}$.

Performance with one iteration: At the first iteration particularly, the variance of each symbol for both TSFE and TOFDM is set to be unit, *i.e.*, $v_n^0 = v_n^1 = \cdots v_n^{M-1} = 1$. Hence, both TSFE and TOFDM reduce to a linear MMSE detector and provide exactly the same performance as:

$$BER_k^{TOFDM} = BER_k^{TSFE} \leq \frac{1}{2} exp\left(\frac{1}{2} \cdot \frac{\hat{\mathbf{h}}_k^H \tilde{\mathbf{r}}^{-1} \hat{\mathbf{h}}_k}{\hat{\mathbf{h}}_k^H \tilde{\mathbf{r}}^{-1} \hat{\mathbf{h}}_k - 1}\right) \tag{3.63}$$

where $\tilde{\mathbf{r}} = \sum_{n=1}^{N_t} \hat{\mathbf{h}}_n \hat{\mathbf{h}}_n^H + N_0 \mathbf{I}_{N_r}$.

Performance with a large number of iterations at a high SNR: With the increase of the number of iterations and at a high SNR, $v_n^0 \cong v_n^1 \cong \cdots v_n^{M-1} \cong \bar{v}_n$ approach zero. As a result, $\mathbf{r}^m$ in (3.61) can be approximated by $\mathbf{r}$ in (3.62), and both (3.61) and (3.62) can be approximated by

$$BER_k^{TOFDM} \cong BER_k^{TSFE} \cong \frac{1}{2} exp\left(\frac{1}{2} \hat{\mathbf{h}}_k^H \mathbf{r}^{-1} \hat{\mathbf{h}}_k\right) \tag{3.64}$$

Hence, TSFE and TOFDM achieve similar performance with a large number of iterations at a high SNR in flat fading.

3.5 Complexity Analysis

This section first investigates the complexity of the proposed TSFE, compared to that of TTDE and TOFDM with symbol-spaced sampling. For simplicity, this section focuses on the complexity of Turbo equalisation without considering decoding, which consists of four parts: 1) complexity of FFT/IFFT (for TSFE and TOFDM only); 2) complexity of calculating the equaliser coefficients; 3) complexity of equalisation which denotes the signal processing required to generate the equalised symbols; and 4) complexity of calculating the statistics associated with the LLR, mean, and variance for each symbol. Solution of the equaliser coefficients plays a critical role in the whole complexity, for which TTDE requires approximately $F^3N_r^3/3$ complex multiplications for matrix inversion, while both the low complexity TSFE and TOFDM need to find the inverses of M $N_r \times N_r$ matrices, each requiring approximately $N_r^3/3$ complex multiplications only. This implies the complexity similarity between the low complexity TSFE and TOFDM, as well as the complexity advantage of the low complexity TSFE over its TTDE counterpart (with a large filter length F).

It should be noted that the first iteration costs less computation than each of the remaining iterations, as the initial statistics for the first iteration is already known to the receiver. The above complexity is summarised in Table 3.1 with S-ary modulation, where 1^* and R^* denote the first iteration and each of the remaining iterations, respectively.

A numerical example of the normalised overall complexity in terms of the number of complex multiplications is shown in Table 3.2, with $N_t = 4$ transmit antennas, $N_r = 4$ receive antennas, QPSK modulation ($S = 4$), overall channel memory $N = 6$, and different numbers of iterations. TSFE and TOFDM have the same configuration with a block size of $M = 64$ symbols with a CP of length

Table 3.1: Complexity per Iteration in Terms of Complex Multiplications (A-Low complexity TSFE, B-Symbol-wise TSFE, C-TOFDM, D-TTDE, $C_1 = 0.5N_tM(log_2M)$, $C_2 = 0.5N_rM(log_2M)$, S-ary modulation, N_t-Number of transmit antennas, N_r-Number of receive antennas, N-Channel memory, M-Data block size, F-Filter length for TTDE, 1*–First iteration, and R^*–each of the remaining iterations)

	FFT/ IFFT	Coefficient	Equalisation	Statistics
A-1*	$C_1 + C_2$	$N_r^3M/3 + 2N_tN_r^2M$	N_tN_rM	$N_tN_rM + N_tMP$ $+N_tP + N_t$
A-R^*	$2C_1$	$N_r^3M/3 + 2N_tN_r^2M$ $+N_tN_rM + N_tM$	$2N_tN_rM$	$N_tMP + N_tP$ $+N_t$
B-1*	$C_1 + C_2$	$N_r^3M/3 + 2N_tN_r^2M$	N_tN_rM	$N_tN_rM + N_tMP$ $+N_tP + N_t$
B-R^*	C_1	$N_r^3M^4/3 + 2N_tN_r^2M^3$ $+2N_tN_rM^2 + N_tM$	$N_t(N_r + 1)M^2$ $+N_tN_rM$	$2N_tMP + N_tP$
C-1*	C_2	$N_r^3M/3 + 2N_tN_r^2M$	N_tN_rM	$N_tN_rM + 2N_tMP$ $+N_tP$
C-R^*	0	$N_r^3M/3 + 2N_tN_r^2M$ $+N_tN_rM + N_tM$	$2N_tN_rM$	$2N_tMP + N_tP$
D-1*	0	$F^3N_r^3/3 + 2F^3N_tN_r^2$	FN_tN_rM	$FN_tN_r + N_tMP$ $+N_tP + N_t$
D-R^*	0	$F^3N_r^3/3 + 2F^3N_tN_r^2$ $+FN_tN_r + N_tM$	$2FN_tN_rN$ $+2FN_tN_rM$	$N_tMP + N_tP$ $+N_t$

N, while TTDE has a block size of $M = 128$ symbols with total $2N$ redundant symbols, where N symbols eliminate IBI, and the other N symbols are used for the filtering purpose (*i.e.*, the filter length $F = N + 1$). In this case, all the structures achieve the same spectral efficiency. The low complexity TSFE obviously requires a complexity comparable to that of TOFDM, much less than that of TTDE, especially with the increase of the number of iterations. Thanks to the block-wise processing, the low complexity TSFE with 5 iterations saves around 20000 times of complexity over the symbol-wise TSFE.

Compared to the complexities of FD-TLE [60] and TTDE [47], the complexity of the proposed oversampled TSFE are also investigated. Solution to the equaliser

Table 3.2: Normalised Complexity with $N_t = 4$ Transmit Antennas, $N_r = 4$ Receive Antennas, Channel Memory $N = 6$, QPSK modulation ($S = 4$), $M = 64$ Symbols per Block (TSFE and TOFDM)/$M = 128$ Symbols per Block (TTDE)

	1 iteration	2 iterations	5 iterations
Low complexity TSFE	1	2.1	5.4
Symbol-wise TSFE	1	27614	110450
TOFDM [47]	1.1	2.1	5.4
TTDE [47]	4.8	10.7	28.5

Table 3.3: Nomalised Complexity of TSFE, FD-TLE and TTDE with $M = 128$ Symbols per Block, $N_s = 2$ Samples per Symbol Period, $N_t = 4$ Transmit Antennas, $N_r = 4$ Receive Antennas, Channel Memory $N = 25$ and QPSK Modulation

Receiver	1 iteration	2 iterations	5 iterations
TSFE	1	2.1	5.1
FD-TLE [60]	2084	4171	10431
TTDE [47]	7.9	16.8	44.1

coefficients plays a critical role in the whole complexity, for which TSFE calculate the inverses of N_sM matrices of size $N_r \times N_r$, and therefore requires approximately $N_sMN_r^3/3$ complex multiplications. While FD-TLE performs iterative FDE by minimising the cost function which involves N_sM samples, and therefore requires approximately $N_s^3M^3N_r^3/3$ complex multiplications for matrix inversion. TTDE uses a time-domain linear filter spanning $(N + 1)$ symbol periods, and therefore the order of $N_s^3(N + 1)^3N_r^3/3$ complex multiplications are needed for calculating equaliser coefficients. A numerical example of the normalised complexity is shown in Table 3.3, with the same configuration as in Table 3.1 and Table 3.2. Thanks to block processing, the low complexity TSFE with 5 iterations saves around 2000 and 9 times of complexity over FD-TLE and TTDE, respectively.

3.6 Simulation

3.6.1 Simulation Setup

Simulation chooses a rate 1/2, memory 2 RSC encoder [7] with generator $(1 + D + D^2, 1 + D^2)$ to generate the ECC bits. The physical channel is modeled by following the exponential power delay profile [65] with a root mean squared (RMS) delay spread of σ. Both transmit and receive filters use a raised-cosine pulse with a roll-off factor of 0.35. TTDE has a filter decision delay $N_d = 1$, which is optimised using the scheme in [65]. The SNR is defined as the spatial average ratio of the received signal power to noise power. Up to 30000 simulation runs are used.

Figure 3.3-3.5 demonstrate the performance of the symbol-spaced TSFE, which uses the same configuration as in Table 3.2. With a symbol rate of 1.25 M-Baud, a default RMS delay spread of $\sigma = 1$ μs (*i.e.*, $\sigma = 1.25$ T) is used, except in Figure 3.4.

Figure 3.6 shows the performance of the oversampled TSFE, with the same setup as in Table 3.3. With and a symbol rate of 5 M-Baud, a RMS delay spread of $\sigma = 1$ μs (*i.e.*, $\sigma = 5$ T) is employed.

3.6.2 Simulation Results

Figure 3.3 demonstrates the average BER performance of the low complexity TSFE, compared to the symbol-wise TSFE, and its TOFDM and TTDE counterparts, assuming perfect CSI and no Doppler effect. It can be observed that the low complexity TSFE provides close performance to the symbol-wise TSFE, with a tremendous complexity (e.g., around 20000 times with 5 iterations). Thus, in the following, this section focuses on the low complexity TSFE which is denoted

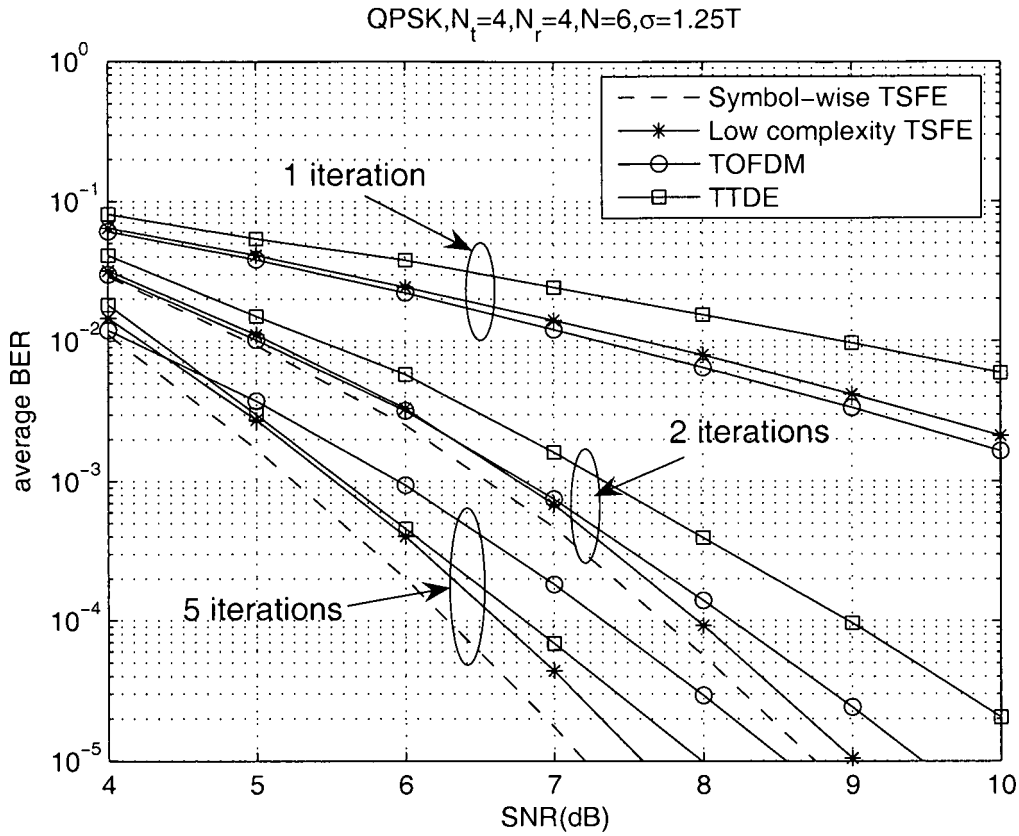

Figure 3.3: Performance of symbol-spaced TSFE, TOFDM, and TTDE with $N_t = 4$ transmit antennas, $N_r = 4$ receive antennas, RMS delay $\sigma = 1.25\ T$, and perfect CSI.

by TSFE for simplicity. Compared to TTDE, TSFE provides better performance at much lower complexity, though the performance gap decreases with the increase of the number of iterations. It can be explained that TSFE employs the whole observation block in its filter, which is much longer than the filter length of TTDE. The FDE based TSFE also outperforms TOFDM with a relatively large number of iterations. The performance gain with 5 iterations is over 1 dB at BER $= 10^{-5}$.

Figure 3.4 shows the impact of the RMS delay spread on performance of TSFE, TOFDM and TTDE at a fixed SNR = 7 dB. The horizontal axis denotes

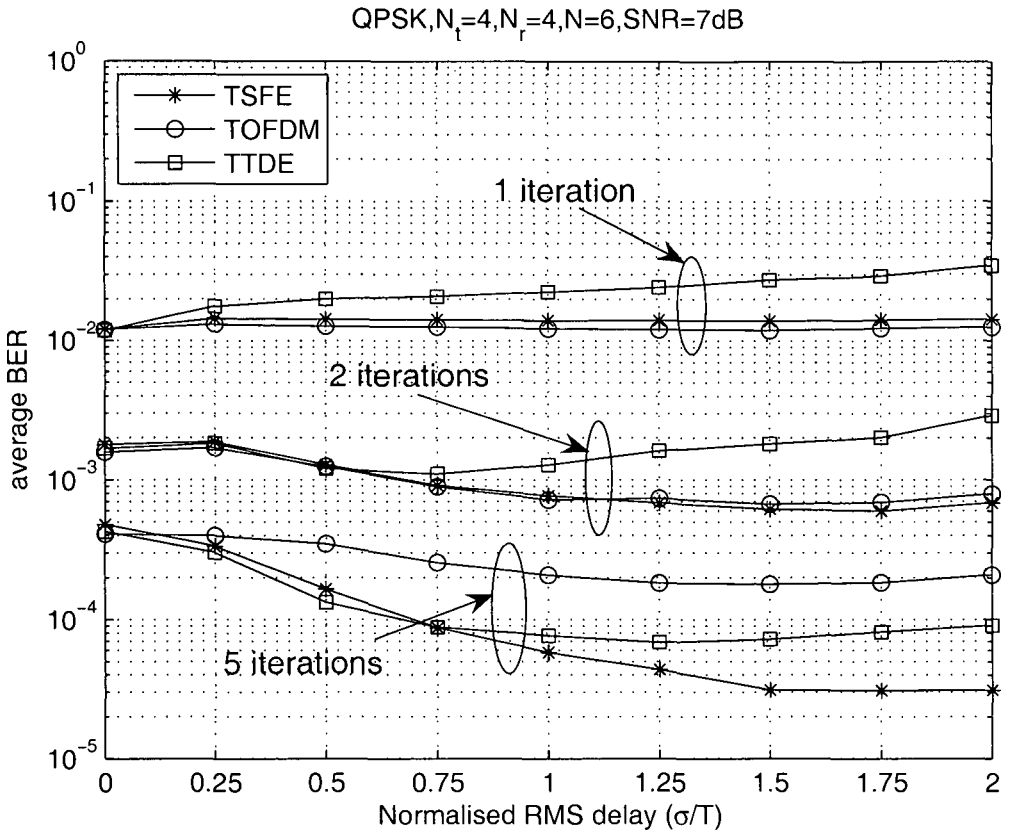

Figure 3.4: Impact of the RMS delay spread on the performance of symbol-spaced TSFE, TOFDM, and TTDE with $N_t = 4$ transmit antennas, $N_r = 4$ receive antennas, SNR = 7 dB, and perfect CSI.

the RMS delay spread normalised to the symbol period. With the same number of iterations, TSFE, TOFDM and TTDE achieve similar performance at a low RMS delay spread. With a relatively high delay spread, however, TSFE outperforms TOFDM and TTDE. This is because TSFE can capture the most multipath channel energy among all the three structures in highly dispersive channels. At a high RMS delay spread, TSFE also outperforms its flat fading case. With 5 iterations, the BER of TSFE at an RMS delay spread of $\sigma = 2\ T$ is around 17 times lower than its BER for flat fading. While TOFDM remains a relatively stable performance over different RMS delay spreads, with a BER improvement of only

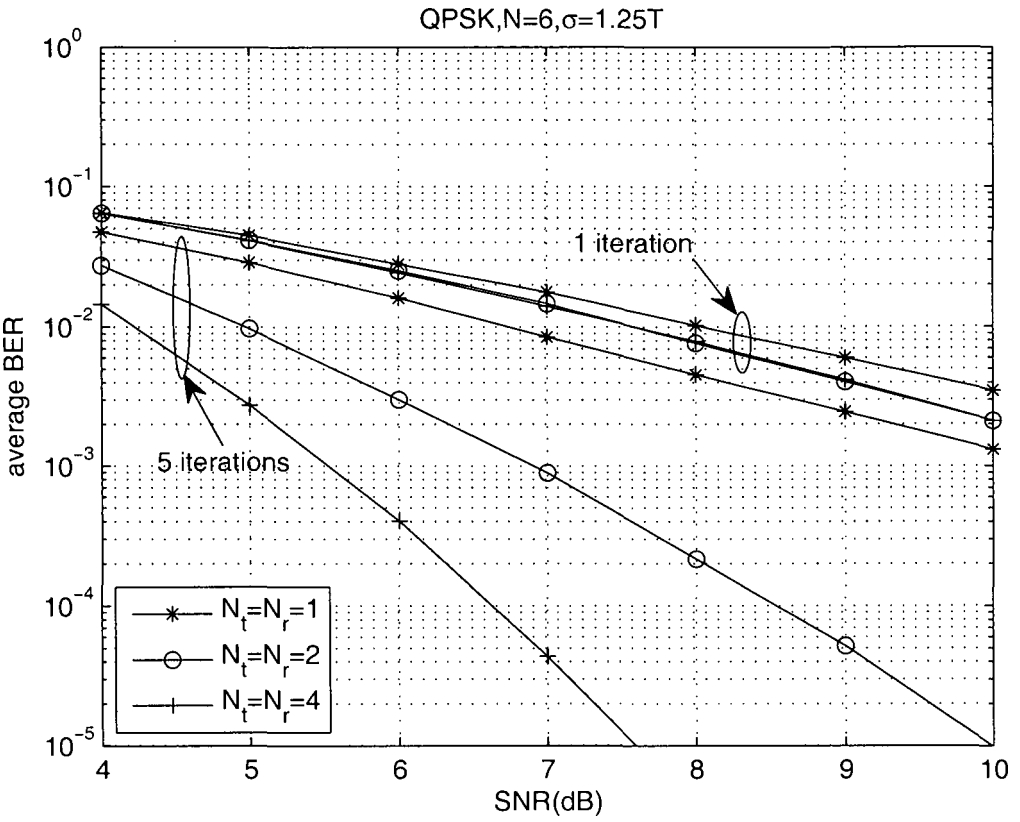

Figure 3.5: Impact of the numbers of antennas on performance of symbol-spaced TSFE with RMS delay $\sigma = 1.25\ T$, and perfect CSI.

2 times at $\sigma = 2\ T$ compared to the flat fading case with 5 iterations. Meanwhile, TTDE suffers from performance degradation in highly dispersive channels with $\sigma > T$.

Figure 3.5 shows the impact of the numbers of transmit and receive antennas on performance of TSFE, with $N_t = N_r = 1$, $N_t = N_r = 2$, and $N_t = N_r = 4$, respectively. With only one iteration, TSFE with different numbers of antennas achieve similar performance given that the numbers of transmit antennas and receive antennas are equal (*i.e.*, $N_t = N_r$), since equally likely code bits are assumed. With the increase of the number of iterations, however, the more

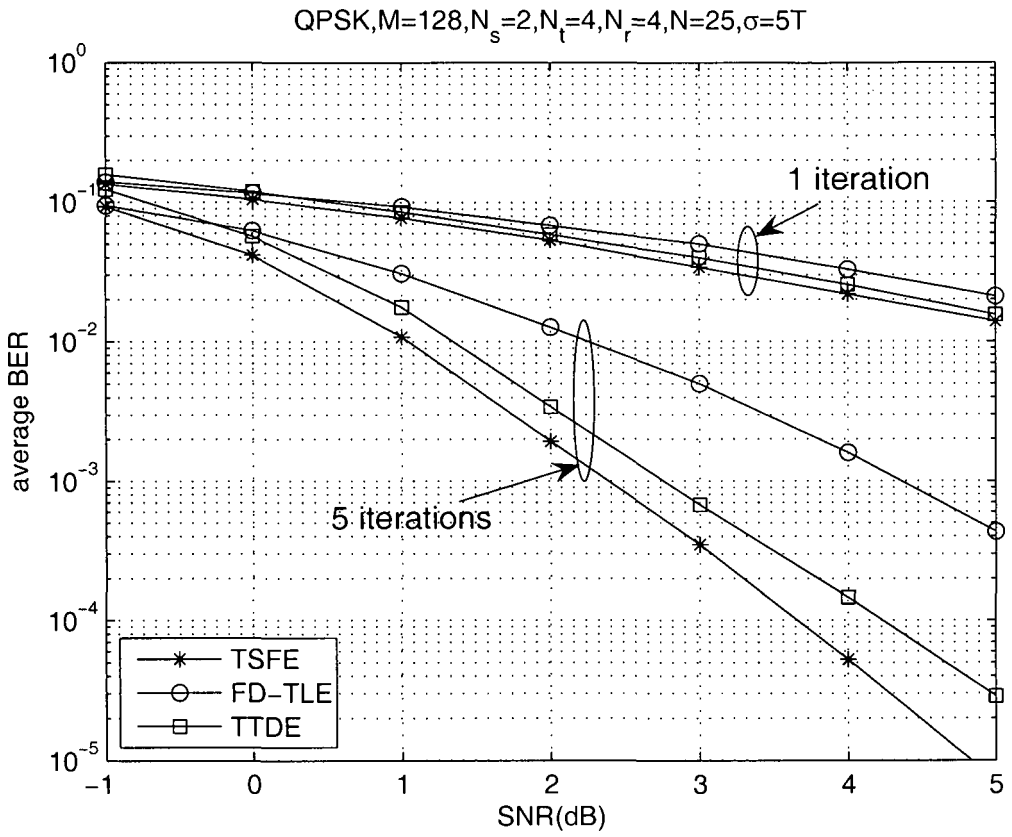

Figure 3.6: Performance of oversampled TSFE, FD-TLE, and TTDE with $M = 128$ symbols per block, $N_s = 2$ samples per symbol period, $N_t = 4$ transmit antennas, $N_r = 4$ receive antennas, RMS delay $\sigma = 5\ T$, perfect CSI and no Doppler effect.

antennas are used given $N_t = N_r$, the better the performance of TSFE is. Using 5 iterations, TSFE with $N_t = N_r = 4$ respectively achieves a performance gain of around 1.5 dB over TSFE with $N_t = N_r = 2$, and a gain of around 5 dB with $N_t = N_r = 1$, at BER $= 10^{-3}$. This is because the performance of TSFE is enhanced with the increase of the total length of the coded bit sequence $\mathbf{c}$ (proportional to the number of transmit antennas N_t), while the spatial diversity (*i.e.*, the number of receive antennas N_r) increases correspondingly. This should be compared to the conventional equalisation methods which generally suffer from

performance degradation with more transmit antennas used given $N_t = N_r$, due to the enhanced interference between substreams from different transmit antennas. It can also be observed that given $N_t = N_r$, the more antennas, the larger the impact of the number of iterations on performance. With $N_t = N_r = 1$, little performance improvement can be achieved with more iterations use. With $N_t = N_r = 4$, however, TSFE with 5 iterations can achieve a significant performance gain of more than 6 dB over the 1 iteration case at BER = 10^{-3}.

The BER performance of the oversampled TSFE is shown in Figure 3.6, assuming perfect CSI and no Doppler effect. With 5 iterations, TSFE has a performance gain of around 2 dB over FD-TLE [60] at BER = 10^{-3}, with a complexity reduction of around 2000 times over the latter as shown in Table 3.3. This is because FD-TLE utilises only the first-order statistics of signals for Turbo equalisation, while TSFE benefits from both the first-order and second-order statistics. TSFE also outperforms TTDE due to the higher frequency diversity achieved by TSFE, while requiring a complexity of around 9 times less than the latter with 5 iterations.

3.7 Summary

This chapter has proposed a low complexity adaptive TSFE structure for SC MIMO block transmission, incorporating the MMSE based frequency-domain Turbo equalisation, combining the advantages of MIMO Turbo equalisation and block processing for SC-FDE. Deriving the equaliser coefficients based on the 'average variance' technique [43, 44, 45] and performing equalisation on each frequency bin independently, the proposed block-wise low complexity TSFE achieves a significant complexity reduction over the symbol-wise TSFE, TTDE [47] and

TFDE [47] for SC MIMO systems, e.g., around 20000 and 2600 times of complexity reduction over the symbol-wise TSFE and TFDE with 5 iterations, respectively. With the same bandwidth efficiency, it provides the performance which is close to that of the symbol-wise TSFE, equal to that of TFDE, and better than that of TTDE. With a moderate code rate, it is shown both theoretically and numerically that SC TSFE achieves much better performance than its TOFDM counterpart [47] for MC systems, at a comparable complexity. The performance gains of TSFE over TTDE and TOFDM increase with the increase of channel delay spread. TSFE also significantly outperforms its flat fading case with the increase of the channel delay spread, due to the frequency diversity. Given that the number of transmit antennas is equal to the number of receive antennas, the more antennas employed, the better the performance of TSFE due to the increased spatial diversity, and the larger the impact of the number of iterations on performance. The complexity of the oversampled TSFE increases linearly with the number of samples per symbol period and the number of subcarriers, which is much lower than the complexities of FD-TLE [60] and TTDE [47].

Chapter 4

Adaptive Iterative Frequency-Domain Channel Estimation

This chapter investigates adaptive iterative channel estimation for time-varying channels, which was not considered in the previous work on Turbo equalisation for SC block transmission [43]. The hard-input frequency-domain channel estimation is an easy extension of the work in [37] to MIMO, which, however, incurs error propagation due to the inaccuracy of hard decision. Compared to hard-input channel estimation, soft-input iterative (Turbo) channel estimation makes the advantage of the likelihood information of each of the transmitted bits, which effectively mitigate the error propagation during channel estimation.

In this chapter, three categories of iterative channel estimation schemes are investigated. The first is hard-input channel estimation, which is based on the LMS and RLS criteria and utilises the hard decision in each iteration. Second, a class of Turbo frequency-domain SCE schemes, extended from the hard-input

SCE counterparts, are introduced. Third, the Kalman filtering based Turbo channel estimation and its general case of the NRLS based Turbo channel estimation are proposed. For the first and third category, an UCE and a SCE are proposed under each channel estimation criterion, (*i.e.*, LMS, RLS, Kalman filtering and NRLS).

An intensive performance analysis in terms of the MSE of the channel estimate is provided for Turbo Kalman channel estimation and Turbo NRLS channl estimation. The performance analysis of the other two categories of iterative channel estimation is not shown, since the analytical MSE is calculated using the error-covariance matrix, which are only available for Kalman based Turbo channel estimation. The complexity analysis of the hard-input channel estimation and the simplified Turbo RLS SCE (TRLS-SCE) is demonstrated, whose complexities are much lower than that of nolinear Kalman based Turbo channel estimation. Thus, the complexity analysis focuses on the hard-input channel estimation and the simplified TRLS-SCE, which both provide better tradeoff between performance and complexity than Kalman based Turbo channel estimation. Simulation results are provided to demonstrate the performance of the proposed iterative channel estimation schemes. Finally, the summary is given.

4.1 Hard-Input Iterative Channel Estimation

By extending the work in [37] to MIMO systems, this section proposes two types of hard decision based adaptive channel estimation schemes, incorporated with TSFE. One is based on the assumption of independent frequency bins, referred to as UCE. The other, referred to as SCE, utilises the correlation between adjacent frequency bins. The channel estimates can be updated based on the LMS or RLS

criterion.

Each data frame consists of a training sequence of *nTrain* blocks and a data sequence of *nData* blocks. The receiver first operates in the training mode where the training blocks are used to obtain the initial channel estimates. Let q denote the block index. In the code-aided channel estimation mode, adaptive channel estimation is based on the hard decisions, and the estimation results are passed to the next iteration of TSFE, as shown in Figure 3.1.

(3.3) can be rewritten as

$$X_l^{m(q)} = \mathbf{\Gamma}_l^{m(q)} \mathbf{D}_l^{m(q)} + N_l^{m(q)} \tag{4.1}$$

where $\mathbf{\Gamma}_l^{m(q)} = \left[H_{l1}^{m(q)} \cdots H_{lN_t}^{m\ (q)}\right]$ and $\mathbf{D}^{m(q)} = \left[D_1^{m(q)} \cdots D_{N_t}^{m\ (q)}\right]^T$. Letting $\mathbf{\Gamma}_l^{(q)} = \left[\mathbf{\Gamma}_l^{0(q)} \cdots \mathbf{\Gamma}_l^{M-1(q)}\right]$, $\mathbf{N}_l^{(q)} = \left[N_l^{0(q)} \cdots N_l^{M-1(q)}\right]$, and $\tilde{\mathbf{D}}^{(q)} = mat(\mathbf{D}^{0(q)} \cdots \mathbf{D}^{M-1(q)})$, the received signal vector $\mathbf{X}_l^{(q)} = \left[X_l^{0(q)} \cdots X_l^{M-1(q)}\right]$ with all the frequency bins can be defined as

$$\mathbf{X}_l^{(q)} = \mathbf{\Gamma}_l^{(q)} \tilde{\mathbf{D}}^{(q)} + \mathbf{N}_l^{(q)} \tag{4.2}$$

Let $\boldsymbol{\tau}_l^{(q)} = \left[h_{l1}^{0\ (q)} \cdots h_{l1}^{N(q)} \cdots h_{lN_t}^{0\ (q)} \cdots h_{lN_t}^{N\ (q)}\right]$ denote the CIR vector of length $N_t(N+1)$, with respect to the lth receive antenna. Define $\tilde{\mathbf{F}} = \left[\mathbf{F}^0 \cdots \mathbf{F}^{M-1}\right]$, where $\mathbf{F}^m = mat(\mathbf{O}^m \cdots \mathbf{O}^m)$ is an $N_t(N+1) \times N_t$ block Toeplitz matrix with $\mathbf{O}^m = \left[e^{-j2\pi 0m/M} \cdots e^{-j2\pi Nm/M}\right]^T$. Thus, $\mathbf{\Gamma}_l^{(q)}$ can be expressed as:

$$\mathbf{\Gamma}_l^{(q)} = \boldsymbol{\tau}_l^{(q)} \tilde{\mathbf{F}} \tag{4.3}$$

Then,

$$\mathbf{X}_l^{(q)} = \boldsymbol{\tau}_l^{(q)} \tilde{\mathbf{F}} \tilde{\mathbf{D}}^{(q)} + \mathbf{N}_l^{(q)} \tag{4.4}$$

4.1.1 LMS Unstructured Channel Estimation (LMS-UCE)

LMS-UCE channel estimation aims to minimise

$$J(\hat{\mathbf{\Gamma}}_l^{(q)}) = E\left\{\|\mathbf{X}_l^{(q)} - \mathbf{\Gamma}_l^{(q)}\tilde{\mathbf{D}}^{(q)}\|^2\right\}(l = 1, \cdots, N_r) \tag{4.5}$$

with respect to $\hat{\mathbf{\Gamma}}_l^{(q)}$ that is the estimate of $\mathbf{\Gamma}_l^{(q)}$. This produces

$$\hat{\mathbf{\Gamma}}_l^{(q)} = \hat{\mathbf{\Gamma}}_l^{(q-1)} + \mu \mathbf{e}_l^{(q)}\tilde{\mathbf{D}}^{(q)H} \tag{4.6}$$

where μ is the step size, and

$$\mathbf{e}_l^{(q)} = \mathbf{X}_l^{(q)} - \hat{\mathbf{\Gamma}}_l^{(q-1)}\tilde{\mathbf{D}}^{(q)} \tag{4.7}$$

4.1.2 RLS Unstructured Channel Estimation (RLS-UCE)

RLS-UCE aims at minimising the cost function

$$J(\hat{\mathbf{\Gamma}}_l^{(q)}) = \sum_{i=0}^{q} \lambda^{q-i}\|\mathbf{X}_l^{(i)} - \mathbf{\Gamma}_l^{(q)}\tilde{\mathbf{D}}^{(i)}\|^2(l = 1, \cdots, N_r) \tag{4.8}$$

with respect to $\hat{\mathbf{\Gamma}}_l^{(q)}$, where λ is the forgetting factor. $\hat{\mathbf{\Gamma}}_l^{(q)}$ is updated by the recursive equation

$$\hat{\mathbf{\Gamma}}_l^{(q)} = \hat{\mathbf{\Gamma}}_l^{(q-1)} + \mathbf{e}_l^{(q)}\tilde{\mathbf{D}}^{(q)H}\mathbf{G}^{(q)} \tag{4.9}$$

where $\mathbf{e}_l^{(q)}$ is defined in (4.7), and

$$\mathbf{G}^{(q)} = DIAG\left(\mathbf{G}^{0(q)} \cdots \mathbf{G}^{M-1(q)}\right) \tag{4.10}$$

is a block diagonal matrix with $\mathbf{G}^{m(q)}$ is given by

$$\mathbf{G}^{m(q)} = \frac{\mathbf{S}^{m(q)}}{\lambda + \mathbf{G}^{m(q)^H}\mathbf{S}^{m(q)}\mathbf{D}^{m(q)}} \tag{4.11}$$

where $\mathbf{S}^{m(q)}$ satisfies the following recursion

$$\mathbf{S}^{m(q+1)} = \lambda^{-1}\mathbf{S}^{m(q)}\left[\mathbf{I}_{N_t} - \mathbf{D}^{m(q)}\mathbf{D}^{m(q)^H}\mathbf{G}^{m(q)}\right] \tag{4.12}$$

Note that $\mathbf{G}^{m(q)}$ and $\mathbf{S}^{m(q)}$ are independent of index l, implying that they are the same for all the receive antennas.

4.1.3 LMS Structured Channel Estimation (LMS-SCE)

The cost function of LMS-SCE is given by

$$J(\hat{\boldsymbol{\tau}}_l^{(q)}) = E\left\{\|\mathbf{X}_l^{(q)} - \hat{\boldsymbol{\tau}}_l^{(q)}\tilde{\mathbf{F}}\tilde{\mathbf{D}}^{(q)}\|^2\right\}(l = 1, \cdots, N_r) \tag{4.13}$$

with respect to $\hat{\boldsymbol{\tau}}_l^{(q)}$ that is the estimate of $\boldsymbol{\tau}_l^{(q)}$. This produces

$$\hat{\boldsymbol{\tau}}_l^{(q)} = \hat{\boldsymbol{\tau}}_l^{(q-1)} + \mu\mathbf{e}_l^{(q)}\tilde{\mathbf{D}}^{(q)^H}\tilde{\mathbf{F}}^H \tag{4.14}$$

4.1.4 RLS Structured Channel Estimation (RLS-SCE)

The objective of RLS-SCE is to minimise the cost function

$$J(\hat{\boldsymbol{\Gamma}}_l^{(q)}) = \sum_{i=0}^{q}\lambda^{q-i}\|\mathbf{X}_l^{(i)} - \hat{\boldsymbol{\tau}}_l^{(q)}\tilde{\mathbf{F}}\tilde{\mathbf{D}}^{(i)}\|^2(l = 1, \cdots, N_r) \tag{4.15}$$

This requires prohibitive complexity as no recursion can be used to compute the inverse of a matrix. However, RLS-SCE will be investigated in Section 4.2 as

a part of TRLS-SCE channel estimation, which helps improved the convergence speed.

The channel estimation accuracy can be measured by the normalised MSE between the channel frequency response $\mathbf{\Gamma}_l^{(q)}$ and its estimate $\hat{\mathbf{\Gamma}}_l^{(q)}$ for each block, expressed as:

$$MSE^{(q)} = \frac{\sum_{l=1}^{N_r} E\|\hat{\mathbf{\Gamma}}_l^{(q)} - \mathbf{\Gamma}_l^{(q)}\|^2}{\sum_{l=1}^{N_r} E\|\mathbf{\Gamma}_l^{(q)}\|^2} \tag{4.16}$$

4.1.5 Complexity Analysis

Table 4.1: Complexity of Hard-Input Adaptive Channel Estimation for TSFE per Iteration

Channel estimation	Symbolic complexity $C_1 = 0.5N_tM(log_2M)$	Normalised complexity $N_t = N_r = 4, M = 64$
LMS-UCE	$C_1 + 2N_tN_rM$	1
RLS-UCE	$C_1 + 2N_tN_rM + N_t^3M$ $+N_t^2N_rM + 3N_t^2M + N_tM$	5.1
LMS-SCE	$C_1 + 2N_tN_rM + 2N_rC_1$	3.2

The complexity required by the hard-input channel estimation is investigated. The complexity of LMS-UCE, RLS-UCE and LMS-SCE for each iteration is shown in Table 4.1, both symbolically and numerically (with $N_t = N_r = 4$ antennas and a block size of $M = 64$). It can be seen that LMS-UCE requires the least complexity and RLS-UCE requires the most complexity.

4.2 Soft-Input Iterative (Turbo) Channel Estimation

This section investigates adaptive soft-input iterative (Turbo) frequency-domain channel estimation for MIMO SC-FDE, which is an extension of hard-input iterative channel estimation in Section 4.1. Compared to Turbo time-domain channel

estimation [57] which is performed on each symbol, the proposed Turbo frequency-domain channel estimation is performed on each block, and its complexity for each block is comparable to the complexity of the former algorithm for each symbol, thanks to the FFT and IFFT. Compared to Turbo frequency-domain channel estimation for MC systems [66], the proposed channel estimation scheme for SC systems is performed on each independent block instead of hundreds of blocks. Therefore, the proposed Turbo frequency-domain channel estimation for SC systems requires a much lower complexity than both Turbo time-domain channel estimation [57] and Turbo frequency-domain channel estimation for MC systems [66]. It is also incorporated with a low complexity oversampled TSFE structure, where oversampling of the received signals is employed to prevent the loss of useful energy. The complexity of TSFE increases linearly with the number of samples per block, and is much lower than the complexities of TTDE [47] and FD-TLE [60], which increase nonlinearly with the number of samples per block. In particular, a simplified TRLS-SCE channel estimation algorithm is proposed, which provides nearly the same performance as TRLS-SCE, with a tremendous complexity reduction. In the scenario of PSK modulations, the simplified TRLS-SCE requires the same complexity as TLMS-SCE. The simplified TRLS-SCE requires a low training overhead to achieve a performance comparable to the case with perfect CSI.

The proposes adaptive Turbo frequency-domain channel estimation is incorporated with the oversampled TSFE in Chapter 3. All the elements perform in the frequency domain. Assume that each data frame consists of a training sequence of $nTrain$ blocks and a data sequence of $nData$ blocks, and all blocks are synchronised. The receiver first operates in the training mode to obtain the initial channel estimates. Letting q denote the block index, in the code-aided

channel estimation mode, Turbo channel estimation is based on the soft decisions $E(D_n^{m(q)})$ on the LLRs of signals from each iteration, and the estimates are passed to the next iteration of TSFE.

Define $\mathbf{\Gamma}_l^{(q)} = \left[\mathbf{\Gamma}_l^{0(q)} \cdots \mathbf{\Gamma}_l^{N_sM-1(q)}\right]$, where $\mathbf{\Gamma}_l^{m(q)} = \left[H_{l1}^{m(q)} \cdots H_{lN_t}^{m(q)}\right] (l = 1, \cdots, N_r; m = 0, \cdots, M-1)$ denotes the channel frequency response vector with respect to the lth receive antenna and the mth frequency bin that consists of elements from all transmit antennas. Let $\boldsymbol{\tau}_l^{(q)} = \left[h_{l1}^{0\,(q)} \cdots h_{l1}^{N_s(N+1)-1\,(q)} \cdots h_{lN_t}^{0\,(q)} \cdots h_{lN_t}^{N_s(N+1)-1(q)}\right]$ denote the CIR vector of length $N_tN_s(N+1)$, with respect to the lth receive antenna. Also define $\tilde{\mathbf{F}} = \left[\mathbf{F}^0 \cdots \mathbf{F}^{N_sM-1}\right]$, where $\mathbf{F}^m = mat(\mathbf{O}^m \cdots \mathbf{O}^m)$ is an $N_tN_s(N+1) \times N_t$ block Toeplitz matrix with $\mathbf{O}^m = \left[e^{-j2\pi 0m/(N_sM)} \ldots e^{-j2\pi[N_s(N+1)-1]m/(N_sM)}\right]^T$. Thus, $\mathbf{\Gamma}_l^{(q)}$ can be expressed as:

$$\mathbf{\Gamma}_l^{(q)} = \boldsymbol{\tau}_l^{(q)} \tilde{\mathbf{F}} \tag{4.17}$$

Let $\tilde{\mathbf{D}}^{(q)} = mat(\mathbf{D}^{0(q)} \cdots \mathbf{D}^{N_sM-1(q)})$, where $\mathbf{D}^{m(q)} = \left[D_1^{m(q)} \cdots D_{N_t}^{m\,(q)}\right]^T$, $\mathbf{X}_l^{(q)} = \left[X_l^{0(q)} \cdots X_l^{N_sM-1(q)}\right]$, $\mathbf{N}_l^{(q)} = \left[N_l^{0(q)} \cdots N_l^{N_sM-1(q)}\right]$. Then, it is obtained that

$$\mathbf{X}_l^{(q)} = \boldsymbol{\tau}_l^{(q)} \tilde{\mathbf{F}} \tilde{\mathbf{D}}^{(q)} + \mathbf{N}_l^{(q)} \tag{4.18}$$

The channel estimation accuracy can be measured by (4.16).

4.2.1 Turbo LMS Structured Channel Estimation (TLMS-SCE)

TLMS-SCE channel estimation is first investigated, which is an extension of the hard-input LMS-SCE channel estimation in the last section. In the training mode,

TLMS-SCE channel estimation is to minimise:

$$J(\hat{\boldsymbol{\tau}}_l^{(q)}) = E\left\{\|\mathbf{X}_l^{(q)} - \hat{\boldsymbol{\tau}}_l^{(q)}\tilde{\mathbf{F}}\tilde{\mathbf{D}}^{(q)}\|^2\right\} (l = 1, \cdots, N_r) \tag{4.19}$$

with respect to $\hat{\boldsymbol{\tau}}_l^{(q)}$ that is the estimate of $\boldsymbol{\tau}_l^{(q)}$. This produces

$$\hat{\boldsymbol{\tau}}_l^{(q)} = \hat{\boldsymbol{\tau}}_l^{(q-1)} + \mu \mathbf{e}_l^{(q)} \tilde{\mathbf{D}}^{(q)^H} \tilde{\mathbf{F}}^H \tag{4.20}$$

where μ is the step size, and

$$\mathbf{e}_l^{(q)} = \mathbf{X}_l^{(q)} - \hat{\boldsymbol{\tau}}_l^{(q-1)}\tilde{\mathbf{F}}\tilde{\mathbf{D}}^{(q)} \tag{4.21}$$

In the code-aided channel estimation mode, the cost function is still given by (4.19) and its solution is given by:

$$\hat{\boldsymbol{\tau}}_l^{(q)} = \hat{\boldsymbol{\tau}}_l^{(q-1)} + \mu \bar{\mathbf{e}}_l^{(q)} E(\tilde{\mathbf{D}}^{(q)})^H \tilde{\mathbf{F}}^H \tag{4.22}$$

where $E(\tilde{\mathbf{D}}^{(q)}) = mat(E(\mathbf{D}^{0(q)}) \cdots E(\mathbf{D}^{N_s M-1(q)}))$ with $E(\mathbf{D}^{m(q)}) = \left[E(D_1^{m(q)}) \cdots E(D_{N_t}^{m(q)})\right]^T$, and $\bar{\mathbf{e}}_l^{(q)}$ is given by

$$\bar{\mathbf{e}}_l^{(q)} = \mathbf{X}_l^{(q)} - \hat{\boldsymbol{\tau}}_l^{(q-1)}\tilde{\mathbf{F}} E(\tilde{\mathbf{D}}^{(q)}) \tag{4.23}$$

4.2.2 Turbo RLS Structured Channel Estimation (TRLS-SCE)

To enhance the convergence behavior of channel estimation, TRLS-SCE channel estimation is investigated, which aims to minimise the following cost function in

the training mode:

$$J(\hat{\boldsymbol{\tau}}_l^{(q)}) = \sum_{i=1}^{q} \lambda^{q-i} \|\mathbf{X}_l^{(i)} - \hat{\boldsymbol{\tau}}_l^{(q)} \tilde{\mathbf{F}} \tilde{\mathbf{D}}^{(i)}\|^2 (l = 1, \cdots, N_r) \tag{4.24}$$

with respect to $\hat{\boldsymbol{\tau}}_l^{(q)}$. λ denotes the forgetting factor. The solution to $\hat{\boldsymbol{\tau}}_l^{(q)}$ is given by

$$\hat{\boldsymbol{\tau}}_l^{(q)} = \boldsymbol{\Psi}_l^{(q)^H} \boldsymbol{\Phi}^{(q)^{-1}} \tag{4.25}$$

where

$$\boldsymbol{\Phi}^{(q)} = \lambda \boldsymbol{\Phi}^{(q-1)} + \tilde{\mathbf{F}} \tilde{\mathbf{D}}^{(q)} \tilde{\mathbf{D}}^{(q)^H} \tilde{\mathbf{F}}^H \tag{4.26}$$

$$\boldsymbol{\Psi}_l^{(q)} = \lambda \boldsymbol{\Psi}_l^{(q-1)} + \tilde{\mathbf{F}} \tilde{\mathbf{D}}^{(q)} \mathbf{X}_l^{(q)^H} \tag{4.27}$$

In the code-aided channel estmation mode, the cost function is given by

$$J(\hat{\boldsymbol{\tau}}_l^{(q)}) = \sum_{i=1}^{q} \lambda^{q-i} E\left\{ \|\mathbf{X}_l^{(i)} - \hat{\boldsymbol{\tau}}_l^{(q)} \tilde{\mathbf{F}} \tilde{\mathbf{D}}^{(i)}\|^2 \right\} (l = 1, \cdots, N_r) \tag{4.28}$$

The solution to $\hat{\boldsymbol{\tau}}_l^{(q)}$ is still given by (4.25) with

$$\boldsymbol{\Phi}^{(q)} = \lambda \boldsymbol{\Phi}^{(q-1)} + \tilde{\mathbf{F}} E\left(\tilde{\mathbf{D}}^{(q)} \tilde{\mathbf{D}}^{(q)^H} \right) \tilde{\mathbf{F}}^H \tag{4.29}$$

$$\boldsymbol{\Psi}_l^{(q)} = \lambda \boldsymbol{\Psi}_l^{(q-1)} + \tilde{\mathbf{F}} \left(E\left(\tilde{\mathbf{D}}^{(q)} \tilde{\mathbf{D}}^{(q)^H} \right) \tilde{\mathbf{F}}^H \hat{\boldsymbol{\tau}}_l^{(q-1)^H} + E(\tilde{\mathbf{D}}^{(q)}) \bar{\mathbf{e}}_l^{(q)^H} \right) \tag{4.30}$$

The derivation of TRLS-SCE channel estimation in the code-aided channel estimation mode is shown in the Appendix D.

The above TRLS-SCE channel estimation can be simplified by assuming that $E\left(\tilde{\mathbf{D}}^{(q)} \tilde{\mathbf{D}}^{(q)^H} \right)$ in (4.29) and (4.30) is a diagonal matrix, since the off-diagonal elements in $E\left(\tilde{\mathbf{D}}^{(q)} \tilde{\mathbf{D}}^{(q)^H} \right)$ average out to zero so long as λ is close to 1 [57]. In the scenario of PSK modulations, $E\left(\tilde{\mathbf{D}}^{(q)} \tilde{\mathbf{D}}^{(q)^H} \right) \simeq M \mathbf{I}_{N_s N_t M}$, regardless of the

LLRs. Hence, (4.29) and (4.30) respectively reduce to:

$$\mathbf{\Phi}^{(q)} \simeq \frac{M}{1-\lambda}\tilde{\mathbf{F}}\tilde{\mathbf{F}}^{H} \simeq \frac{N_s M^2}{1-\lambda}\mathbf{I}_{\mathbf{N_s N_t(N+1)}} \tag{4.31}$$

$$\mathbf{\Psi}_l^{(q)} \simeq \lambda \mathbf{\Psi}_l^{(q-1)} + \tilde{\mathbf{F}}\left(M\tilde{\mathbf{F}}^{H}\hat{\boldsymbol{\tau}}_l^{(q-1)^H} + E(\tilde{\mathbf{D}}^{(q)})\bar{\mathbf{e}}_l^{(q)^H}\right) \tag{4.32}$$

Using (4.25), (4.31) and (4.32), it is found that

$$\hat{\boldsymbol{\tau}}_l^{(q)} = \hat{\boldsymbol{\tau}}_l^{(q-1)} + \frac{1-\lambda}{N_s M^2}\bar{\mathbf{e}}_l^{(q)} E(\tilde{\mathbf{D}}^{(q)})^H \tilde{\mathbf{F}}^H \tag{4.33}$$

Comparing (4.22) with (4.33), it can be deduced that with PSK modulations the simplified TRLS-SCE channel estimation reduces to TLMS-SCE channel estimation. For non-PSK modulations, $E\left(\tilde{\mathbf{D}}^{(q)}\tilde{\mathbf{D}}^{(q)^H}\right) \simeq M\mathbf{I}_{N_s N_t M}$ does not hold any more, however, the assumption that $E\left(\tilde{\mathbf{D}}^{(q)}\tilde{\mathbf{D}}^{(q)^H}\right)$ is a diagonal matrix still helps reduce the complexity of TRLS-SCE channel estimation.

4.2.3 Complexity Analysis

The normalised complexity of the proposed simplified TRLS-SCE channel estimation (which is equivalent to TLMS-SCE channel estimation in the code-aided channel estimation mode) in terms of the number of complex multiplications used for a data frame (which accounts for the training mode and code-aided channel estimation mode) is demonstrated, compared to the complexities of the standard TRLS-SCE channel estimation. The updates of $\mathbf{\Phi}^{(q)}$ in (4.29) and $\mathbf{\Psi}_l^{(q)}$ in (4.30) account for the most complexity of the TRLS-SCE channel estimation. Compared to standard TRLS-SCE channel estimation whose complexity is on the order of M^3, the simplified TRLS-SCE channel estimation has a complexity on the order of M due to the assumption that $E\left(\tilde{\mathbf{D}}^{(q)}\tilde{\mathbf{D}}^{(q)^H}\right)$ in (4.29) and (4.30) is diagonal.

It is demonstrated that the simplified TRLS-SCE channel estimation achieves a complexity reduction of 33 times over TRLS-SCE channel estimation.

4.3 Kalman Filtering based Turbo Channel Estimation

This section investigates adaptive Turbo channel estimation for MIMO SC-FDE systems, based on the Kalman filtering and NRLS criteria. Two types of channel estimation schemes are proposed under each criterion: 1) UCE which operates on each frequency bin independently; 2) SCE which exploits the correlation between adjacent frequency bins. This work is different in three aspects. Firstly, to the best of the knowledge, this is the first work to investigate the Kalman based Turbo channel estimation for SC-FDE systems using the wide-sense stationary (WSS) uncorrelated scattering (US) channel model. Secondly, the NRLS based Turbo channel estimation schemes are developed for channels where the state space model for Turbo Kalman channel estimation is not guaranteed. Thirdly, a MIMO SC-FDE system is considered, where the proposed Turbo channel estimation schemes are incorporated with low complexity Turbo space-frequency equalisation (TSFE) [61]. Simulation results show that the Turbo SCE schemes provide a better BER performance than their Turbo UCE counterparts, and a close performance to the case with perfect CSI. This section provides an intensive performance analysis of the Turbo SCE schemes in terms of the MSE, which is a good match with the numerical results. The impacts of Doppler spreads, RMS delay spreads and SNRs on the performance of the Turbo SCE schemes are also shown in simulation results.

This section first proposes Turbo Kalman channel estimation and Turbo NRLS

channel estimation, each of which include UCE and SCE. In particular, the performance analysis of SCE is provided, since the SCE schemes outperform their UCE counterparts.

4.3.1 Turbo Kalman Channel Estimation

This section proposes Turbo channel estimation based on the Kalman filtering criterion, where two channel estimation schemes, UCE and SCE are proposed. UCE only estimates the channel response on each frequency bin independently, and SCE estimates the time-domain CIR which exploits the inherent correlation between adjacent frequency bins. The Turbo UCE and SCE schemes require a comparable complexity.

A training sequence of *nTrain* blocks and a data sequence of *nData* blocks constitute a frame, and all blocks are assumed synchronous. The receiver first operates in the training mode to obtain the initial channel estimates. Letting q denote the block index, in the code-aided channel estimation mode, Turbo channel estimation is performed by using the soft decisions $E(D_n^{m(q)})$ on the LLRs of signals from each iteration, and the estimates are passed to the next iteration of TSFE.

The notations in Section 4.1 are kept to derive the proposed channel estimation schemes.

Corresponding to the frequency-domain received signal vector $\mathbf{X}_l^{(q)}$ in (4.2), the time-domain vector counterpart $\mathbf{x}_l^{(q)} = \left[x_l^{0(q)} \cdots x_l^{M-1(q)}\right]$ is given by

$$\mathbf{x}_l^{(q)} = \boldsymbol{\tau}_l^{(q)} \tilde{\mathbf{d}}^{(q)} + \mathbf{n}_l^{(q)} \tag{4.34}$$

where $\tilde{\mathbf{d}}^{(q)} = \left[\mathbf{d}^{0(q)} \cdots \mathbf{d}^{M-1(q)}\right]$ with $\mathbf{d}^{i(q)} = \left[d_1^{i-N(q)} \cdots d_1^{i(q)} \cdots d_{N_t}^{i-N(q)} \cdots d_{N_t}^{i(q)}\right]^H$,

and $\mathbf{n}^{(q)} = \left[n_l^{0(q)} \cdots n_l^{M-1(q)}\right]$.

4.3.1.1 Turbo Kalman Unstructured Channel Estimation (TK-UCE)

TK-UCE is constructed based on the following frequency-domain state space model:

$$\mathbf{\Gamma}_l^{(q)} = \mathbf{\Gamma}_l^{(q-1)}\mathbf{Q}_l + \mathbf{\Delta}_l^{(q)} \tag{4.35}$$

where $\mathbf{Q}_l (l = 1, \cdots, N_r)$ denotes the frequency-domain state transition matrix of size $N_tM \times N_tM$ with respect to the lth $(l = 1, \cdots, N_r)$ receive antenna, and $\mathbf{\Delta}_l^{(q)}$ of size $1 \times N_tM$ denotes the frequency-domain noise vector with a zero mean and the auto-correlation matrix $\mathbf{V}_l = E\left(\mathbf{\Delta}_l^{(q)^H}\mathbf{\Delta}_l^{(q)}\right)$. Assuming no correlation between adjacent frequency bins of the channel response, both $\mathbf{Q}_l$ and $\mathbf{V}_l$ become diagonal.

In the code-aided channel estimation mode, $D_n^{m(q)} (n = 1, \cdots, N_t; m = 0, \cdots, M-1)$ is regarded as the noisy observation of $E(D_n^{m(q)})$, *i.e.*,

$$D_n^{m(q)} = E(D_n^{m(q)}) + \gamma_n^{m(q)} \tag{4.36}$$

where $\gamma_n^{m(q)}$ denotes the noise with a zero mean and a variance of $\sum_{i=0}^{M-1} v_n^{i\,(q)}$. Substituting (4.36) into (4.2) yields

$$\mathbf{X}_l^{(q)} = \mathbf{\Gamma}_l^{(q)} E(\tilde{\mathbf{D}}^{(q)}) + \mathbf{G}_l^{(q)} \tag{4.37}$$

$$\mathbf{G}_l^{(q)} = \mathbf{\Gamma}_l^{(q)} \tilde{\boldsymbol{\gamma}}^{(q)} + \mathbf{N}_l^{(q)} \tag{4.38}$$

where $\mathbf{G}_l^{(q)} = \left[G_l^{0(q)} \cdots G_l^{M-1(q)}\right]$ denotes the frequency-domain colored noise vector, $\tilde{\boldsymbol{\gamma}}^{(q)} = mat(\boldsymbol{\gamma}^{0(q)} \cdots \boldsymbol{\gamma}^{M-1(q)})$, with $\boldsymbol{\gamma}^{m(q)} = \left[\gamma_1^{m(q)} \cdots \gamma_{N_t}^{m\,(q)}\right]^T$, and $E(\tilde{\mathbf{D}}^{(q)}) = mat(E(\mathbf{D}^{0(q)}) \cdots E(\mathbf{D}^{M-1(q)}))$ with $E(\mathbf{D}^{m(q)}) = \left[E(D_1^{m(q)}) \cdots E(D_{N_t}^{m\,(q)})\right]^T$.

Let $c_l^{m(q)}(l = 1, \cdots, N_r; m = 0, \cdots, M-1)$ denote the variance of $G_l^{m(q)}$, which is given by

$$c_l^{m(q)} = tr\left[diag\left(\sum_{i=0}^{M-1} v_1^{i(q)}, \cdots, \sum_{i=0}^{M-1} v_{N_t}^{i\ (q)}\right) E\left(\mathbf{\Gamma}_l^{m(q)^H} \mathbf{\Gamma}_l^{m(q)}\right)\right] + MN_0 \quad (4.39)$$

After some mathematical derivation, the covariance matrix $\mathbf{C}_l^{(q)}$ of the frequency-domain noise vector $\mathbf{G}_l^{(q)}$ is expressed as:

$$\mathbf{C}_l^{(q)} = diag\left(c_l^{0(q)} \cdots c_l^{M-1(q)}\right) \quad (4.40)$$

To obtain $E\left(\mathbf{\Gamma}_l^{m(q)^H} \mathbf{\Gamma}_l^{m(q)}\right)(m = 0, \cdots, M-1)$ in (4.39), the diagonal matrix $\mathbf{Z}_l^{(q)} = E\left(\mathbf{\Gamma}_l^{(q)^H} \mathbf{\Gamma}_l^{(q)}\right)$ is first computed, where the off-diagonal elements are zero under the assumption that no correlation between adjacent frequency bins of the channel response. Due to the fact that both $\mathbf{Q}_l$ and $\mathbf{V}_l$ are diagonal matrices, $\mathbf{Z}_l^{(q)}$ is given by

$$\mathbf{Z}_l^{(q)} = diag\left(\frac{[\mathbf{V}_l]_{1,1}}{1 - [\mathbf{Q}_l]_{1,1}^2}, \cdots, \frac{[\mathbf{V}_l]_{N_tM,N_tM}}{1 - [\mathbf{Q}_l]_{N_tM,N_tM}^2}\right) \quad (4.41)$$

Then, $E\left(\mathbf{\Gamma}_l^{m(q)^H} \mathbf{\Gamma}_l^{m(q)}\right)(m = 0, \cdots, M-1)$ of size $N_t \times N_t$ can be found on the main diagonal in the order of subcarriers.

TK-UCE employs the following recursion to produce the optimal channel estimate with respect to the lth $(l = 1, \cdots, N_r)$ receive antenna, based on the MMSE criterion:

$$\hat{\mathbf{\Gamma}}_l^{(q|q-1)} = \hat{\mathbf{\Gamma}}_l^{(q-1|q-1)} \mathbf{Q}_l \quad (4.42)$$

$$\mathbf{E}_l^{(q|q-1)} = \mathbf{X}_l^{(q)} - \hat{\mathbf{\Gamma}}_l^{(q|q-1)} E(\tilde{\mathbf{D}}^{(q)}) \quad (4.43)$$

$$\mathbf{P}_l^{(q|q-1)} = \mathbf{Q}_l^H \mathbf{P}_l^{(q-1|q-1)} \mathbf{Q}_l + \mathbf{V}_l \quad (4.44)$$

$$\mathbf{K}_l^{(q)} = \left[E(\tilde{\mathbf{D}}^{(q)})^H \mathbf{P}_l^{(q|q-1)} E(\tilde{\mathbf{D}}^{(q)}) + \mathbf{C}_l^{(q)}\right]^{-1} E(\tilde{\mathbf{D}}^{(q)})^H \mathbf{P}_l^{(q|q-1)} \tag{4.45}$$

$$\hat{\mathbf{\Gamma}}_l^{(q|q)} = \hat{\mathbf{\Gamma}}_l^{(q|q-1)} + \mathbf{E}_l^{(q|q-1)} \mathbf{K}_l^{(q)} \tag{4.46}$$

$$\mathbf{P}_l^{(q|q)} = \mathbf{P}_l^{(q|q-1)} \left[\mathbf{I}_{N_t M} - E(\tilde{\mathbf{D}}^{(q)}) \mathbf{K}_l^{(q)}\right] \tag{4.47}$$

where $\hat{\mathbf{\Gamma}}_l^{(q|i)}$ denotes the MMSE estimate of $\mathbf{\Gamma}_l^{(q)}$ given $\{\mathbf{X}_l^0 \cdots \mathbf{X}_l^i\}$, and $\mathbf{P}_l^{(q|i)} = E\left(\mathbf{S}_l^{(q|i)^H} \mathbf{S}_l^{(q|i)}\right)$ with $\mathbf{S}_l^{(q|i)} = \mathbf{\Gamma}_l^{(q)} - \hat{\mathbf{\Gamma}}_l^{(q|i)}$ denoting the frequency-domain channel estimation error, and $\mathbf{K}_l^{(q)}$ denotes the frequency-domain Kalman gain matrix. $\mathbf{P}_l^{(q|q-1)}$ and $\mathbf{P}_l^{(q|q)}$ are referred to as the prediction error-covariance matrix and filtering error-covariance matrix in the frequency domain, respectively.

4.3.1.2 Turbo Kalman Structured Channel Estimation (TK-SCE)

Compared with the assumption of no correlation between adjacent frequency bins in the channel response for TK-UCE, TK-SCE only assumes that each channel tap of the time-domain channel impulse response is an uncorrelated WSS random process, which preserves the correlation across the frequency bins.

TK-SCE is constructed using the following time-domain state space model:

$$\boldsymbol{\tau}_l^{(q)} = \boldsymbol{\tau}_l^{(q-1)} \mathbf{q}_l + \boldsymbol{\delta}_l^{(q)} \tag{4.48}$$

where $\mathbf{q}_l (l = 1, \cdots, N_r)$ denotes the time-domain state transition matrix of size $N_t(N+1) \times N_t(N+1)$ with respect tothe lth ($l = 1, \cdots, N_r$) receive antenna, and $\boldsymbol{\delta}_l^{(q)}$ of size $1 \times N_t(N+1)$ denotes the AWGN vector with the auto-correlation matrix $\mathbf{v}_l = E\left(\boldsymbol{\delta}_l^{(q)^H} \boldsymbol{\delta}_l^{(q)}\right)$. Assuming that each channel tap is an uncorrelated WSS random process that yields the WSSUS model [67], both $\mathbf{q}_l$ and $\mathbf{v}_l$ become diagonal.

In the code-aided channel estimation mode, $d_n^{i\,(q)} (n = 1, \cdots, N_t; i = 0, \cdots, M-$

1) is regarded as the noisy observation of $\mu_n^{i\,(q)}$, *i.e.*,

$$d_n^{i\,(q)} = \mu_n^{i\,(q)} + \phi_n^{i\,(q)} \tag{4.49}$$

where the noise $\phi_n^{i\,(q)}$ has a zero mean and a variance of $v_n^{i\,(q)}$. Substituting (4.49) into (4.34) yields

$$\mathbf{x}_l^{(q)} = \boldsymbol{\tau}_l^{(q)} E(\tilde{\mathbf{d}}^{(q)}) + \mathbf{g}_l^{(q)} \tag{4.50}$$

$$\mathbf{g}_l^{(q)} = \boldsymbol{\tau}_l^{(q)} \tilde{\boldsymbol{\phi}}^{(q)} + \mathbf{n}_l^{(q)} \tag{4.51}$$

where $\mathbf{g}_l^{(q)} = \left[g_l^{0(q)} \cdots g_l^{M-1(q)}\right]$ denotes the time-domain colored noise vector, $E\left(\tilde{\mathbf{d}}^{(q)}\right) = \left[E\left(\mathbf{d}^{0(q)}\right) \cdots E\left(\mathbf{d}^{M-1(q)}\right)\right]$ with $E\left(\mathbf{d}^{i(q)}\right) = \left[\mu_1^{i-N(q)} \cdots \mu_1^{i\,(q)} \cdots \mu_{N_t}^{i-N(q)} \cdots \mu_{N_t}^{i\,(q)}\right]^H$, and $\tilde{\boldsymbol{\phi}}^{(q)} = \left[\boldsymbol{\phi}^{0(q)} \cdots \boldsymbol{\phi}^{M-1(q)}\right]$ with $\boldsymbol{\phi}^{i(q)} = \left[\phi_1^{i-N(q)} \cdots \phi_1^{i\,(q)} \cdots \phi_{N_t}^{i-N(q)} \cdots \phi_{N_t}^{i\,(q)}\right]^H$.

Then, the covariance matrix $\mathbf{r}_l^{(q)}$ of the time-domain noise vector $\mathbf{g}_l^{(q)}$ is expressed as:

$$\mathbf{r}_l^{(q)} = diag\left(r_l^{0(q)} \cdots r_l^{M-1(q)}\right) \tag{4.52}$$

where

$$r_l^{i(q)} = tr\left[diag\left(v_1^{i-N(q)} \cdots v_1^{i\,(q)} \cdots v_{N_t}^{i-N(q)} \cdots v_{N_t}^{i\,(q)}\right) \mathbf{z}_l^{(q)}\right] + N_0 \tag{4.53}$$

with $\mathbf{z}_l^{(q)} = E\left(\boldsymbol{\tau}_l^{(q)H} \boldsymbol{\tau}_l^{(q)}\right)$. The off-diagonal elements of $\mathbf{z}_l^{(q)}$ are zero under the WSSUS channel model. Since both $\mathbf{q}_l$ and $\mathbf{v}_l$ are diagonal matrices, $\mathbf{z}_l^{(q)}$ is given by

$$\mathbf{z}_l^{(q)} = diag\left(\frac{[\mathbf{v}_l]_{1,1}}{1-[\mathbf{q}_l]_{1,1}^2}, \cdots, \frac{[\mathbf{v}_l]_{N_t(N+1),N_t(N+1)}}{1-[\mathbf{q}_l]_{N_t(N+1),N_t(N+1)}^2}\right) \tag{4.54}$$

With the time-domain state space model in (4.48), TK-SCE employs the following recursion to produce the optimal channel estimate with respect to the

lth ($l = 1, \cdots, N_r$) receive antenna:

$$\hat{\boldsymbol{\tau}}_l^{(q|q-1)} = \hat{\boldsymbol{\tau}}_l^{(q-1|q-1)}\mathbf{q}_l \tag{4.55}$$

$$\mathbf{e}_l^{(q|q-1)} = \mathbf{x}_l^{(q)} - \hat{\boldsymbol{\tau}}_l^{(q|q-1)}E(\tilde{\mathbf{d}}^{(q)}) \tag{4.56}$$

$$\mathbf{p}_l^{(q|q-1)} = \mathbf{q}_l^H\mathbf{p}_l^{(q-1|q-1)}\mathbf{q}_l + \mathbf{v}_l \tag{4.57}$$

$$\mathbf{k}_l^{(q)} = \left[E(\tilde{\mathbf{d}}^{(q)})^H\mathbf{p}_l^{(q|q-1)}E(\tilde{\mathbf{d}}^{(q)}) + \mathbf{r}_l^{(q)}\right]^{-1}E(\tilde{\mathbf{d}}^{(q)})^H\mathbf{p}_l^{(q|q-1)} \tag{4.58}$$

$$\hat{\boldsymbol{\tau}}_l^{(q|q)} = \hat{\boldsymbol{\tau}}_l^{(q|q-1)} + \mathbf{e}_l^{(q|q-1)}\mathbf{k}_l^{(q)} \tag{4.59}$$

$$\mathbf{p}_l^{(q|q)} = \mathbf{p}_l^{(q|q-1)}\left[\mathbf{I}_{N_t(N+1)} - E(\tilde{\mathbf{d}}^{(q)})\mathbf{k}_l^{(q)}\right] \tag{4.60}$$

where $\hat{\boldsymbol{\tau}}_l^{(q|i)}$ denotes the MMSE estimate of $\boldsymbol{\tau}_l^{(q)}$ given $\{\mathbf{x}_l^0 \cdots \mathbf{x}_l^i\}$, $\mathbf{k}_l^{(q)}$ denotes the time-domain Kalman gain matrix, and $\mathbf{p}_l^{(q|i)} = E\left(\mathbf{s}_l^{(q|i)^H}\mathbf{s}_l^{(q|i)}\right)$ with $\mathbf{s}_l^{(q|i)} = \boldsymbol{\tau}_l^{(q)} - \hat{\boldsymbol{\tau}}_l^{(q|i)}$ denoting the time-domain channel estimation error. $\mathbf{p}_l^{(q|q-1)}$ and $\mathbf{p}_l^{(q|q)}$ denote the time-domain prediction error-covariance matrix and filtering error-covariance matrix, respectively.

For both TK-UCE and TK-SCE, $v_n^{i\,(q)} > 0 (n = 1, \cdots, N_t; i = 0, \cdots, M-1)$, the variance of the colored noise on each subcarrier or each symbol), is taken into account while calculating the Kalman gain. Thus, the innovation process of TK-UCE and TK-SCE implicates the consideration of the likelihood information of the data, which helps limit the error propagation during the channel estimation. When the hard-input Kalman UCE or hard-input Kalman SCE is applied, *i.e.*, $v_n^{i\,(q)} = 0 (n = 1, \cdots, N_t; m = 0, \cdots, M-1)$, the influence of the likelihood information of the data on the channel estimate is excluded.

4.3.2 Turbo NRLS Channel Estimation

This section proposes Turbo NRLS based channel estimation schemes to address channels where the state space model in (4.35) or (4.48) is not guaranteed. Following the transformation rule from the Kalman filter to the RLS filter [48], this section derives Turbo NRLS unstructured channel estimation (TNRLS-UCE) and Turbo NRLS structured channel estimation (TNRLS-SCE) schemes based on the results of Turbo Kalman channel estimation in Subsection 4.3.1.

4.3.2.1 Turbo NRLS Unstructured Channel Estimation (TNRLS-UCE)

In the code-aided channel estimation mode, TNRLS-UCE aims to minimise

$$J(\hat{\mathbf{\Gamma}}_l^{(q)}) = \sum_{i=1}^{q} \lambda^{q-i} \frac{tr\left[\left(\mathbf{X}_l^{(i)} - \hat{\mathbf{\Gamma}}_l^{(q)} E(\tilde{\mathbf{D}}^{(i)})\right)^H \left(\mathbf{X}_l^{(i)} - \hat{\mathbf{\Gamma}}_l^{(q)} E(\tilde{\mathbf{D}}^{(i)})\right)\right]}{tr\left(\mathbf{C}_l^{(i)}\right)} \quad (l = 1, \cdots, N_r) \tag{4.61}$$

with respect to $\hat{\mathbf{\Gamma}}_l^{(q)}$ that is the estimate of $\mathbf{\Gamma}_l^{(q)}$. Both the forgetting factor λ and $\mathbf{C}_l^{(i)}$ determine the weighting of the recent data. The frequency-domain solution to $\hat{\mathbf{\Gamma}}_l^{(q)}$ is given by the following recursion:

$$\mathbf{E}_l^{(q)} = \mathbf{X}_l^{(q)} - \hat{\mathbf{\Gamma}}_l^{(q-1)} E(\tilde{\mathbf{D}}^{(q)}) \tag{4.62}$$

$$\mathbf{K}_l^{(q)} = \left[E(\tilde{\mathbf{D}}^{(q)})^H \mathbf{P}_l^{(q-1)} E(\tilde{\mathbf{D}}^{(q)}) + \lambda \mathbf{C}_l^{(q)}\right]^{-1} E(\tilde{\mathbf{D}}^{(q)})^H \mathbf{P}_l^{(q-1)} \tag{4.63}$$

$$\hat{\mathbf{\Gamma}}_l^{(q)} = \hat{\mathbf{\Gamma}}_l^{(q-1)} + \mathbf{E}_l^{(q)} \mathbf{K}_l^{(q)} \tag{4.64}$$

$$\mathbf{P}_l^{(q)} = \frac{1}{\lambda} \mathbf{P}_l^{(q-1)} \left[\mathbf{I}_{N_t M} - E(\tilde{\mathbf{D}}^{(q)}) \mathbf{K}_l^{(q)}\right] \tag{4.65}$$

where $\mathbf{P}_l^{(q)} = E\left(\mathbf{S}_l^{(q)^H} \mathbf{S}_l^{(q)}\right)$ with $\mathbf{S}_l^{(q)} = \mathbf{\Gamma}_l^{(q)} - \hat{\mathbf{\Gamma}}_l^{(q)}$. Due to no guarantee of the assumption that no correlation between adjacent frequency bins of the channel

response, $\mathbf{Z}_l^{(q)}$ that determines $\mathbf{C}_l^{(q)}$ can not be computed as in (4.41). Therefore, $\mathbf{Z}_l^{(q)}$ is approximated by

$$\mathbf{Z}_l^{(q)} \approx \hat{\mathbf{\Gamma}}_l^{(q-1)^H} \hat{\mathbf{\Gamma}}_l^{(q-1)} + \mathbf{P}_l^{(q-1)} \tag{4.66}$$

4.3.2.2 Turbo NRLS Structured Channel Estimation (TNRLS-SCE)

In the code-aided channel estimation mode, TNRLS-SCE aims to minimise

$$J(\hat{\boldsymbol{\tau}}_l^{(q)}) = \sum_{i=1}^{q} \lambda^{q-i} \frac{tr\left[\left(\mathbf{x}_l^{(i)} - \hat{\boldsymbol{\tau}}_l^{(q)} E(\tilde{\mathbf{d}}^{(i)})\right)^H \left(\mathbf{x}_l^{(i)} - \hat{\boldsymbol{\tau}}_l^{(q)} E(\tilde{\mathbf{d}}^{(i)})\right)\right]}{tr\left(\mathbf{r}_l^{(i)}\right)} \quad (l = 1, \cdots, N_r) \tag{4.67}$$

with respect to $\hat{\boldsymbol{\tau}}_l^{(q)}$ that is the estimate of $\boldsymbol{\tau}_l^{(q)}$. Both the forgetting factor λ and $\mathbf{r}_l^{(i)}$ determine the weighting of the recent data. The time-domain solution to $\hat{\boldsymbol{\tau}}_l^{(q)}$ is given by the following recursion:

$$\mathbf{e}_l^{(q)} = \mathbf{x}_l^{(q)} - \hat{\boldsymbol{\tau}}_l^{(q-1)} E(\tilde{\mathbf{d}}^{(q)}) \tag{4.68}$$

$$\mathbf{k}_l^{(q)} = \left[E(\tilde{\mathbf{d}}^{(q)})^H \mathbf{p}_l^{(q-1)} E(\tilde{\mathbf{d}}^{(q)}) + \lambda \mathbf{r}_l^{(q)}\right]^{-1} E(\tilde{\mathbf{d}}^{(q)})^H \mathbf{p}_l^{(q-1)} \tag{4.69}$$

$$\hat{\boldsymbol{\tau}}_l^{(q)} = \hat{\boldsymbol{\tau}}_l^{(q-1)} + \mathbf{e}_l^{(q)} \mathbf{k}_l^{(q)} \tag{4.70}$$

$$\mathbf{p}_l^{(q)} = \frac{1}{\lambda} \mathbf{p}_l^{(q-1)} \left[\mathbf{I}_{N_t(N+1)} - E(\tilde{\mathbf{d}}^{(q)}) \mathbf{k}_l^{(q)}\right] \tag{4.71}$$

where $\mathbf{p}_l^{(q)} = E\left(\mathbf{s}_l^{(q)^H} \mathbf{s}_l^{(q)}\right)$ with $\mathbf{s}_l^{(q)} = \boldsymbol{\tau}_l^{(q)} - \hat{\boldsymbol{\tau}}_l^{(q)}$. Due to no guarantee of the WSSUS channel model in practical environments, $\mathbf{z}_l^{(q)}$ that determines $\mathbf{r}_l^{(q)}$ can not be computed as in (4.54). Therefore, $\mathbf{z}_l^{(q)}$ is approximated by

$$\mathbf{z}_l^{(q)} \approx \hat{\boldsymbol{\tau}}_l^{(q-1)^H} \hat{\boldsymbol{\tau}}_l^{(q-1)} + \mathbf{p}_l^{(q-1)} \tag{4.72}$$

In the cases of TNRLS-UCE and TNRLS-SCE, the noise variance changes in each block, while it is assumed to be constant over a block in the conventional hard-input channel estimation.

4.3.3 Performance Analysis

An intensive performance analysis for Kalman based Turbo channel estimation in terms of the MSE of the channel estimate is provided. The analysis focus is the Turbo SCE schemes, since they outperform their Turbo UCE counterparts and provide a close performance to the case with perfect CSI as shown by simulation results.

Without loss of generality, this section assumes QPSK modulation. A reasonable approximation of evaluating the MSE is to consider $\mathbf{p}_l^{(q|i)}$ and $\mathbf{p}_l^{(q)}$ are diagonal, due to the uncorrelation between different channel taps. It should be noted that the dependence of the channel observations should be avoided throughout the analysis, since the analytical calculation of the MSE depends on random LLRs of code bits, instead of deterministic LLRs of code bits. The MSE of TK-SCE is first calculated, then TNRLS-SCE.

The probability density function (pdf) of a Gaussian random variable y with a mean of a and a variance of b is given by

$$f\left(y; a, b^2\right) = \frac{1}{\sqrt{2\pi}b} exp\left[\frac{-(y-a)^2}{2b^2}\right] \tag{4.73}$$

Since each input LLR to the channel estimator can be modeled as an independent identical distributed (i.i.d.) Gaussian random variable with mean $\pm a$ ($a > 0$) and

variance $2a$ [8, 68], the pdf of each LLR, denoted by $f_L(y)$, can be modeled as

$$f_L(y) = \frac{1}{2} f(y; a, 2a) + \frac{1}{2} f(y; -a, 2a) \tag{4.74}$$

where 0 and 1 are assumed be to equally likely in the code sequence and the reliability of LLRs are closely related to a. For each data block, Gaussian LLRs of code bits with mean $\pm a$ and variance $2a$ in (4.74) are generated and then fed to the channel estimator. $\mu_n^i (n = 1, \cdots, N_t; i = 0, \cdots, M-1)$ are regarded as random variables with the Gaussian distribution of input LLRs to the channel estimator. Let $E_L(.)$ denote the expectation subject to the distribution of input LLRs.

4.3.3.1 MSE of TK-SCE

From (4.57), (4.58) and (4.60), it is found that

$$E_L\left(\left[\mathbf{p}_l^{(q|q-1)}\right]_{k,k}\right) = E_L\left(\left[\mathbf{p}_l^{(q-1|q-1)}\right]_{k,k}\right)[\mathbf{q}_l]_{k,k}^2 + [\mathbf{v}_l]_{k,k} \tag{4.75}$$

$$E_L\left(\left[\mathbf{p}_l^{(q|q)}\right]_{k,k}\right) = E_L\left(\left[\mathbf{p}_l^{(q|q-1)}\right]_{k,k}\right)\left(1 - \omega_{l,k}^{(q)} E_L\left(\left[\mathbf{p}_l^{(q|q-1)}\right]_{k,k}\right)\right) \tag{4.76}$$

where $\omega_{l,k}^{(q)}$ related to the transition from $E_L\left(\left[\mathbf{p}_l^{(q|q-1)}\right]_{k,k}\right)$ to $E_L\left(\left[\mathbf{p}_l^{(q|q)}\right]_{k,k}\right)$ needs to be computed for each block to accomplish the recursion of $E_L\left(\left[\mathbf{p}_l^{(q|q)}\right]_{k,k}\right)$, which represents the mean of $\left[\mathbf{p}_l^{(q|q)}\right]_{k,k}$. The recursive computation of $\omega_{l,k}^{(q)}$ is derived in Appendix B.

In general, if an S-ary modulation scheme is employed, the calculation of $\omega_{l,k}^{(q)}$ requires a $log_2(S)$-dimension integration. Based on (4.75), (4.76) and taking $E_L\left(\left[\mathbf{p}_l^{(0|0)}\right]_{k,k}\right) = \left[\mathbf{p}_l^{(0|0)}\right]_{k,k}$, the analytical MSE $E_L\left(\left[\mathbf{p}_l^{(q|q)}\right]_{k,k}\right)$ can be com-

puted recursively. The average MSE at the qth block for TK-SCE is given by

$$J_{TK-SCE}^{(q|q)} = \frac{1}{N_r N_t (N+1)} \sum_{l=1}^{N_r} \sum_{k=1}^{N_t(N+1)} E_L \left(\left[\mathbf{p}_l^{(q|q)} \right]_{k,k} \right) \tag{4.77}$$

In particular, $J_{TK-SCE}^{(0|0)}$ represents the initial MSE for TK-SCE. The numerical MSE of TK-SCE is calculated as

$$\hat{J}_{TK-SCE}^{(q|q)} = \frac{1}{N_r N_t (N+1)} \sum_{l=1}^{N_r} \sum_{k=1}^{N_t(N+1)} \left[\mathbf{p}_l^{(q|q)} \right]_{k,k} \tag{4.78}$$

which is compared with the analytical MSE in (4.77) to demonstrate the accuracy of the performance analysis in Section 4.4.

In comparison, the numerical time-domain MSE of TK-UCE is given by

$$\hat{J}_{TK-UCE}^{(q|q)} = \frac{1}{N_r N_t (N+1)} \sum_{l=1}^{N_r} \sum_{k=1}^{N_t(N+1)} \left[\tilde{\mathbf{F}} \mathbf{P}_l^{(q|q)} \tilde{\mathbf{F}}^H \right]_{k,k} \tag{4.79}$$

4.3.3.2 MSE of TNRLS-SCE

It is found from (4.69) and (4.71) that

$$E_L \left(\left[\mathbf{p}_l^{(q)} \right]_{k,k} \right) = E_L \left(\left[\mathbf{p}_l^{(q-1)} \right]_{k,k} \right) \left(1 - \theta_{l,k}^{(q)} E_L \left(\left[\mathbf{p}_l^{(q-1)} \right]_{k,k} \right) \right) \tag{4.80}$$

where $\theta_{l,k}^{(q)}$ needs to be computed for each block to accomplish the recursive computation of $E_L \left(\left[\mathbf{p}_l^{(q)} \right]_{k,k} \right)$, which represents the mean of $\left[\mathbf{p}_l^{(q)} \right]_{k,k}$. The recursive computation of $\theta_{l,k}^{(q)}$ is derived as in Appendix C.

Based on (4.80) and taking $E_L \left(\left[\mathbf{p}_l^{(0)} \right]_{k,k} \right) = \left[\mathbf{p}_l^{(0)} \right]_{k,k}$, the recursive computation of $E_L \left(\left[\mathbf{p}_l^{(q)} \right]_{k,k} \right)$ can be achieved. The average MSE at the qth block for

TNRLS-SCE is denoted by

$$J^{(q)}_{TNRLS-SCE} = \frac{1}{N_r N_t(N+1)} \sum_{l=1}^{N_r} \sum_{k=1}^{N_t(N+1)} E_L\left(\left[\mathbf{p}_l^{(q)}\right]_{k,k}\right) \tag{4.81}$$

In particular, the initial MSE for TNRLS-SCE is given by $J^{(0)}_{TNRLS-SCE}$. The numerical MSE can also be obtained by

$$\hat{J}^{(q)}_{TNRLS-SCE} = \frac{1}{N_r N_t(N+1)} \sum_{l=1}^{N_r} \sum_{k=1}^{N_t(N+1)} \left[\mathbf{p}_l^{(q)}\right]_{k,k} \tag{4.82}$$

For the purpose of comparison, the numerical MSE of TNRLS-UCE in the time-domain is given by

$$\hat{J}^{(q)}_{TNRLS-UCE} = \frac{1}{N_r N_t(N+1)} \sum_{l=1}^{N_r} \sum_{k=1}^{N_t(N+1)} \left[\tilde{\mathbf{F}}\mathbf{P}_l^{(q)}\tilde{\mathbf{F}}^H\right]_{k,k} \tag{4.83}$$

4.4 Simulation

4.4.1 Simulation Setup

Simulations were carried out to determine the performance of the proposed iterative channel estimation schemes. A MIMO system with $N_t = 4$ transmit antennas and $N_r = 4$ receive antennas is considered. The ECC bits are generated using a rate 1/2, memory $M_c = 2$ terminated RSC encoder with generator $(1 + D + D^2, 1 + D^2)$. Both the transmit and receive filters use a raised-cosine pulse with a roll-off factor of 0.35. The SNR is defined as the spatial average ratio of the signal power to noise power. The physical channel is modeled by following the exponential power delay profile [65]. Each channel path is generated using the 100th order autoregressive (AR) state space model [69] which provides a good

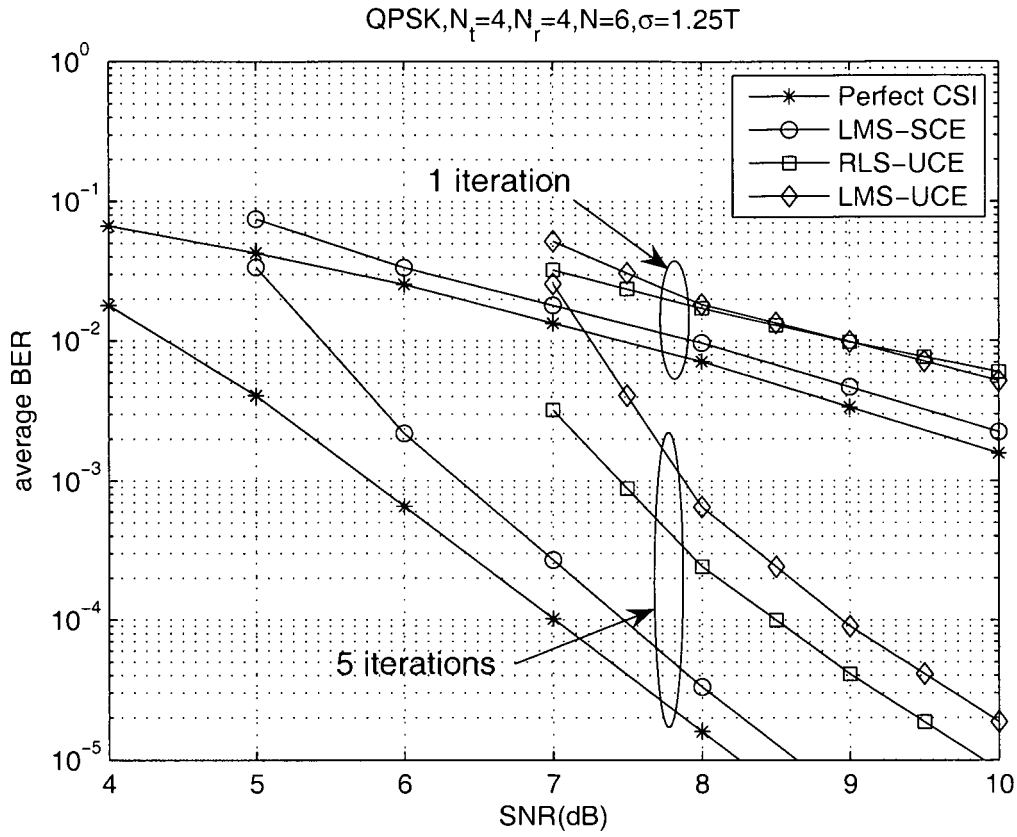

Figure 4.1: Performance of adaptive TSFE with $N_t = 4$ transmit antennas, $N_r = 4$ receive antennas, RMS delay $\sigma = 1.25\ T$, and $f_d T = 1/25000$.

approximation of the Rayleigh fading channel. All the channel taps are mutually independent, and follow a Gaussian Doppler spectrum [70]. The channel is assumed to be block fading, *i.e.*, the CSI is constant over a block.

Figure 4.1 and Figure 4.2 demonstrate the performance of the hard-input iterative channel estimation incorporated with the symbol-spaced TSFE. With a symbol rate of 1.25 M-Baud, a default RMS delay spread of $\sigma = 1\ \mu s$ (*i.e.*, $\sigma = 1.25\ T$) is used. Each data block contains $M = 64$ symbols.

Figure 4.3 and Figure 4.4 show the performance of TRLS-SCE channel estimation. The symbol rate is 5 M-Baud, and the RMS delay spread is $\sigma = 1\ \mu s$

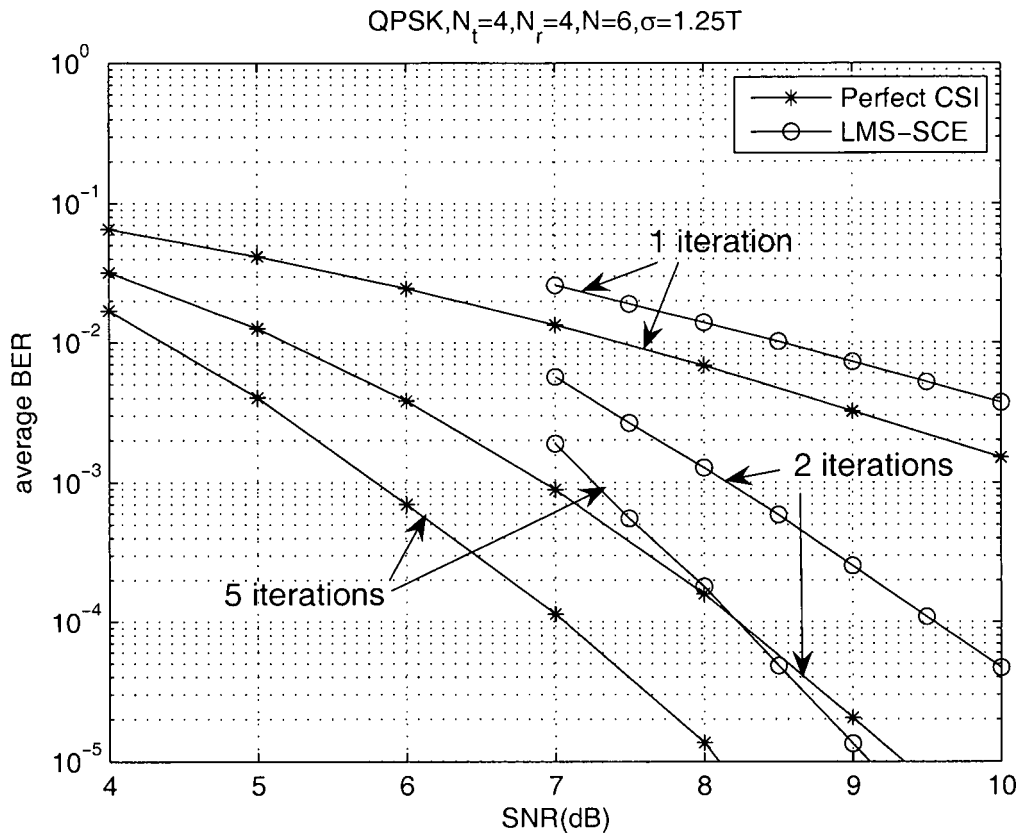

Figure 4.2: Performance of adaptive TSFE with $N_t = 4$ transmit antennas, $N_r = 4$ receive antennas, RMS delay $\sigma = 1.25\ T$, and $f_dT = 1/6250$.

(*i.e.*, $\sigma = 5\ T$). A sampling rate of $N_s = 2$ (*i.e.*, 2 samples per symbol period) and a block size of $M = 128$ employed.

The performance of the Kalman based Turbo channel estimation is demonstrated in Figure 4.5-4.12. For Turbo Kalman and Turbo NRLS channel estimation, there is the following setup. Given a Doppler spread f_d, $\mathbf{Q}_l = J_0(2\pi f_d T)\mathbf{I}_{N_tM}$ in (4.35) and $\mathbf{q}_l = J_0(2\pi f_d T)\mathbf{I}_{N_t(N+1)}$ in (4.48) are applied to TK-UCE and TK-SCE, respectively. At Doppler spread $f_d = 50$ Hz (*i.e.*, $f_dT = 10^{-5}$), $\mathbf{V}_l = 2\times10^{-4}\mathbf{I}_{N_tM}$ and $\mathbf{v}_l = 2\times10^{-6}\mathbf{I}_{N_t(N+1)}$ are used to optimise the performance of TK-UCE and TK-SCE respectively, and both TNRLS-UCE and TNRLS-SCE

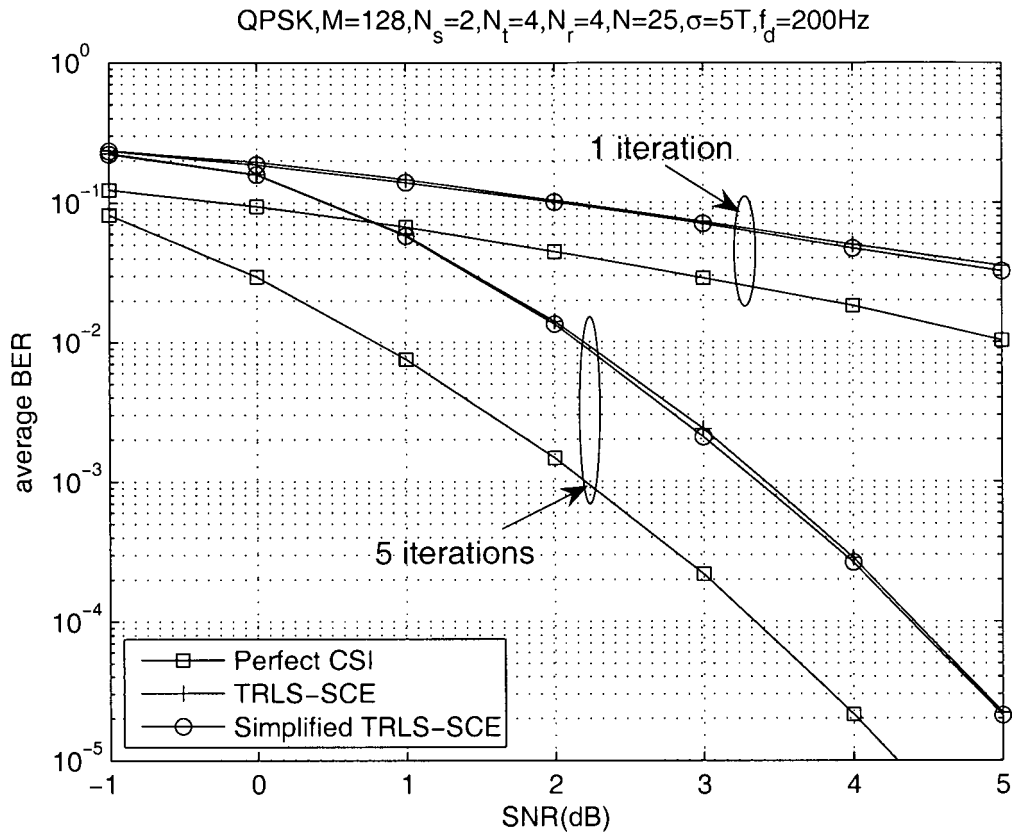

Figure 4.3: Performance of adaptive Turbo frequency-domain channel estimation based oversampled TSFE with $M = 128$ symbols per block, $N_s = 2$ samples per symbol period, $N_t = 4$ transmit antennas, $N_r = 4$ receive antennas, RMS delay $\sigma = 5\ T$ and Doppler spread $f_d = 200$ Hz.

are configured with a forgetting factor of $\lambda = 0.985$. At Doppler spread $f_d = 200$ Hz (*i.e.*, $f_d T = 4 \times 10^{-5}$), the forgetting factor of $\lambda = 0.955$ is configured for both TNRLS-UCE and TNRLS-SCE, and $\mathbf{V}_l = 2{\times}10^{-3}\mathbf{I}_{N_t M}$ and $\mathbf{v}_l = 2{\times}10^{-5}\mathbf{I}_{N_t(N+1)}$ are chosen for TK-UCE and TK-SCE, respectively.

4.4.2 Simulation Results

The performance of TSFE over time-varying channels, employing the hard-input adaptive channel estimation methods, is first investigated in Figure 4.1 and Figure

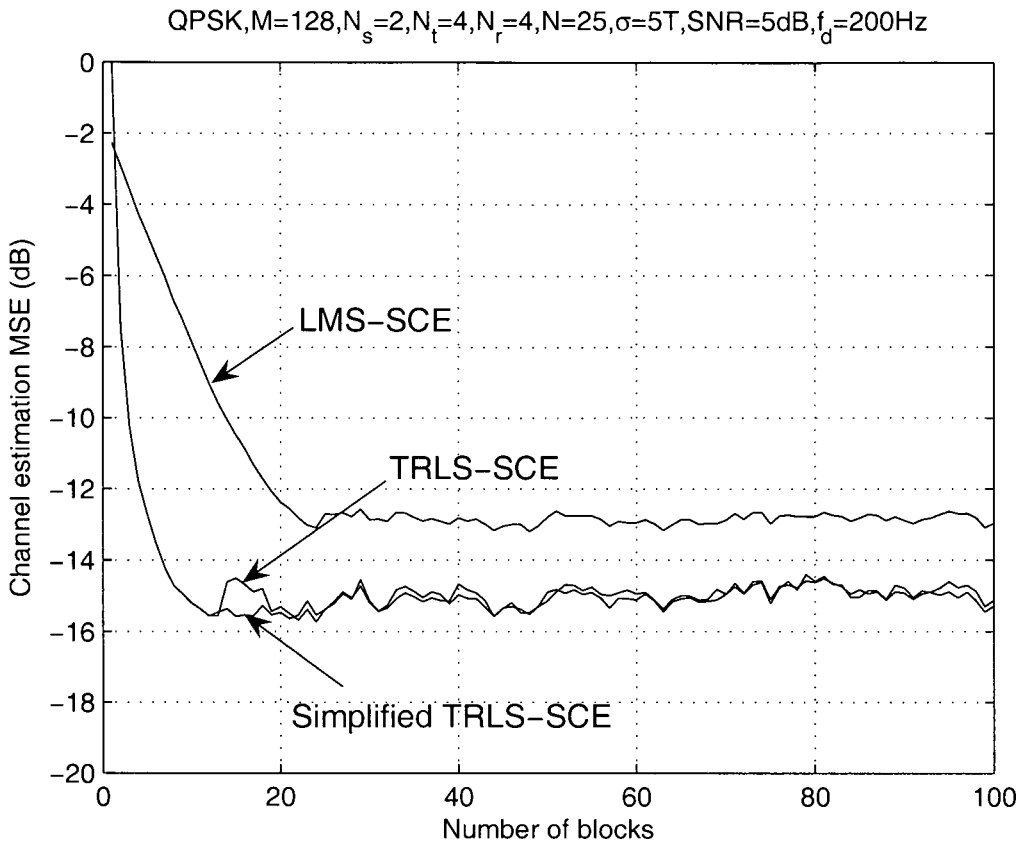

Figure 4.4: Learning curves of adaptive Turbo frequency-domain channel estimation with $M = 128$ symbols per block, 5 iterations, $N_s = 2$ samples per symbol period, $N_t = 4$ transmit antennas, $N_r = 4$ receive antennas, SNR = 5 dB, RMS delay $\sigma = 5\ T$ and Doppler spread $f_d = 200$ Hz.

4.2. The Doppler spreads are $f_d = 50$ Hz and 200 Hz, which correspond to the Doppler spreads normalised to the symbol rate as $f_dT = 1/25000$ and $f_dT = 1/6250$, respectively. Each data frame consists of a training sequence of $nTrain$ blocks and a data sequence of $nData$ blocks. Figure 4.1 shows the performance of TSFE based on LMS-UCE (with $nTrain = 100$, $nData = 600$ and $\mu = 3 \times 10^{-4}$), RLS-UCE ($nTrain = 45$, $nData = 600$ and $\lambda = 0.99$) and LMS-SCE (with $nTrain = 40$, $nData = 600$ and $\mu = 1.8 \times 10^{-5}$) at a moderate Doppler spread of $f_dT = 1/25000$, compared to the perfect CSI case. LMS-SCE can adapt to

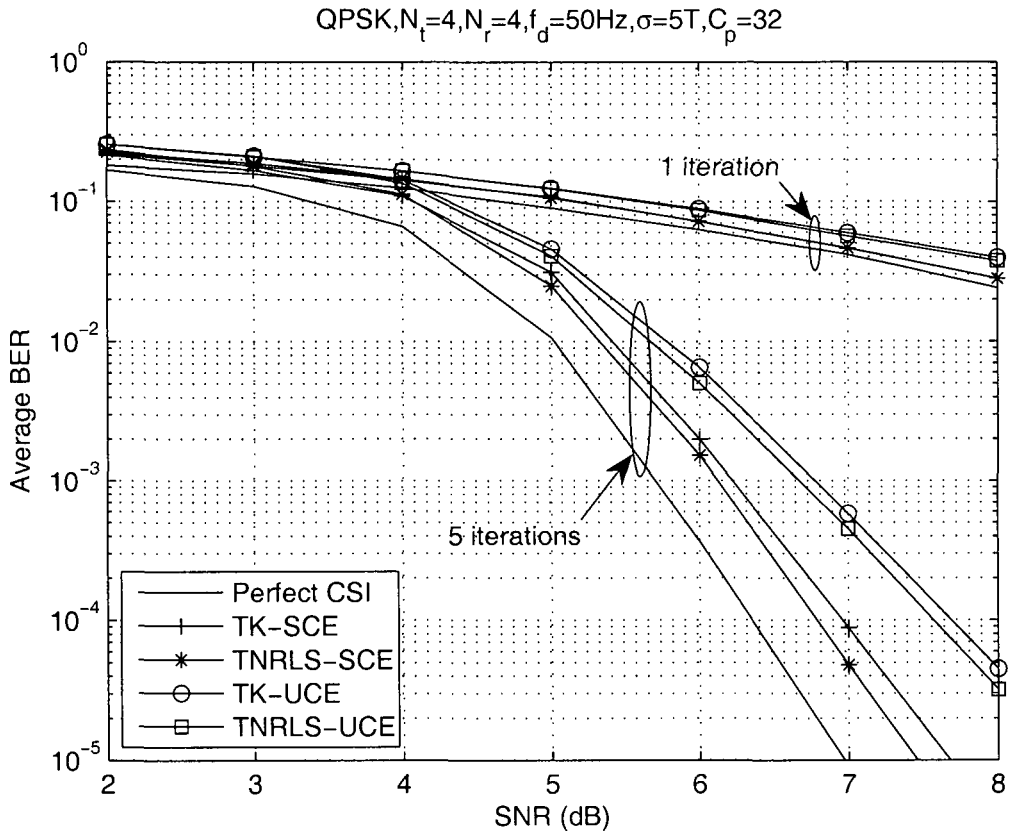

Figure 4.5: Performance of adaptive Turbo channel estimation based TSFE with $M = 128$ symbols per block, $N_t = 4$ transmit antennas, $N_r = 4$ receive antennas, RMS delay $\sigma = 5\ T$ and Doppler spread $f_d = 50$ Hz.

the channel variations effectively, which has an SNR penalty of only 0.5 dB at BER $= 10^{-4}$ using 5 iterations over its perfect CSI case. Both RLS-UCE and LMS-UCE can track the channel variations at SNR higher than 7 dB, achieving the performance gaps of about 1 dB and 1.5 dB over LMS-SCE using 5 iterations at BER $= 10^{-4}$, respectively.

At a relatively high Doppler spread $f_dT = 1/6250$, Figure 4.2 demonstrates the performance of TSFE with LMS-SCE (with $nTrain = 20$, $nData = 300$ and $\mu = 3 \times 10^{-5}$), which remains a stable performance gap of around only 1 dB compared to the perfect CSI case, over the SNR range from 7 dB to 10 dB.

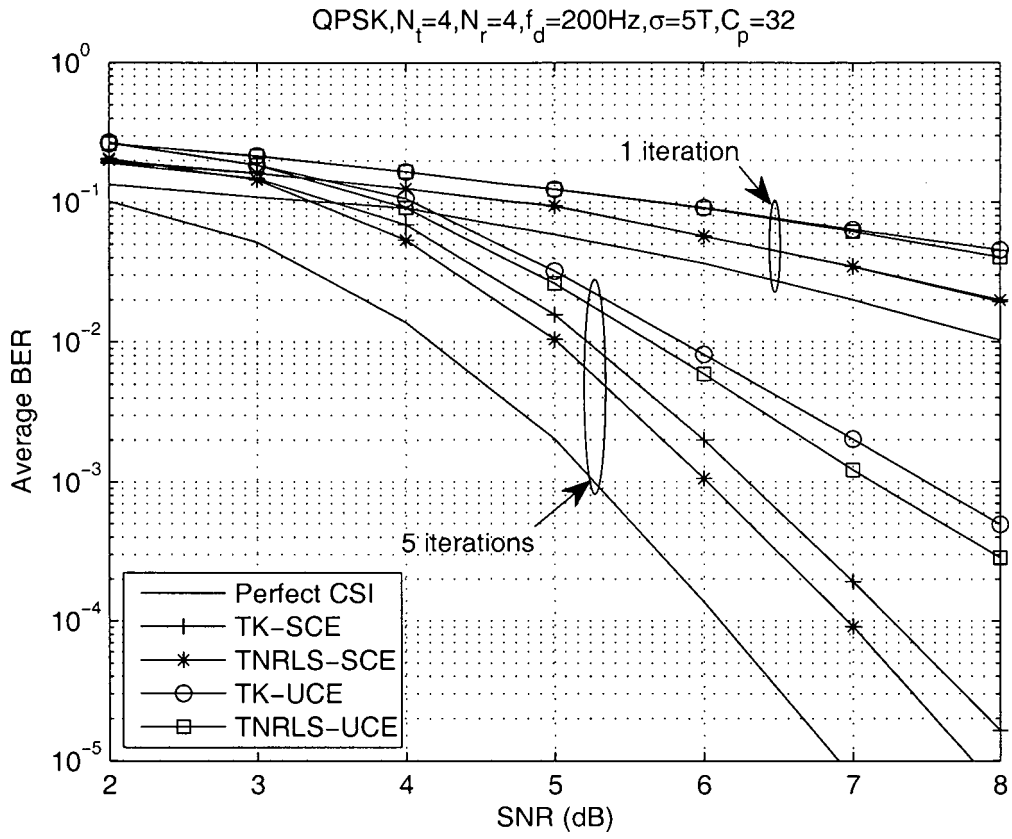

Figure 4.6: Performance of adaptive Turbo channel estimation based TSFE with $M = 128$ symbols per block, $N_t = 4$ transmit antennas, $N_r = 4$ receive antennas, RMS delay $\sigma = 5\ T$ and Doppler spread $f_d = 200$ Hz.

This implies the effectiveness of the LMS-SCE based TSFE in the fast fading environment, which utilises the fading correlation between adjacent frequency bins.

The second category of iterative channel estimation, TRLS-SCE, is investigated in Figure 4.3 and Figure 4.4. Figure 4.3 demonstrates the BER performance of the TRLS-SCE schemes incorporated with oversampled TSFE. A Doppler spread of $f_d = 200$ Hz (*i.e.*, $f_d T = 4 \times 10^{-5}$) is assumed here. Both TRLS-SCE and the simplified TRLS-SCE schemes use a forgetting factor of $\lambda = 0.94$, and $nTrain = 12$ training blocks and $nData = 300$ data blocks are employed in

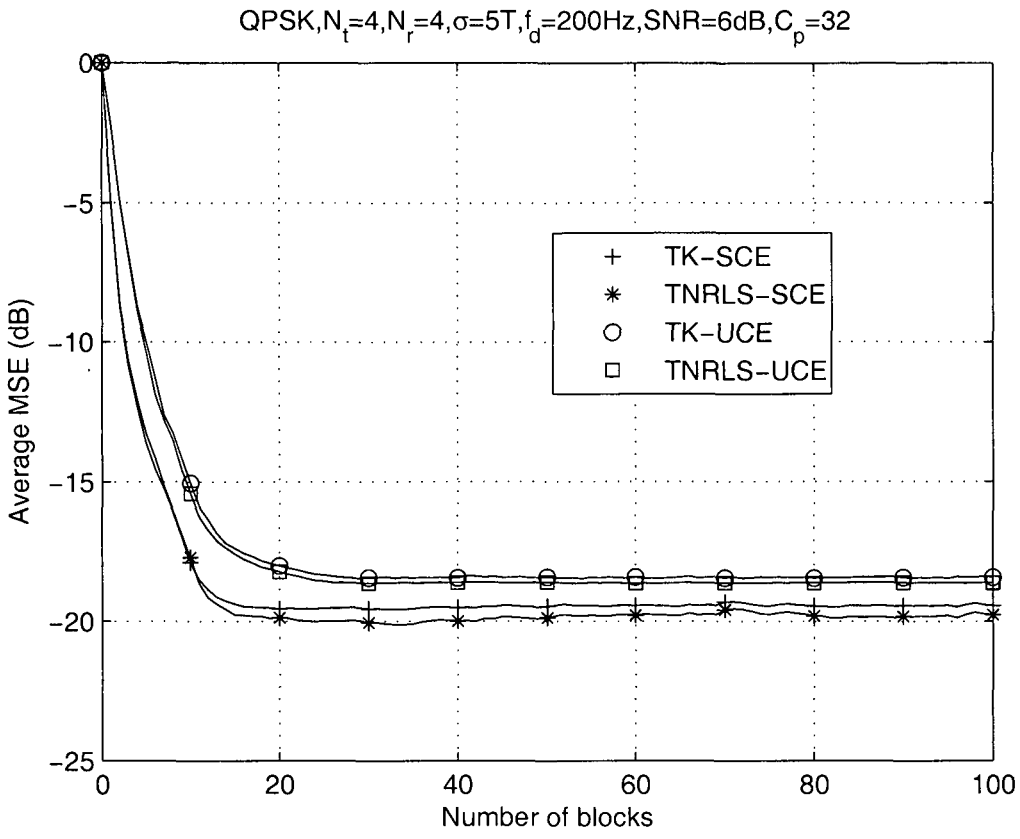

Figure 4.7: Learning curves of TSFE incorporated Turbo channel estimation with $M = 128$ symbols per block, 5 iterations, $N_t = 4$ transmit antennas, $N_r = 4$ receive antennas, SNR = 6 dB, RMS delay $\sigma = 5\ T$ and Doppler spread $f_d = 200$ Hz.

a frame, leading to a training overhead of only 3.8%. The simplified TRLS-SCE scheme provides nearly the same performance as TRLS-SCE, with a complexity reduction of around 33 times over the latter as discussed in Subsection 4.2.3. Compared to the case with perfect CSI, the simplified TRLS-SCE has a performance loss of only 1 dB at BER = 10^{-4} with 5 iterations.

Figure 4.4 shows the convergence performance of the two RLS-SCE channel estimation algorithms in terms of the normalised channel estimation MSE defined in (4.16) versus the number of blocks. The same configuration as in Figure 4.3

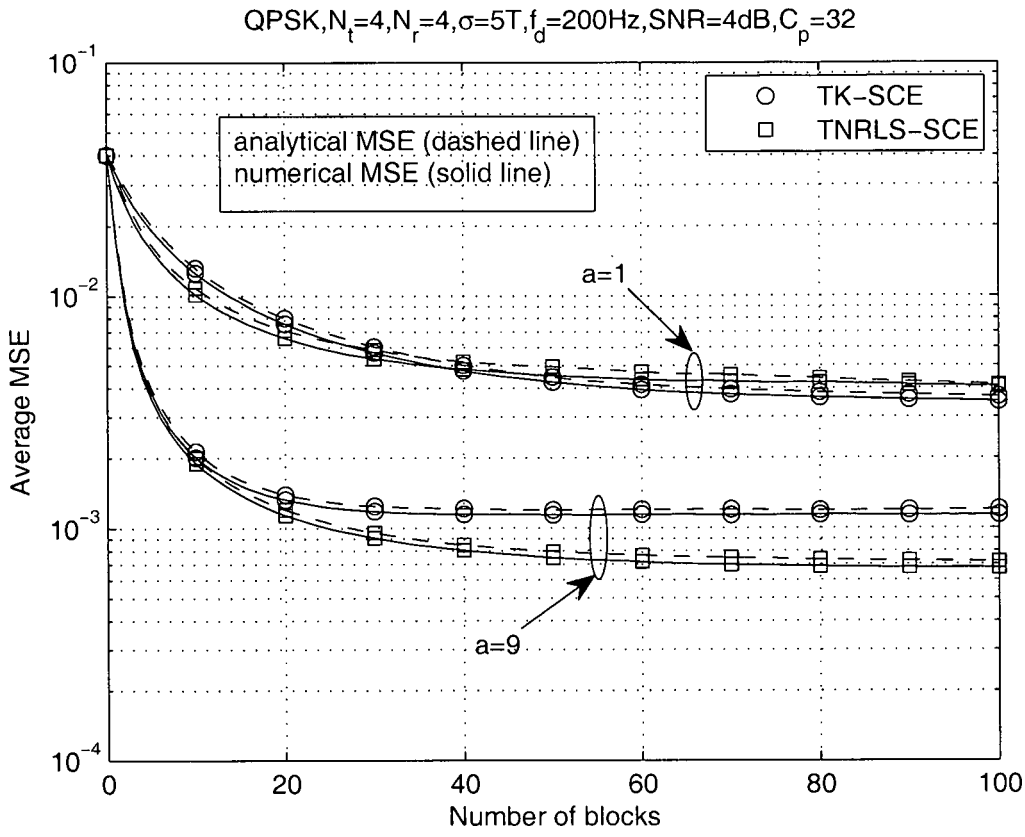

Figure 4.8: Learning curves of TK-SCE and TNRLS-SCE with $M = 128$ symbols per block, $J^{(0|0)}_{TK-SCE} = J^{(0)}_{TNRLS-SCE} = 0.04$, $N_t = 4$ transmit antennas, $N_r = 4$ receive antennas, SNR = 4 dB, RMS delay $\sigma = 5\ T$ and Doppler spread $f_d = 200$ Hz.

is employed except that SNR = 5 dB. The LMS-SCE algorithm [61] with a step size of $\mu = 2 \times 10^{-6}$ is used for comparison, which was proven to have a faster convergence speed than other frequency-domain channel estimation algorithms [61]. TRLS-SCE estimation schemes have a higher convergence speed with only 12 training blocks needed to achieve the steady state, while LMS-SCE [61] requires 24 training blocks. The simplified TRLS-SCE provides nearly the same steady-state MSE as TRLS-SCE, which is around 4 dB lower than that achieved by LMS-SCE.

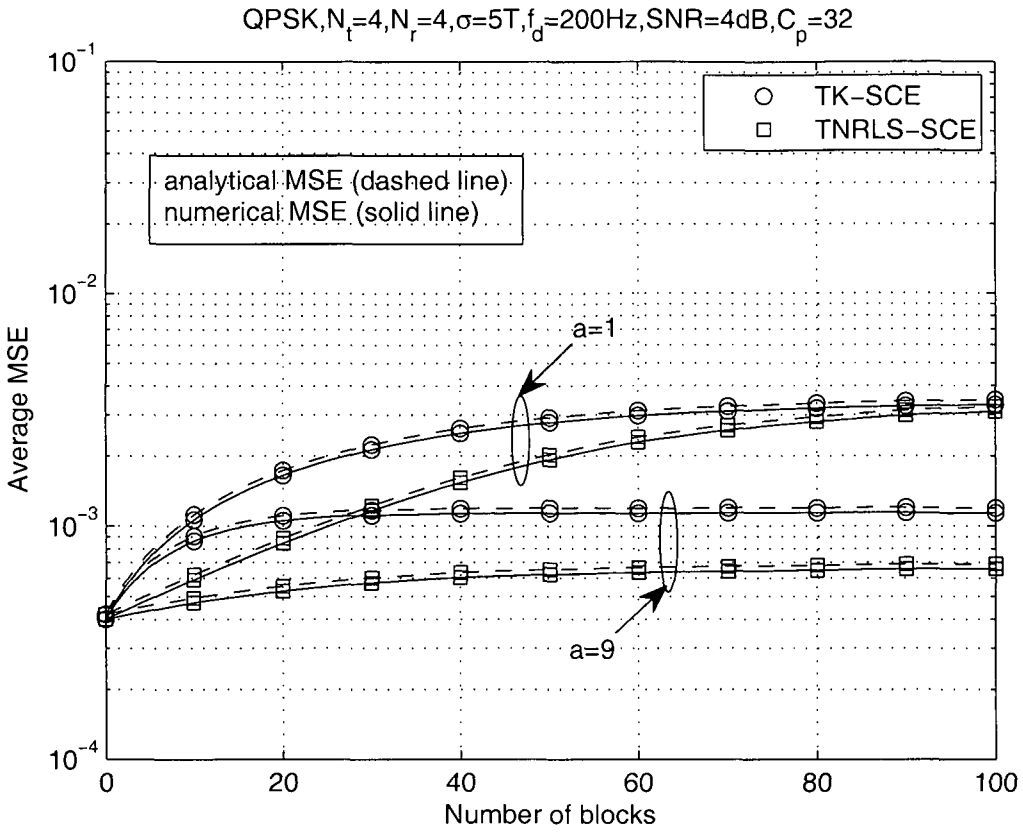

Figure 4.9: Learning curves of TK-SCE and TNRLS-SCE with $M = 128$ symbols per block, $J^{(0|0)}_{TK-SCE} = J^{(0)}_{TNRLS-SCE} = 4\times10^{-4}$, $N_t = 4$ transmit antennas, $N_r = 4$ receive antennas, SNR = 4 dB, RMS delay $\sigma = 5\,T$ and Doppler spread $f_d = 200$ Hz.

Finally, the performance of the Kalman based Turbo channel estimation is shown in Figure 4.5-4.12. Figure 4.5 demonstrates the BER performance of the four proposed adaptive Turbo channel estimation schemes incorporated with TSFE [61] at Doppler spread $f_d = 50$ Hz (*i.e.*, $f_dT = 10^{-5}$). Both TNRLS-SCE and TK-SCE have a low training overhead of 2.5% with $nTrain = 30$, and both TNRLS-UCE and TK-UCE require a higher training overhead of 4.1% with $nTrain = 50$. TNRLS-SCE and TK-SCE with 5 iterations have a performance loss of only 0.5 dB compared to the case with perfect CSI at BER = 10^{-4}. Us-

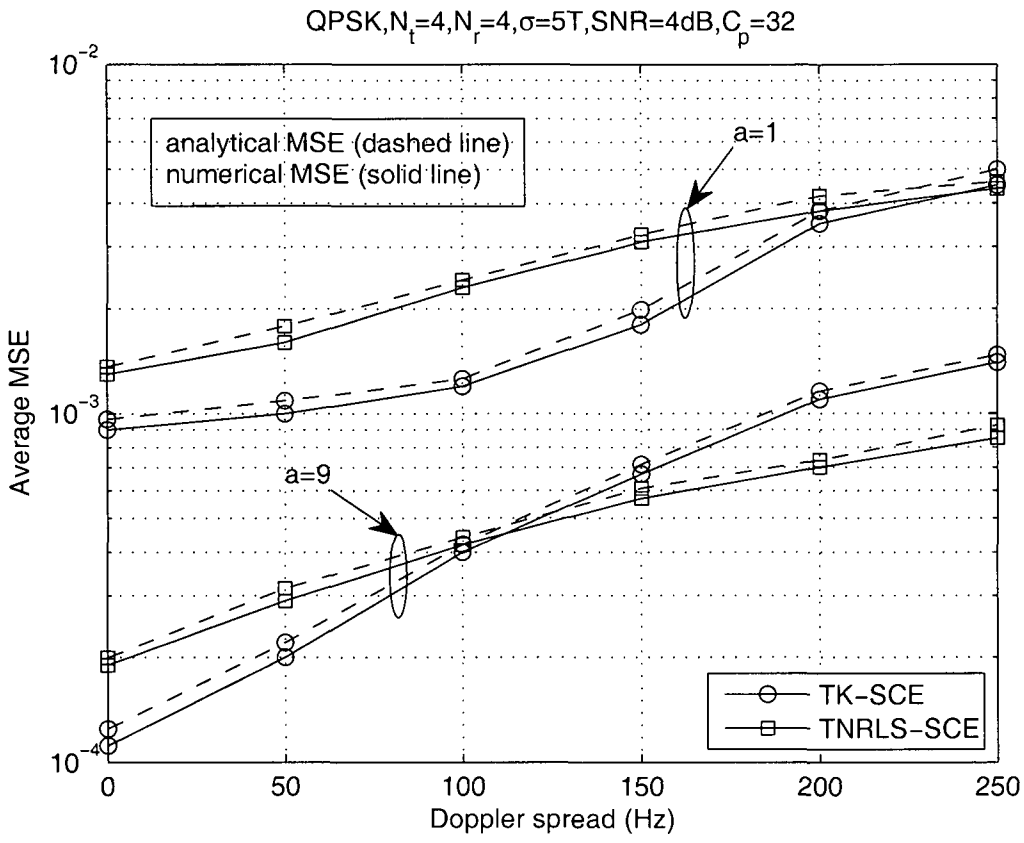

Figure 4.10: Impact of different Doppler spreads over steady MSEs of TK-SCE and TNRLS-SCE with $M = 128$ symbols per block, $N_t = 4$ transmit antennas, $N_r = 4$ receive antennas, SNR = 4 dB and RMS delay $\sigma = 5\ T$.

ing 5 iterations, the Turbo UCE schemes have a performance gap of over 1 dB to the case with perfect CSI, In slow fading channels the Turbo SCE schemes outperform the Turbo UCE schemes by around 0.7 dB.

Figure 4.6 shows the BER performance of the four channel estimators, incorporated with TSFE at a higher Doppler spread of $f_d = 200$ Hz (*i.e.*, $f_dT = 4 \times 10^{-5}$). The training overhead of 2.5% remains for TNRLS-SCE and TK-SCE, with $nTrain = 15$, and both TNRLS-UCE and TK-UCE have a higher training overhead of 4.1%, with $nTrain = 25$. The TNRLS-SCE scheme provides the best performance among all the four schemes. With 5 iterations and at BER = 10^{-4},

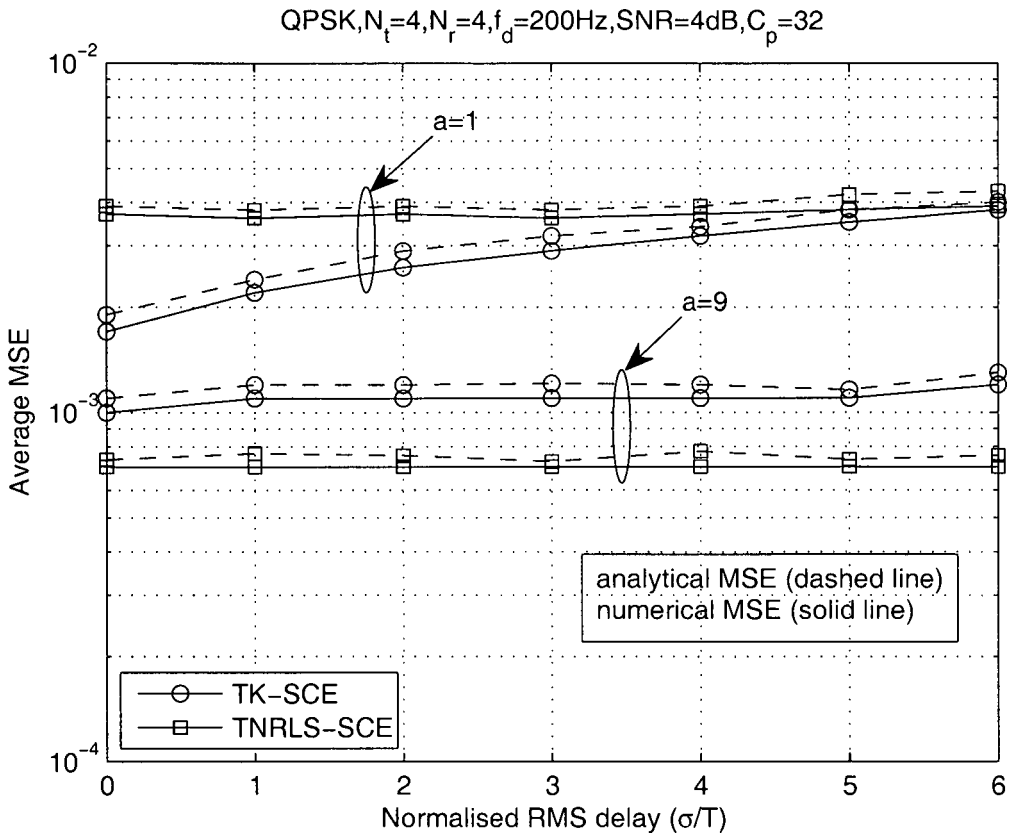

Figure 4.11: Impact of different RMS delays over steady MSEs of TK-SCE and TNRLS-SCE with $M = 128$ symbols per block, $N_t = 4$ transmit antennas, $N_r = 4$ receive antennas, SNR = 4 dB and Doppler spread $f_d = 200$ Hz.

TNRLS-SCE achieves a performance gain of around 0.3 dB over TK-SCE, and around 2 dB over TNRLS-UCE and TK-UCE. Compared to the case with perfect CSI, TNRLS-SCE with 5 iterations has a performance loss of only 0.8 dB at BER $= 10^{-4}$.

The learning curves of the proposed Turbo channel estimators at Doppler spread $f_d = 200$ Hz and SNR = 6 dB are illustrated in Figure 4.7, where the same configuration as in Figure 4.6 is employed. The horizontal and vertical axes indicate the number of blocks and average MSE, respectively. Due to the existence of the decoder, the numerical MSEs ($\hat{J}^{(q|q)}_{TK-UCE}$ in (4.79), $\hat{J}^{(q|q)}_{TK-SCE}$ in (4.78),

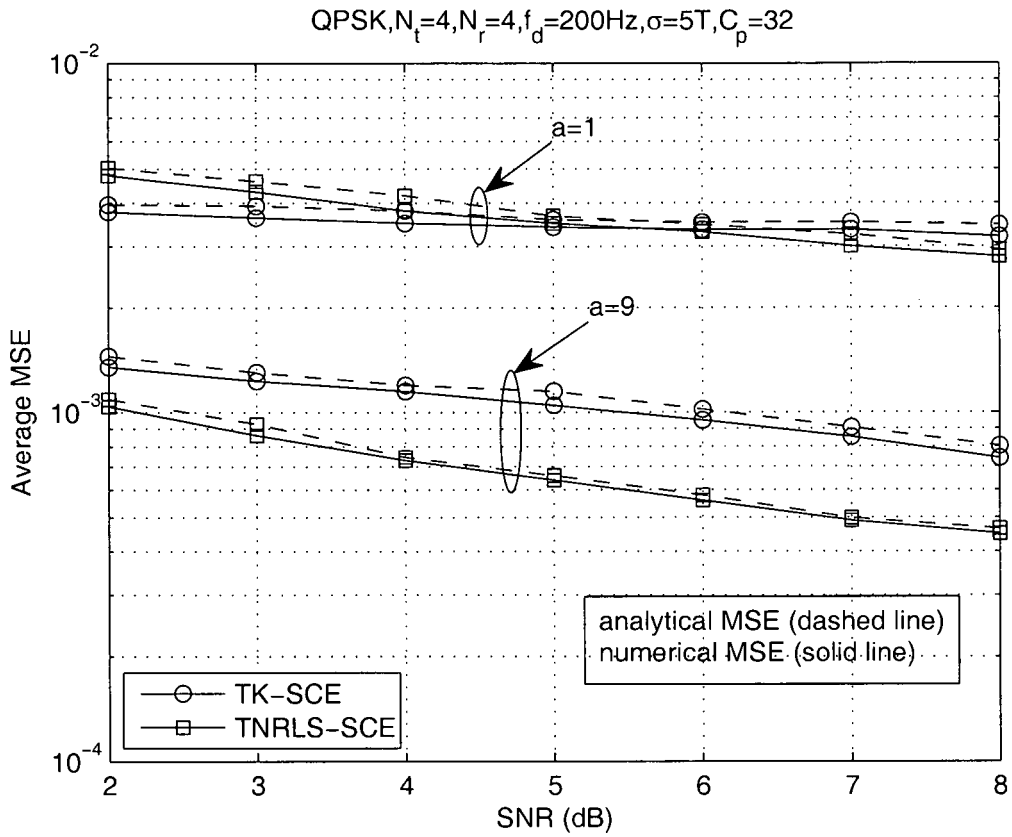

Figure 4.12: Impact of different SNRs over steady MSEs of TK-SCE and TNRLS-SCE with $M = 128$ symbols per block, $N_t = 4$ transmit antennas, $N_r = 4$ receive antennas, RMS delay $\sigma = 5\ T$, and Doppler spread $f_d = 200$ Hz.

$\hat{J}^{(q)}_{TNRLS-UCE}$ in (4.83) and $\hat{J}^{(q)}_{TNRLS-SCE}$ in (4.82)) are employed. In the code-aided channel estimation mode, 5 iterations are used. TNRLS-SCE outperforms TK-SCE with a marginal MSE gain, while TNRLS-UCE and TK-UCE provide a close performance. Compared to the Turbo UCE schemes, the Turbo SCE schemes achieve a steady-state MSE of around 1.5 dB lower, with a slightly higher convergence speed, benefiting from the correlation between adjacent frequency bins.

Figures 4.8-4.12 focus on performance of the Turbo SCE schemes, since they outperform their Turbo UCE counterparts and provide a close performance to the

case with perfect CSI, as shown in Figures 4.5-4.6. By generating Gaussian LLRs of code bits with mean $\pm a$ and variance $2a$ as in (4.74) and feeding them to the channel estimator, the simulation eliminates the impact of Turbo equalisation on the performance of Turbo channel estimation. $a = 1, 9$ are used for the absolute value of the mean of the input LLRs in Figures 4.8-4.12, where the accuracy of the performance analysis in Subsection 4.3.3 is demonstrated by the good match between the analytical MSEs and the numerical MSEs. The analytical MSEs $J^{(q|q)}_{TK-SCE}$ in (4.77) and $J^{(q)}_{TNRLS-SCE}$ in (4.81) are represented by dashed lines, and the numerical MSEs $\hat{J}^{(q|q)}_{TK-SCE}$ in (4.78) and $\hat{J}^{(q)}_{TNRLS-SCE}$ in (4.82) are denoted by solid lines.

Figure 4.8 shows the convergence behavior of TNRLS-SCE and TK-SCE in terms of MSE versus the number of blocks, using a rough initial MSE of channel estimates $J^{(0)}_{TNRLS-SCE} = J^{(0|0)}_{TK-SCE} = 0.04$. The Doppler spread is $f_d = 200$ Hz and SNR = 4 dB. With a parameter of $a = 1$, TNRLS-SCE and TK-SCE both take around 60 blocks to converge and achieve a comparable steady-state MSE of around 4×10^{-3}. With an increased parameter of $a = 9$, TNRLS-SCE and TK-SCE respectively require only around 40 blocks and 30 blocks to achieve the reduced steady-state MSEs, which are 7×10^{-4} for TNRLS-SCE and 1.1×10^{-3} for TK-SCE. This implies that with the increase of a, the absolute value of the mean of the input LLRs, both TNRLS-SCE and TK-SCE achieve a lower steady-state MSE with a higher convergence speed. With a large valued a, TNRLS-SCE outperforms TK-SCE in terms of the steady-state MSE, at a moderate cost of the convergence speed. A similar conclusion can be drawn from Figure 4.9, which has the same configuration as Figure 4.8 except for a very small initial MSE of $J^{(0)}_{TNRLS-SCE} = J^{(0|0)}_{TK-SCE} = 4\times10^{-4}$. In this case, the MSE increases until convergence. Figures 4.10-4.12 show the impact of Doppler spreads, RMS delay

spreads and SNRs on the steady-state MSEs of the Turbo SCE schemes.

Figure 4.10 demonstrates the impact of Doppler spreads f_d varying from 0 Hz (*i.e.*, no Doppler effect) to 250 Hz on the steady-state MSEs of the Turbo SCE schemes, with SNR = 4 dB and RMS delay spread $\sigma = 5\ T$. The steady-state MSEs of TNRLS-SCE and TK-SCE both increase with the reinforcement of the Doppler effect. With a parameter of $a = 1$, TNRLS-SCE outperforms TK-SCE at $f_d < 200$ Hz, and both the channel estimators achieve a comparable steady-state MSE under a stronger Doppler effect. With an increased parameter of $a = 9$, TNRLS-SCE achieves a lower steady-state MSE than TK-SCE at $f_d > 100$ Hz and TK-SCE still outperforms TNRLS-SCE at $f_d < 100$ Hz. This implies that TNRLS-SCE is more robust against medium to fast fading channels than TK-SCE.

In Figure 4.11, the effect of the RMS delay spreads, varying from 0 (*i.e.*, flat fading channels) to 6 T (*i.e.*, $\sigma = 1.2\ \mu s$), is shown, with Doppler spread $f_d = 200$ Hz and SNR = 4 dB. With a parameter of $a = 9$, both TNRLS-SCE and TK-SCE are insensitive to frequency selectivity, and the former obtains a steady-state MSE, which is around 3×10^{-4} lower compared to the latter. With a decreased parameter of $a = 1$, TNRLS-SCE is still robust against frequency selective fading channels, and the steady-state MSE of TK-SCE increases with the increase of the RMS delay spread.

The impact of different SNRs on the steady-state MSEs of Turbo SCE is shown in Figure 4.12, with Doppler spread $f_d = 200$ Hz and RMS delay spread $\sigma = 5\ T$. The SNR ranges from 2 dB to 8 dB. TNRLS-SCE tracks channel variations more effectively than TK-SCE, especially at a high SNR. Only with low SNR < 5 dB and $a = 1$, TK-SCE slightly outperforms TNRLS-SCE. With an increased parameter of $a = 9$, TNRLS-SCE outperforms TK-SCE in the whole

range of SNRs.

4.5 Summary

Two types of hard-input iterative channel estimation methods have been incorporated with TSFE, assuming uncorrelated frequency bins (for UCE) and correlated frequency bins (for SCE). In particular, the LMS-SCE based TSFE is effective to track the channel variations, with performance close to the perfect CSI case even in the fast fading environment. LMS-SCE also has a reasonably low complexity as well as the highest convergence speed among all the channel estimation methods.

One of the contributions of this chapter is to proposed adaptive TRLS-SCE frequency-domain channel estimation schemes for MIMO SC-FDE, incorporated with the low complexity TSFE. While achieving a tremendous complexity reduction, the simplified TRLS-SCE channel estimation provides nearly the same performance as TRLS-SCE channel estimation. It requires a low training overhead below 4% to provide a performance comparable to the case with perfect CSI. TRLS-SCE channel estimation also outperforms the so-called LMS-SCE channel estimation [61] in terms of the convergence speed.

The third category of Turbo channel estimation for MIMO SC-FDE systems, based on the Kalman filtering and NRLS criteria, is also investigated. Under each criterion, a SCE scheme and a UCE scheme are proposed to update the channel estimate iteratively. By utilising the correlation across frequency bins, the Turbo SCE schemes outperform their Turbo UCE counterparts with a comparable complexity, and provide a performance close to the case with perfect CSI. A performance analysis has been provided in terms of the analytical MSEs of the Turbo SCE schemes, which provide a good match with the numerical results.

With the increase of parameter a, the absolute value of the mean of the input LLRs to the channel estimator, both TNRLS-SCE and TK-SCE achieve a lower steady-state MSE with a higher convergence speed. In particular, given a large valued a, which is close to the practical channel model in wireless communications, TNRLS-SCE outperforms TK-SCE in terms of the steady-state MSE, with a wide range of SNRs and RMS delay spreads, and a medium to high Doppler spread.

Chapter 5

Adaptive Turbo Multiuser Detection and Co-Channel Interference Suppression for MIMO SC-FDMA Systems

SC-FDMA [71, 72], an evolution of OFDMA, has been proposed as a strong candidate for the uplink communications of future wireless systems by the Third Generation Partnership Project (3GPP) [73], due to its simplicity of implementation and robustness against highly dispersive channels. Compared to OFDMA, SC-FDMA has a lower PAPR [71, 74], while achieving a similar performance and requiring the same overall complexity. SC-FDMA can also be regarded as a special case of cyclic prefix code division multiple access (CP-CDMA), and significantly outperforms the latter at high user loads [75].

Among the little work on SC-FDMA in the literature, most has focused on PAPR [73, 74, 76] and channel-dependant scheduling [73, 76] problems. In [72],

a multiuser SC-FDMA system was proposed, which combines FDE [6, 5] and iterative interference cancellation at the receiver. However, [72] did not consider channel coding, channel estimation and multiple antennas for each user. To the best of the knowledge, no work has been reported on adaptive Turbo equalisation and CCIS for SC-FDMA, which are practical challenges in system design.

Adaptive Turbo equalisation has been shown to be effective to combat frequency selective and time-varying channels, by utilising the soft decisions on signals for iterative equalisation and channel estimation. Most previous work on adaptive Turbo equalisation focused on time-domain processing. However, the characteristics of SC-FDMA lead to a preference for frequency-domain processing due to its low complexity. In [61], a Turbo space-frequency equalisation (TSFE) structure was proposed for SC MIMO systems. In [58], a low complexity Turbo adaptive frequency-domain channel estimator was proposed. However, [61] and [58] were based on time-division multiple access (TDMA) systems. It was indicated in [76] that SC-FDMA can perform adaptive channel estimation on each user's distinct subcarrier set, which is robust against dispersive channels and has a low complexity. However, no implementation details were included in [58].

CCI has become an increasingly critical challenge in wireless communications. It was shown that Turbo equalisation is robust to CCI if the correlation matrix of CCI is estimated properly [77]. In [78] and [79], filters to suppress the asynchronous CCI were proposed for OFDM systems. However, no work has been reported on CCI suppression for SC-FDMA systems. This chapter investigate an uplink MIMO SC-FDMA system with adaptive Turbo multiuser detection and CCI suppression. The work is different in that a new solution to adaptive Turbo channel estimation for SC-FDMA in the presence of unknown CCI is proposed, with multiple antennas employed for each user as well as the base station. TSFE

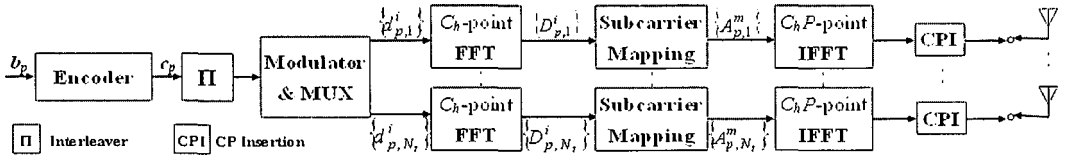

Figure 5.1: Block diagram of the transmitter of user $p(p = 0, \cdots, P-1)$ in a MIMO SC-FDMA system.

[61] is extended for the case of Turbo SC-FDMA in the presence of unknown CCI. Turbo SC-FDMA is found to significantly outperform Turbo OFDMA counterpart especially in dispersive channels with a comparable complexity. To combat unknown CCI, temporal low pass smoothing and an efficient matrix decomposition technique are utilised to effectively improve the accuracy in estimation of the spatial correlation matrix of unknown CCI plus noise. The proposed CCI suppression scheme, incorporated with the simplified Turbo RLS channel estimation and Turbo SC-FDMA, outperforms the previously proposed CCI suppression scheme. In particular, the proposed CCI suppression scheme provides very close performance to the case with perfect CSI.

Section 5.1 first presents the system model of adaptive Turbo SC-FDMA. The Turbo detection and CCIS structure for SC-FDMA is proposed in Section 5.2. Section 5.3 investigates simplified Turbo frequency-domain RLS channel estimation. Section 5.4 introduces estimation of spatial correlation matrix of unknown CCI plus noise. Simulation results are shown in Section 5.5, and the conclusion is drawn in Section 5.6.

5.1 System Model

An uplink MIMO SC-FDMA system with N_t transmit antennas for each of the P desired users, and N_r receive antennas at the base station is considered. The

system first considers the system without CCI, then with CCI. The block diagram of the transmitter of user $p(p = 0, \cdots, P-1)$ is depicted by Figure 5.1. For simplicity, all users are assumed to employ the same modulation and the same length of bit sequences. For the pth $(p = 0, \cdots, P-1)$ user, the information bit sequence $\mathbf{b}_p$ is encoded into an ECC sequence $\mathbf{c}_p$, which is then interleaved and passed to the modulator. The modulator maps the interleaved version of $\mathbf{c}_p$ into the corresponding symbols according to the symbol alphabet $\boldsymbol{\alpha} = \{\alpha_1, \cdots, \alpha_S\}$, where $\alpha_s (s = 1, \cdots, S)$ has unit symbol energy. The modulated data sequence is then split into N_t transmission subsequences, each containing C_h symbols. Let $d^i_{p,n} (i = 0, \cdots, C_h - 1)$ denote the ith symbol in a subsequence transmitted by the nth $(n = 1, \cdots, N_t)$ antenna. On each transmit antenna, the subsequence $\left\{d^i_{p,n}\right\}$ is first transferred into the frequency-domain subsequence $\left\{D^i_{p,n}\right\}$ by C_h-point FFT, which is latter mapped to subcarriers. The mapped frequency-domain subsequence $\left\{A^m_{p,n}\right\}$ has C_h non-zero elements and $C_h(P-1)$ zeros as follows:

$$A^m_{p,n} = \begin{cases} D^i_{p,n}, & m = iP + p \\ 0, & otherwise \end{cases} \tag{5.1}$$

where the interleaved mapping [76] is employed, which leads to the least fluctuation over the time-domain transmitted signals, and more importantly avoids allocating adjacent subcarriers simultaneously in a deep fade to the same user. The mapped frequency-domain sequence $\left\{A^m_{p,n}\right\} (m = 0, \cdots, C_h P - 1)$ is finally transferred back to the time domain by $C_h P$-point IFFT for final block transmission.

The overall channel memory is assumed to be N, lumping the effects of the transmit filter, receive filter and physical channel. To implement SC-FDE, each block is prepended with a CP, which is the replica of the last N symbols in the

block. The CP is discarded at the receiver to remove the inter-block interference and to make the channel appear to be circular. The received signals are transferred into the frequency domain by C_hP-point FFT. Define $\tilde{\mathbf{X}}^m$ of length N_r as the receive signal vector at the mth ($m = 0, \cdots, C_hP - 1$) subcarrier, which is given by

$$\tilde{\mathbf{X}}^m = P \sum_{p=0}^{P-1} \sum_{n=1}^{N_t} \tilde{\mathbf{H}}_{p,n}^m A_{p,n}^m + \tilde{\mathbf{N}}^m \tag{5.2}$$

where the constant P makes the transmitted signal unit energy, $\tilde{\mathbf{H}}_{p,n}^m$ denotes the channel response vector at the mth subcarrier with respect to the nth ($n = 1, \cdots, N_t$) transmit antenna associated with the pth ($p = 0, \cdots, P - 1$) user, and $\tilde{\mathbf{N}}^m$ the DFT of the AWGN with the single-sided PSD N_0.

According to (5.1), $\tilde{\mathbf{X}}^m (m = 0, \cdots, C_h - 1)$ can be associated with an independent user. Thus, let $\mathbf{X}_p^m (m = 0, \cdots, C_h - 1; (p = 0, \cdots, P - 1))$ as:

$$\mathbf{X}_p^m = P \sum_{n=1}^{N_t} \mathbf{H}_{p,n}^m D_{p,n}^m + \mathbf{N}_p^m \tag{5.3}$$

where $\mathbf{X}_{m\%p}^{\lfloor m/p \rfloor} = \tilde{\mathbf{X}}^m$, $\mathbf{H}_{p,n}^m = \tilde{\mathbf{H}}_{p,n}^{mP+p}$, and $\mathbf{N}_{m\%p}^{\lfloor m/p \rfloor} = \tilde{\mathbf{N}}^m$.

Let $\mathbf{G}_p^m$ denote the CCI plus noise vector on the mth ($m = 0, \cdots, C_h - 1$) subcarrier associated with the pth ($p = 0, \cdots, P - 1$) user, which is modeled as a time-uncorrelated colored zero-mean Gaussian random process. The received signals with CCI can be written as:

$$\mathbf{X}_p^m = P \sum_{n=1}^{N_t} \mathbf{H}_{p,n}^m D_{p,n}^m + \mathbf{G}_p^m \tag{5.4}$$

As in [61], the mean $\mu_{p,n}^i$ and variance $v_{p,n}^i$ of $d_{p,n}^i$ are computed based on the LLR:

$$\mu_{p,n}^i = E(d_{p,n}^i) = \sum_{\alpha_s \in \boldsymbol{\alpha}} \alpha_s P(d_{p,n}^i = \alpha_s) \tag{5.5}$$

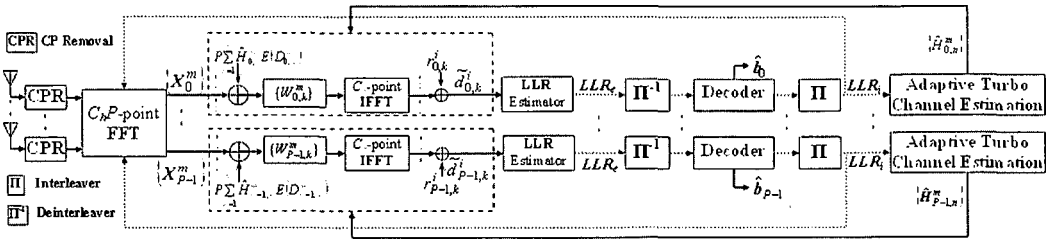

Figure 5.2: Block diagram of the receiver with adaptive Turbo multiuser detection and CCI suppression.

$$v_{p,n}^{i} = Cov(d_{p,n}^{i}, d_{p,n}^{i}) = \sum_{\alpha_s \in \boldsymbol{\alpha}} |\alpha_s|^2 P(d_{p,n}^{i} = \alpha_s) - |\mu_{p,n}^{i}|^2 \tag{5.6}$$

In particular, if only one user is employed in the system (*i.e.*, $P = 1$), MIMO SC-FDMA reduces to MIMO SC-FDE as depicted in Figure 3.1, where the CCI is still modeled as the time-uncorrelated colored zero-mean Gaussian random process.

5.2 Turbo Multiuser Detection and CCI Suppression

Figure 5.2 depicts the iterative receiver for MIMO SC-FDMA, where C_hP subcarriers on each receive antenna are separated according to (5.1) before equalisation. Each user employs its own Turbo equaliser, adaptive Turbo channel estimator, and decoder to detect signals. For a particular user $p(p = 0, \cdots, P-1)$, the frequency-domain received signals are first equalised by a low complexity block-wise weight vector, and the residual interference is then removed by a time-domain constant. The LLR estimator [61] and decoder exchange the extrinsic LLRs through the deinterleaver and interleaver. The estimate of the information bit sequence, denoted by $\hat{\mathbf{b}}_p$, is generated by the decoder.

The block-wise TSFE in [61] is extended to the case of multiuser MIMO

SC-FDMA in the presence of unknown CCI. The equalisation coefficients are determined to minimise the MSE cost function:

$$J_{p,k}^{i} = E\left|\tilde{d}_{p,k}^{i} - d_{p,k}^{i}\right|^{2} \tag{5.7}$$

Let $\mathbf{W}_{p,k}^{m}$ denote the length N_r weight vector for the mth ($m = 1, \cdots, C_h - 1$) subcarrier at the kth ($k = 1, \cdots, N_t$) transmit antenna of the pth ($p = 0, \cdots, P - 1$) user, and $\hat{\mathbf{H}}_{p,n}^{m}$ the estimate of $\mathbf{H}_{p,n}^{m}$. It can be derived that $\mathbf{W}_{p,k}^{m}$ is given by

$$\mathbf{W}_{p,k}^{m} = \frac{\bar{\mathbf{R}}_{p}^{m^{-1}} \hat{\mathbf{H}}_{p,k}^{m}}{1 + \frac{P(1-\bar{v}_{p,k})}{C_h} \sum_{m=0}^{C_h-1} \hat{\mathbf{H}}_{p,k}^{m^H} \bar{\mathbf{R}}_{p}^{m^{-1}} \hat{\mathbf{H}}_{p,k}^{m}} \tag{5.8}$$

where $\bar{v}_{p,n} = \frac{1}{C_h} \sum_{i=0}^{C_h-1} v_{p,n}^{i}$, the average variance over the block, is applied to reduce the computational complexity [61], and $\bar{\mathbf{R}}_{p}^{m}$ is given by

$$\bar{\mathbf{R}}_{p}^{m} = P \sum_{n=1}^{N_t} \bar{v}_{p,n} \hat{\mathbf{H}}_{p,n}^{m} \hat{\mathbf{H}}_{p,n}^{m^H} + \mathbf{\Lambda}_{p}^{m} \tag{5.9}$$

where $\mathbf{\Lambda}_{p}^{m}$ denotes the correlation matrix of CCI plus noise on the mth ($m = 0, \cdots, C_h - 1$) subcarrier.

The resulting equaliser output $\tilde{d}_{p,k}^{i}$ is give by

$$\tilde{d}_{p,k}^{i} = \frac{1}{C_h} \sum_{m=1}^{C_h-1} \mathbf{W}_{p,k}^{m^H} \left[\mathbf{X}_{p}^{m} - P \sum_{n=1}^{N_t} \hat{\mathbf{H}}_{p,n}^{m} E\left(D_{p,n}^{m}\right) \right] e^{j2\pi mi/C_h} + r_{p,k}^{i} \tag{5.10}$$

where $E\left(D_{p,n}^{m}\right)$ ($m = 0, \cdots, C_h - 1$) is the DFT of $\mu_{p,n}^{i}$, and

$$r_{p,k}^{i} = \frac{P\mu_{p,k}^{i}}{C_h} \sum_{m=0}^{C_h-1} \mathbf{W}_{p,k}^{m^H} \hat{\mathbf{H}}_{p,k}^{m} \tag{5.11}$$

It is shown in Figure 5.2 that $\left\{\mathbf{W}_{p,k}^{m}\right\}$ ($m = 0, \cdots, C_h - 1; p = 0, \cdots, P - 1$) is

employed to detect substream $\left\{d_{p,k}^{i}\right\}(i=0,\cdots,C_h-1)$ in the frequency domain. Then, the frequency-domain equalised signals are transferred back into the time domain, and the residual interference is removed by adding a constant $r_{p,k}^{i}$.

5.3 Simplified Turbo RLS Channel Estimation

The simplified RLS based Turbo channel estimation performs for each user independently. All blocks are assumed to be synchronous. The channel estimator first operates in the training mode as in [58]. In the code-aided channel estimation mode, soft decisions on signals in each iteration are used for Turbo channel estimation.

Let q denote the block index. Define $\mathbf{X}_{p,l}^{(q)}$ of size $1\times C_h$ as the all-subcarrier received signal vector at the lth ($l=1,\cdots,Nr$) receive antenna corresponding to the pth user and $\mathbf{N}_{p,l}^{(q)}$ the corresponding noise vector. Also define $\tilde{\mathbf{D}}_{p}^{(q)} = mat(\mathbf{D}_{p}^{0(q)}\cdots\mathbf{D}_{p}^{C_h-1(q)})$ and $\mathbf{\Gamma}_{p,l}^{(q)} = \left[\mathbf{\Gamma}_{p,l}^{0\ (q)}\cdots\mathbf{\Gamma}_{p,l}^{C_h-1(q)}\right]$, where $\mathbf{D}_{p}^{m(q)} = \left[D_{p,1}^{m\ (q)}\cdots D_{p,N_t}^{m\ (q)}\right]^T$ and $\mathbf{\Gamma}_{p,l}^{m\ (q)} = \left[H_{p,l1}^{m\ (q)}\cdots H_{p,lN_t}^{m\ (q)}\right](m=0,\cdots,C_h-1)$ denotes the channel response vector at the mth subcarrier with respect to the lth receive antenna. Then,

$$\mathbf{X}_{p,l}^{(q)} = P\mathbf{\Gamma}_{p,l}^{(q)}\tilde{\mathbf{D}}_{p}^{(q)} + \mathbf{N}_{p,l}^{(q)} \tag{5.12}$$

At the lth receive antenna, $\mathbf{\Gamma}_{p,l}^{(q)}$ can be expressed as:

$$\mathbf{\Gamma}_{p,l}^{(q)} = \boldsymbol{\tau}_{p,l}^{(q)}\tilde{\mathbf{F}}_{p}\,, \tag{5.13}$$

where $\boldsymbol{\tau}_{p,l}^{(q)}(p=0,\cdots,P-1)$ of size $1\times N_t(N+1)$ is the channel impulse response vector with respect to the lth receive antenna, and $\tilde{\mathbf{F}}_p$ of size $N_t(N+1)\times N_tC_h$ is the Fourier transformation matrix corresponding to the interleaved mapping.

The Turbo RLS channel estimator aims to minimise

$$J(\hat{\boldsymbol{\tau}}_{p,l}^{(q)}) = \sum_{i=1}^{q} \lambda^{q-i} E\left\{\|\mathbf{X}_{p,l}^{(i)} - P\hat{\boldsymbol{\tau}}_{p,l}^{(q)} \tilde{\mathbf{F}}_p \tilde{\mathbf{D}}_p^{(i)}\|^2\right\} (l = 1, \cdots, N_r) \tag{5.14}$$

with respect to $\hat{\boldsymbol{\tau}}_{p,l}^{(q)}$ that is the estimate of $\boldsymbol{\tau}_{p,l}^{(q)}$. λ is the forgetting factor. The solution to $\hat{\boldsymbol{\tau}}_{p,l}^{(q)}$ is given by

$$\hat{\boldsymbol{\tau}}_{p,l}^{(q)} = \boldsymbol{\Psi}_{p,l}^{(q)^H} \boldsymbol{\Phi}_p^{(q)^{-1}} \tag{5.15}$$

where

$$\boldsymbol{\Phi}_p^{(q)} = \lambda \boldsymbol{\Phi}_p^{(q-1)} + P^2 \tilde{\mathbf{F}}_p E\left(\tilde{\mathbf{D}}_p^{(q)} \tilde{\mathbf{D}}_p^{(q)^H}\right) \tilde{\mathbf{F}}_p^H \tag{5.16}$$

$$\boldsymbol{\Psi}_{p,l}^{(q)} = \lambda \boldsymbol{\Psi}_{p,l}^{(q-1)} + P\tilde{\mathbf{F}}_p \left(PE\left(\tilde{\mathbf{D}}_p^{(q)} \tilde{\mathbf{D}}_p^{(q)^H}\right) \tilde{\mathbf{F}}_p^H \hat{\boldsymbol{\tau}}_{p,l}^{(q-1)^H} + E(\tilde{\mathbf{D}}_p^{(q)}) \bar{\mathbf{e}}_{p,l}^{(q)^H}\right) \tag{5.17}$$

where $E(\tilde{\mathbf{D}}_p^{(q)}) = mat(E(\mathbf{D}_p^{0(q)}) \cdots E(\mathbf{D}_p^{C_h-1(q)}))$ with $E(\mathbf{D}_p^{m(q)}) = \left[E(D_{p,1}^{m\ (q)}) \cdots E(D_{p,N_t}^{m\ (q)})\right]^T$.

$E\left(\tilde{\mathbf{D}}_p^{(q)} \tilde{\mathbf{D}}_p^{(q)^H}\right)$ is a diagonal matrix, since its off-diagonal elements average out to zero so long as λ is close to 1 [58]. In the scenario of PSK modulations, $E\left(\tilde{\mathbf{D}}_p^{(q)} \tilde{\mathbf{D}}_p^{(q)^H}\right) \simeq C_h \mathbf{I}_{N_t C_h}$ regardless of LLRs. Thus, (5.16) and (5.17) respectively reduce to

$$\boldsymbol{\Phi}_p^{(q)} \simeq \frac{C_h P^2}{1-\lambda} \tilde{\mathbf{F}}_p \tilde{\mathbf{F}}_p^H \tag{5.18}$$

$$\boldsymbol{\Psi}_{p,l}^{(q)} \simeq \lambda \boldsymbol{\Psi}_{p,l}^{(q-1)} + P\tilde{\mathbf{F}}_p \left(C_h P \tilde{\mathbf{F}}_p^H \hat{\boldsymbol{\tau}}_{p,l}^{(q-1)^H} + E(\tilde{\mathbf{D}}_p^{(q)}) \bar{\mathbf{e}}_{p,l}^{(q)^H}\right) \tag{5.19}$$

where $\bar{\mathbf{e}}_{p,l}^{(q)} = \mathbf{X}_{p,l}^{(q)} - P\hat{\boldsymbol{\Gamma}}_{p,l}^{(q-1)} E\left(\tilde{\mathbf{D}}_p^{(q)}\right)$. Using (5.18), (5.19) and (5.15), it is achieved that

$$\hat{\boldsymbol{\tau}}_{p,l}^{(q)} = \hat{\boldsymbol{\tau}}_{p,l}^{(q-1)} + \frac{1-\lambda}{C_h P} \bar{\mathbf{e}}_{p,l}^{(q)} E(\tilde{\mathbf{D}}_p^{(q)})^H \tilde{\mathbf{F}}_p^H \left(\tilde{\mathbf{F}}_p \tilde{\mathbf{F}}_p^H\right)^{-1} \tag{5.20}$$

In particular, $\tilde{\mathbf{F}}_p \tilde{\mathbf{F}}_p^H = C_h \mathbf{I}_{N_t(N+1)}$ with the interleaved mapping as shown in (5.1).

Therefore, (5.20) reduces to

$$\hat{\tau}_{p,l}^{(q)} = \hat{\tau}_{p,l}^{(q-1)} + \frac{1-\lambda}{C_h^2 P}\bar{e}_{p,l}^{(q)} E(\tilde{\mathbf{D}}_p^{(q)})^H \tilde{\mathbf{F}}_p^H \tag{5.21}$$

Compared to the original Turbo RLS channel estimator whose complexity is on the order of C_h^3, the simplified Turbo RLS channel estimator requires a much lower complexity on the order of C_h. What subcarrier mapping scheme is employed has no big impact on the overall computational complexity on the simplified RLS channel estimation, since $\left(\tilde{\mathbf{F}}_p \tilde{\mathbf{F}}_p^H\right)^{-1}$ is off-line computation.

5.4 Estimation of Spatial Correlation Matrix of Interference plus Noise

The spatial correlation matrix of interference plus noise $\mathbf{\Lambda}_p^m (m = 0, \cdots, C_h - 1)$ in (5.9) is estimated for each user independently.

5.4.1 Temporal CCI Suppression

A temporal CCI suppression (TCCIS) method is first investigated, where $\tilde{\mathbf{\Lambda}}_p^m$, the coarse estimate of $\mathbf{\Lambda}_p^m$, is obtained by averaging temporal samples over B training and data blocks [80]:

$$\tilde{\mathbf{\Lambda}}_p^m = \frac{1}{B}\sum_{q=1}^{B} \frac{1}{C_h P} \tilde{\mathbf{G}}_p^m \tilde{\mathbf{G}}_p^{m^H} \tag{5.22}$$

where $\tilde{\mathbf{G}}_p^m$ is the estimate of $\mathbf{G}_p^m$ in 5.4. $\tilde{\mathbf{G}}_p^m$ is given by

$$\tilde{\mathbf{G}}_p^m = \mathbf{X}_p^m - P\sum_{n=1}^{N_t} \hat{\mathbf{H}}_{p,n}^m D_{p,n}^m \tag{5.23}$$

in the training mode, and

$$\tilde{\mathbf{G}}_p^m = \mathbf{X}_p^m - P\sum_{n=1}^{N_t} \hat{\mathbf{H}}_{p,n}^m E\left(D_{p,n}^m\right) \tag{5.24}$$

in the code-aided channel estimation mode, respectively.

5.4.2 Low-Pass CCI Suppression

The performance of TCCIS can be improved by using the correlation between frequency bins to refine the temporal estimate $\tilde{\mathbf{\Lambda}}_p^m$. This is referred to as the low-pass CCI suppression (LPCCIS) scheme. The tentative estimate $\tilde{\mathbf{\Lambda}}_p^m$ is first obtained using 5.22. It is of interest to note that the estimated auto PSD of signal from the ith antenna can be represented by the ith diagonal element vector $\tilde{\boldsymbol{\eta}}_{p,ii}(p = 0, \cdots, P-1; i = 1, \cdots, N_r)$, which is given by

$$\tilde{\boldsymbol{\eta}}_{p,ii} = \left[\left[\tilde{\mathbf{\Lambda}}_p^0\right]_{i,i} \cdots \left[\tilde{\mathbf{\Lambda}}_p^{C_h-1}\right]_{i,i}\right] \tag{5.25}$$

The estimated mutual PSD between signals from the ith and jth antenna can be represented by the i,j-th element vector $\tilde{\boldsymbol{\eta}}_{p,ij}(p = 0, \cdots, P-1; i \neq j)$, which is given by

$$\tilde{\boldsymbol{\eta}}_{p,ij} = \left[\left[\tilde{\mathbf{\Lambda}}_p^0\right]_{i,j} \cdots \left[\tilde{\mathbf{\Lambda}}_p^{C_h-1}\right]_{i,j}\right] \tag{5.26}$$

The estimated auto PSD $\tilde{\boldsymbol{\eta}}_{p,ii}$ is transformed into the time-domain vector $\tilde{\boldsymbol{\xi}}_{p,ii}$ and the estimated mutual PSD $\tilde{\boldsymbol{\eta}}_{p,ij}$ is transformed into the time-domain vector $\tilde{\boldsymbol{\xi}}_{p,ij}$, respectively, for further processing.

Since the correlation function has the "low-pass" property [78], the middle $C_h - (2N+2)$ elements of $\tilde{\boldsymbol{\xi}}_{p,ii}$ and $\tilde{\boldsymbol{\xi}}_{p,ij}$ are nulled, respectively, as $\hat{\boldsymbol{\xi}}_{p,ii}$ and $\hat{\boldsymbol{\xi}}_{p,ij}$, which are finally transformed back to the frequency domain to obtained the

refined estimate $\hat{\boldsymbol{\eta}}_{p,ii}$ and $\hat{\boldsymbol{\eta}}_{p,ii}$. The low-pass smoothing can be summarised as follows:

$$\begin{aligned}\hat{\boldsymbol{\eta}}_{p,ii} &= \mathbf{F}\hat{\boldsymbol{\xi}}_{p,ii} \\ &= \mathbf{FL}\tilde{\boldsymbol{\xi}}_{p,ii} \\ &= \mathbf{FLF}^H\tilde{\boldsymbol{\eta}}_{p,ii}\end{aligned} \tag{5.27}$$

and

$$\hat{\boldsymbol{\eta}}_{p,ij} = \mathbf{FLF}^H\tilde{\boldsymbol{\eta}}_{p,ij} \tag{5.28}$$

where

$$\mathbf{L} = diag(\underbrace{1,\cdots,1}_{N+1},\ \underbrace{0,\cdots,0}_{C_h-(2N+2)},\underbrace{1,\cdots,1}_{N+1}) \tag{5.29}$$

However, if operating the above low-pass filter on each element vector independently, the structure of the $N_r \times N_r$ matrix $\tilde{\boldsymbol{\Lambda}}_p^m$, which is Hermitian and positive definite (PD), and has $N_r \times (N_r+1)/2$ parameters constrained, will be destroyed.

5.4.3 Cholesky Decomposition

In the area of multivariate statistics, it is a common approach to decompose the complicate covariance matrices into simpler components for further processing. There are three popular methods to use for matrix decomposition: variance correlation decomposition, spectral decomposition (singular value decomposition (SVD)) and Cholesky decomposition. While the entries of the correlation and orthogonal matrices in the variance-corrleation and spectral decompositions are still constrained, those in the lower triangle matrix of the Cholesky decomposition are always unconstrained. As a result, it becomes a unconstrained refinement

if smoothing the Cholesky decomposition of spatial covariances across different tones instead of the covariance itself, and the Hermitian and positive definite structure can be maintained. The low-triangle matrix of the Cholesky decomposition provides sufficient statistics for the covariance estimation, and can be written as:

$$\tilde{\mathbf{\Lambda}}_p^m = \tilde{\mathbf{Z}}_p^{m^H} \tilde{\mathbf{Z}}_p^m \tag{5.30}$$

where $\tilde{\mathbf{Z}}_p^m$ is an upper triangle matrix and is also called "squareroot" of the matrix $\tilde{\mathbf{\Lambda}}_p^m$. Let $\tilde{\zeta}_{p,ij} = \left[\left[\tilde{\mathbf{Z}}_p^0\right]_{i,j} \cdots \left[\tilde{\mathbf{Z}}_p^{C_h-1}\right]_{i,j}\right] (i = 1, \cdots, N_r; p = 0, \cdots, P-1; i \leq j)$, which is transferred into the time-domain vector $\tilde{\mathbf{M}}_{p,ij}$. As same as the operation on $\tilde{\boldsymbol{\eta}}_{p,ij}$, $\tilde{\mathbf{M}}_{p,ij}$ is first low-pass filtered, and then transferred back into the frequency domain to obtain $\hat{\zeta}_{p,ij} = \left[\left[\hat{\mathbf{Z}}_p^0\right]_{i,j} \cdots \left[\hat{\mathbf{Z}}_p^{C_h-1}\right]_{i,j}\right]$, where $\hat{\mathbf{Z}}_p^m$ denotes the refined estimate of $\tilde{\mathbf{Z}}_p^m$. Finally the refined estimate $\hat{\mathbf{\Lambda}}_p^m$ is reconstructed as:

$$\hat{\mathbf{\Lambda}}_p^m = \hat{\mathbf{Z}}_p^{m^H} \hat{\mathbf{Z}}_p^m \tag{5.31}$$

The Cholesky decomposition method has been used in [81] for simultaneous estimation of several covariance matrix. It was also shown that the estimation of a covariance matrix is equivalent to estimating a sequence of varying-coefficient and varying-order regression models with unconstrained coefficients.

5.5 Simulation

This section used simulation results to show performance of the proposed uplink SC-FDMA system. The performance of Turbo MIMO SC-FDE (the special case of Turbo MIMO SC-FDMA ($P = 1$)) with CCI suppression is first investigated, then Turbo MIMO SC-FDMA with CCI suppression. Since the simplified Turbo

RLS and the Turbo RLS channel estimators can be shown to provide very close performance, only the simplified Turbo RLS channel estimation incorporated with Turbo detection and CCIS is employed.

5.5.1 Simulation Setup

The MIMO SC-FDMA system employs $P = 8$ desired users, each having $N_t = 4$ transmit antennas, and there are $N_r = 4$ receive antennas at the base station. Simulation chooses a rate 1/2, memory 2 recursive systematic convolutional encoder with generator $(1 + D + D^2, 1 + D^2)$. With a symbol period of $T = 0.1$ μs, each user's overall symbol rate reaches 40 M-Baud. Each data block consists of $C_h = 128$ QPSK symbols. Both the transmit and receive filters use a raised-cosine pulse with a roll-off factor of 0.35. The physical channel is modeled by the exponential power delay profile [65] with a RMS delay spread of $\sigma = 0.5$ μs (*i.e.*, $\sigma = 5$ T). The overall channel is of memory $N = 25$. The signal-to-interference ratio (SIR) is defined as the ratio of each desired user's signal power to the overall unknown users' signal power. The SNR is defined as the spatial average ratio of the received signal power to noise power.

For the MIMO SC-FDE system, the single-user case of the MIMO SC-FDMA system, the configuration is the same as MIMO SC-FDMA, except that the symbol period is $T = 0.8$ μs and the RMS delay spread is $\sigma = 1.25$ T.

5.5.2 Simulation Results

5.5.2.1 Turbo MIMO SC-FDE with CCI Suppression

Figure 5.3 shows the BER performance of the adaptive TSFE with TCCIS and LPCCIS, compared to the case with perfect CSI. A moderate Doppler spread of

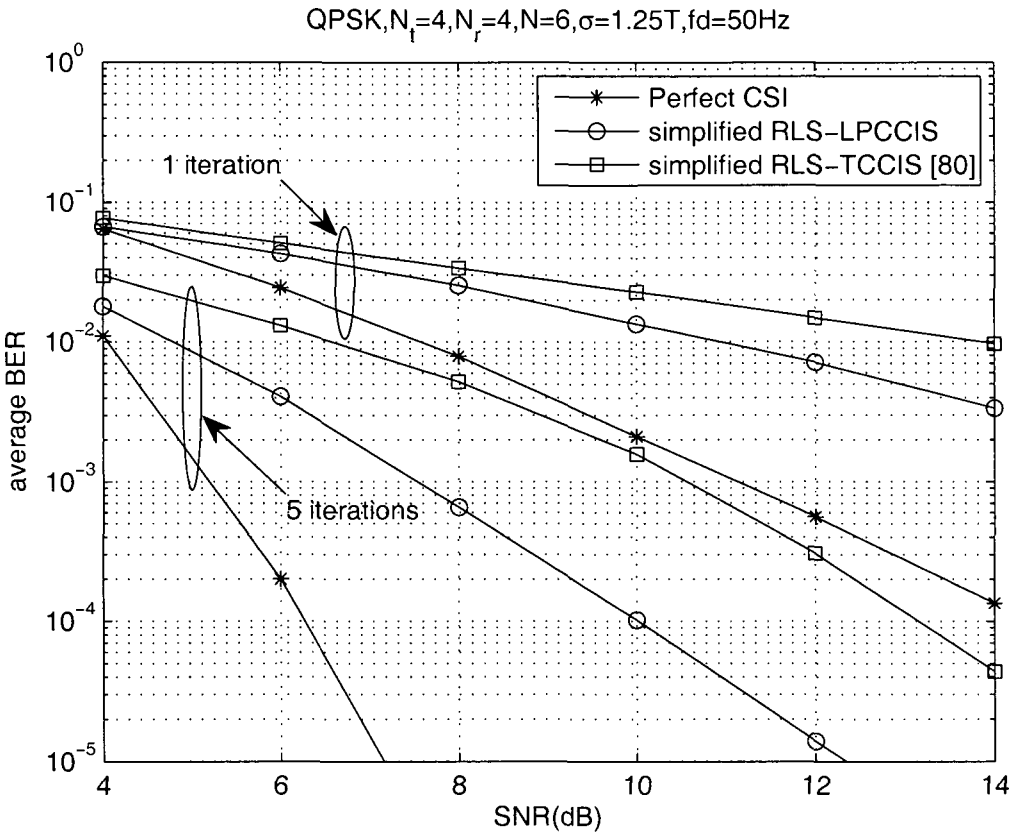

Figure 5.3: Performance of SC-FDE with adaptive Turbo detection and CCI suppression with $N_t = 4$ transmit antennas, $N_r = 4$ receive antennas, SIR = 0 dB, RMS delay $\sigma = 1.25\ T$, and Doppler spread $f_d = 50$ Hz.

$f_d = 50$ Hz and SIR = 0 dB are assumed. At this strong CCI circumstance, TSFE with LPCCIS outperforms TSFE with TCCIS by around 3 dB at BER= 10^{-4}, using 5 iterations. LPCCIS and TCCIS with 5 iterations both provide a performance of over 3 dB worse than the case with perfect CSI at BER= 10^{-4}. In this case, TSFE with both LPCCIS and TCCIS are not able to benefit from the multiuser diversity, which is the naturally inherent characteristic to Turbo SC-FDMA systems.

At higher SIR = 5 dB and Doppler spread $f_d = 50$ Hz, Figure 5.4 shows the performance improvement of the adaptive TSFE with CCI suppression, compared

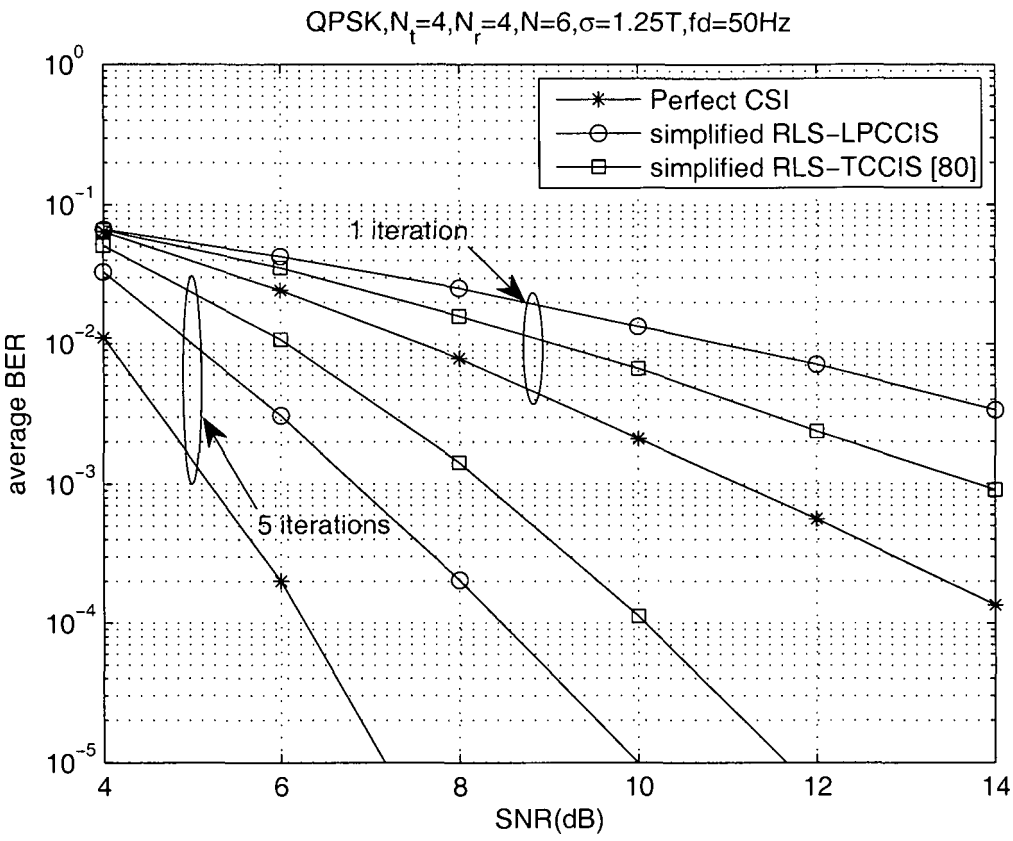

Figure 5.4: Performance of SC-FDE with adaptive Turbo detection and CCI suppression with $N_t = 4$ transmit antennas, $N_r = 4$ receive antennas, SIR = 5 dB, RMS delay $\sigma = 1.25\ T$, and Doppler spread $f_d = 50$ Hz.

to the case with perfect CSI. With the decrease of CCI and 5 iterations, the performance gap between LPCCIS and the case with perfect CSI is narrowed to around 2 dB at BER = 10^{-4} with no multiuser diversity available. At BER = 10^{-4}, there is still a 1.5 dB performance gap between TCCIS and LPCCIS with 5 iterations.

Figure 5.5 demonstrates the impact of higher Doppler spread $f_d = 200$ Hz on the performance of the adaptive TSFE with TCCIS and LPCCIS. SIR maintains 5 dB. Using 5 iterations and incorporated with adaptive TSFE, LPCCIS outperforms TCCIS by around 2 dB and underperforms the case with perfect CSI

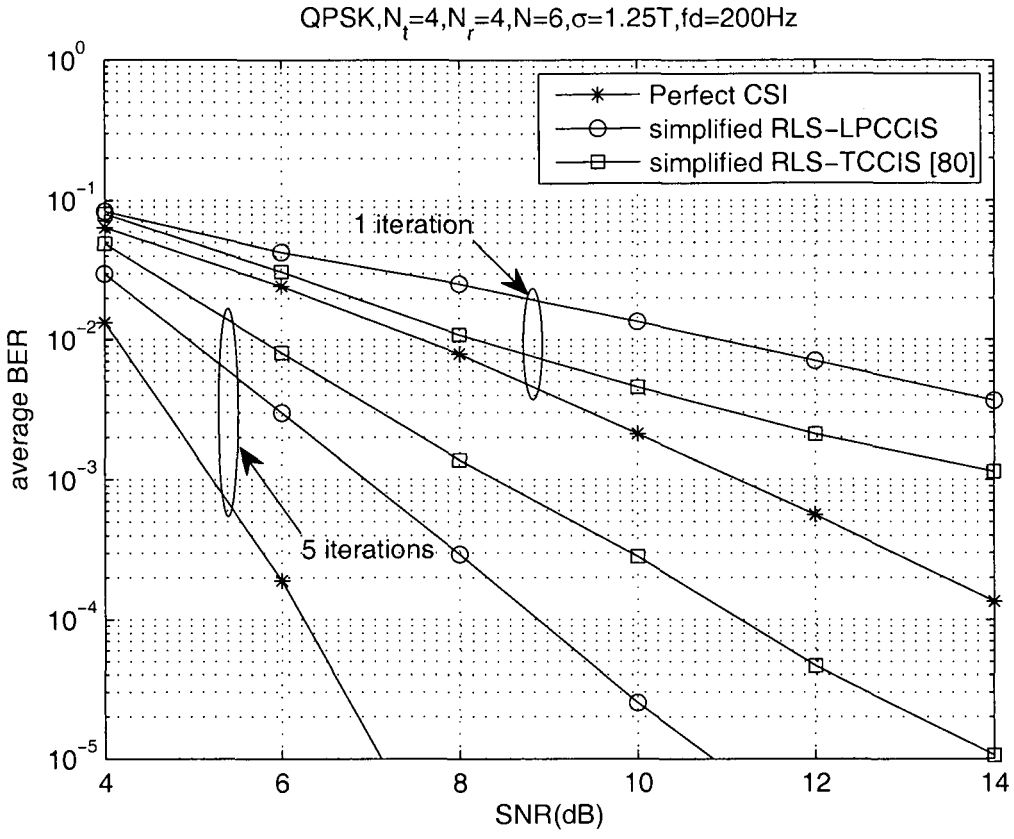

Figure 5.5: Performance of SC-FDE with adaptive Turbo detection and CCI suppression with $N_t = 4$ transmit antennas, $N_r = 4$ receive antennas, SIR = 5 dB, RMS delay $\sigma = 1.25\ T$, and Doppler spread $f_d = 200$ Hz.

also by aroudn 2 dB, respectively. In terms performance loss, the performance of LPCCIS is robust against the increase of Doppler effect.

5.5.2.2 Turbo MIMO SC-FDMA with CCI Suppression

Figure 5.6 demonstrates the average BER performance of Turbo SC-FDMA compared to its Turbo OFDMA counterpart, assuming perfect CSI and no Doppler effect. Different from Turbo SC-FDE, Turbo SC-FDMA is multiuser access scheme, which can benefit from the interleaved mapping [76]. It can be observed that Turbo SC-FDMA provides a significant performance improvement over Turbo

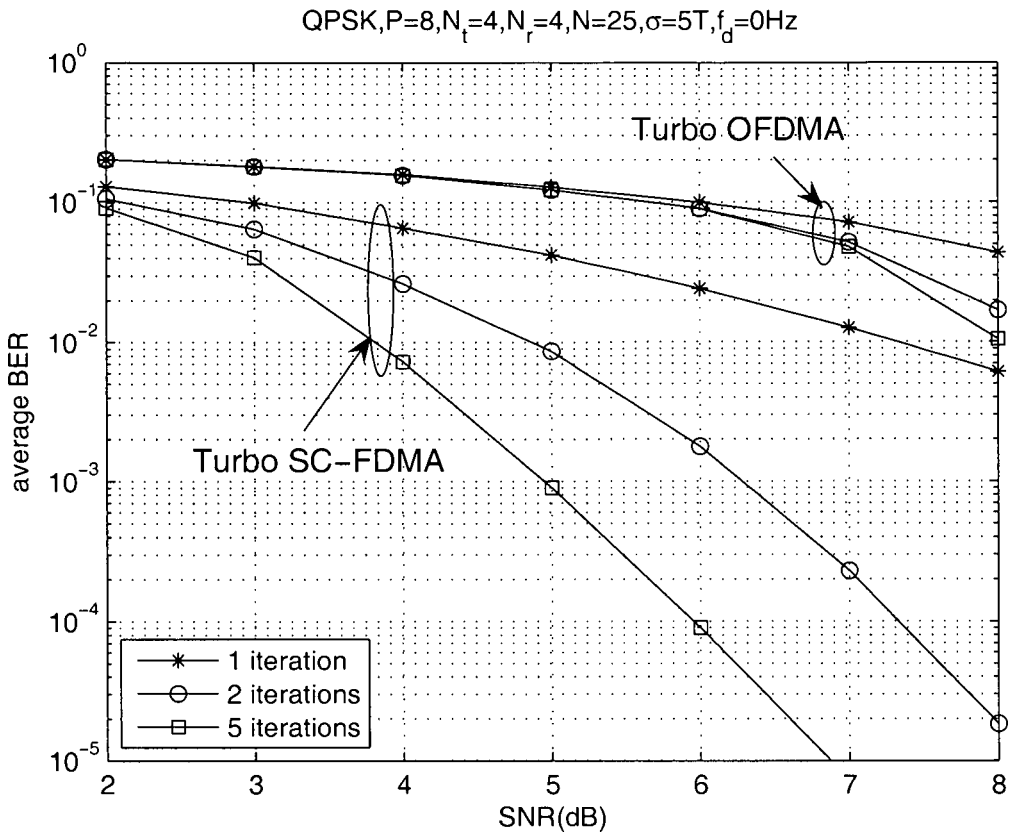

Figure 5.6: Performance of Turbo SC-FDMA and Turbo OFDMA with $N_t = 4$ transmit antennas for each of the $P = 8$ users, $N_r = 4$ receive antennas, and RMS delay $\sigma = 5\ T$.

OFDMA by achieving higher frequency diversity due to applying TSFE for each user. This is consistent with the comparison between Turbo SC-FDE and Turbo OFDM in [61]. In particular, Turbo SC-FDMA achieves a tremendous performance improvement with the increase of the number of iterations even at a relatively low SNR, while the number of iterations has little impact on performance of Turbo OFDMA at a low SNR.

Figure 5.7 investigates the performance of the adaptive Turbo SC-FDMA with CCIS at a Doppler spread $f_d = 50$ Hz and SIR = 5 dB. With the configuration 12 training blocks and 468 data blocks in each frame, the training overhead is only

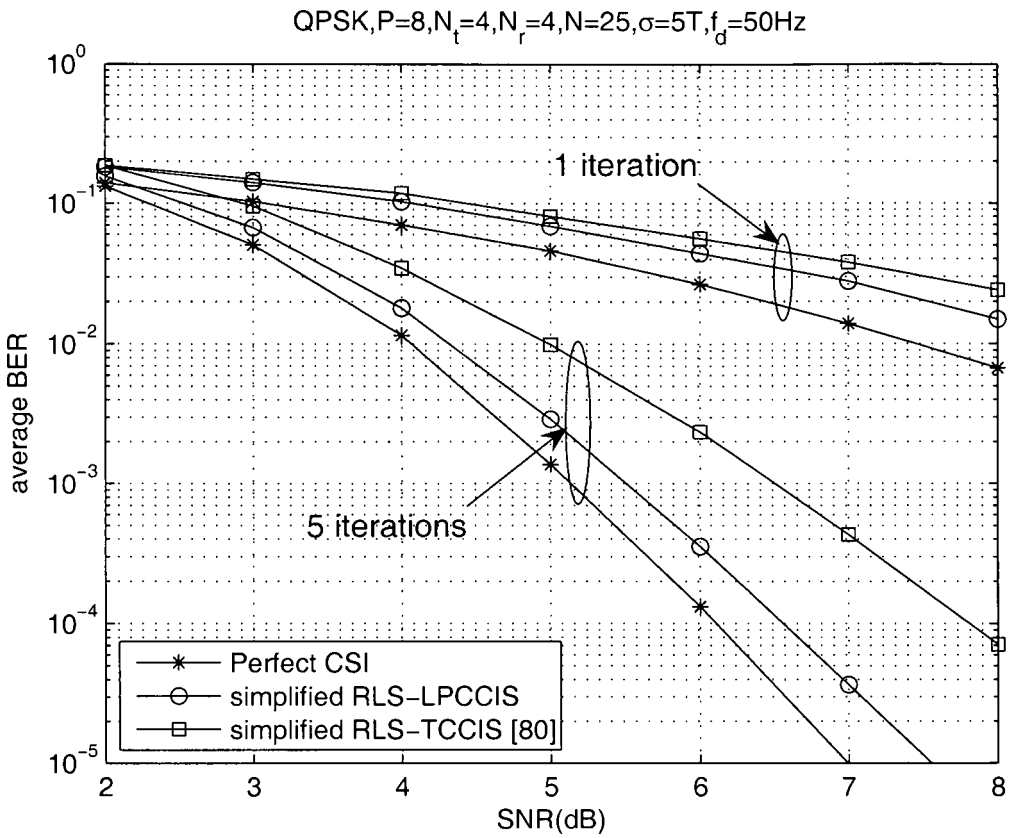

Figure 5.7: Performance of SC-FDMA with adaptive Turbo detection and CCI suppression with $N_t = 4$ transmit antennas for each of the $P = 8$ users, $N_r = 4$ receive antennas, SIR = 5 dB, RMS delay $\sigma = 5\ T$, and Doppler spread $f_d = 50$ Hz.

2.5%. The forgetting factor is $\lambda = 0.95$. Using 5 iterations, LPCCIS outperforms TCCIS [80] by over 1 dB at BER = 10^{-4}. The performance gap between LPCCIS and the case with perfect CSI is just 0.4 dB at BER = 10^{-4} using 5 iterations.

The impact of stronger CCI on performance is shown in Figure 5.8, with a reduced SIR of 3dB. The training overhead still remains only 2.5%, with all the other setup is the same as in Figure 5.7. Using 5 iterations, LPCCIS provides around 1 dB gain over TCCIS [80] with the simplified RLS channel estimation, and is around 1 dB away from the case with perfect CSI at BER = 10^{-4}.

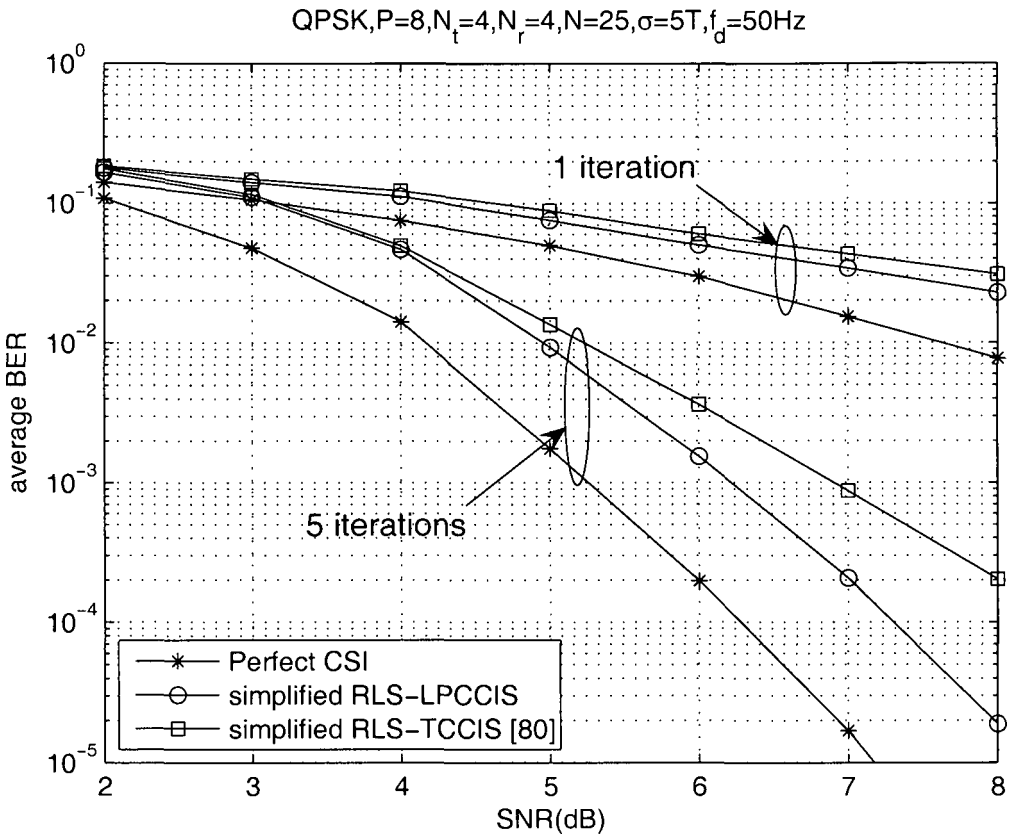

Figure 5.8: Performance of SC-FDMA with adaptive Turbo detection and CCI suppression with $N_t = 4$ transmit antennas for each of the $P = 8$ users, $N_r = 4$ receive antennas, SIR = 3 dB, RMS delay $\sigma = 5\ T$, and Doppler spread $f_d = 50$ Hz.

5.6 Summary

This chapter has proposed an adaptive Turbo multiuser detection and CCI suppression structure for the uplink MIMO SCFDMA system. Turbo SC-FDMA is found to significantly outperform its Turbo OFDMA counterpart. In the presence of unknown CCI, the proposed simplified Turbo RLS channel estimation along with LPCCIS provides performance close to the case with perfect CSI, and outperforms the existing temporal CCI suppression scheme. By achieving the additional multiuser diversity, LPCCIS incorporated with TSFE achieves better

BER performance in the MIMO SC-FDMA system than the MIMO SC-FDE system, the single-user case of the MIMO SC-FDMA system.

Chapter 6

Conclusion and Future Work

6.1 Conclusion

The thesis has investigated iterative channel equalisation and estimation for MIMO SC systems, aiming to combat frequency selective fading channels and to improve the throughput and diversity with a low computational complexity. A TSFE structure, which combines the advantages of MIMO FDE and Turbo equalisation, has been proposed. To be incorporated with TSFE in time-varying and unknown channels, iterative channel estimation has also been investigated to estimate the CSI.

Chapter 3 has proposed a low complexity adaptive TSFE structure for SC MIMO block transmission. The proposed block-wise low complexity TSFE achieves a significant complexity reduction over the symbol-wise TSFE, TTDE [47] and TFDE [47] for SC MIMO systems. With the same bandwidth efficiency, it provides the performance which is close to that of the symbol-wise TSFE, equal to that of TFDE, and better than that of TTDE. With a moderate code rate, it is shown both theoretically and numerically that SC TSFE achieves much better

performance than its TOFDM counterpart [47] for MC systems, at a comparable complexity. The performance gains of TSFE over TTDE and TOFDM increase with the increase of channel delay spread. TSFE also significantly outperforms its flat fading case with the increase of the channel delay spread, due to the frequency diversity. The oversampled TSFE is also investigated, whose complexity increases linearly, which is much lower than the complexities of FD-TLE [60] and TTDE [47].

Chapter 4 has investigated adaptive iterative channel estimation for time-varying channels. One of the contributions of this chapter is to proposed adaptive Turbo RLS frequency-domain channel estimation schemes for MIMO SC-FDE. While achieving a tremendous complexity reduction, the simplified TRLS-SCE provides nearly the same performance as TRLS-SCE. Turbo channel estimation based on Kalman filtering and NRLS criteria, is also investigated. By utilising the correlation across frequency bins, the Turbo SCE schemes outperform their Turbo UCE counterparts with a comparable complexity, and provide a performance close to the case with perfect CSI. Both TNRLS-SCE and TK-SCE achieve a lower steady-state MSE with a higher convergence speed. In particular, TNRLS-SCE outperforms TK-SCE in terms of the steady-state MSE, with a wide range of SNRs and RMS delay spreads, and a medium to high Doppler spread.

Chapter 5 has applied TSFE as well as the simplified Turbo RLS channel estimation to the uplink MIMO SCFDMA system. Turbo SC-FDMA is found to significantly outperform its Turbo OFDMA counterpart. In the presence of unknown CCI, the proposed simplified Turbo RLS channel estimation along with LPCCIS provides performance close to the case with perfect CSI, and outperforms the existing temporal CCI suppression scheme. By achieving the additional multiuser diversity, LPCCIS incorporated with TSFE achieves better BER per-

formance in the MIMO SC-FDMA system than the MIMO SC-FDE system, the single-user case of the MIMO SC-FDMA system.

6.2 Future Work

To continue the research having been done, I have the following ideas for future research activity, which will still focus on Turbo (iterative) processing for MIMO SC-FDE systems.

- Turbo processing can help improve the reliability of the data as well as the channel estimation. The same idea can be applied to improve the accuracy of carrier synchronisation, which is to compensate for the effect of frequency offset and phase noise generated by local oscillator instabilities.

- The BER performance of Turbo SC-FDMA can be improved by optimising the subcarrier mapping to different users. The similar subcarrier mapping scheme can be applied to Turbo OFDMA. The comparison will reveal how differently the same subcarrier mapping scheme works on Turbo SC-FDMA and Turbo OFDMA.

- The existence of the CP reduces the bandwidth efficiency of SC-FDE, especially in highly dispersive channels. The desired system is to reduce the length of CP, which, however, imposes extra signal processing complexity on equalisation and channel estimation, especially under Turbo processing discipline. The low complexity adaptive Turbo TSFE with a reduced CP will be another focus in future research.

Appendix A

Derivation of The Equaliser Coefficients for the Symbol-wise TSFE

Based on the independence of the bits $\left\{c_{n,q}^{i}\right\}$, $Cov(d_{n}^{i}, d_{n}^{i})$ for all $n \neq n'$ and $i \neq i'$. The equaliser coefficients $\mathbf{U}_{k}^{i}$ and b_{k}^{i} of TSFE are determined to minimise the MSE J_{k}^{i} in (3.31). By setting $\partial J_{k}^{i}/\partial b_{k}^{i} = 0$, it can be derived that the feedback coefficient is related to $\mathbf{U}_{k}^{i}$ by

$$b_{k}^{i} = \mu_{k}^{i} - \frac{1}{M}\mathbf{U}_{k}^{i\,H} \sum_{n=1}^{N_t} \sum_{m=0}^{M-1} \mu_{n}^{i-m} \hat{\mathbf{H}}_{n} \mathbf{f}^{m} \tag{A.1}$$

Then, the linear weight vector $\mathbf{U}_{k}^{i}$ is obtained by setting $\partial J_{k}^{i}/\partial \mathbf{U}_{k}^{i} = 0$:

$$\mathbf{U}_{k}^{i} = \mathbf{\Upsilon}^{i^{-1}} \sum_{n=1}^{N_t} \sum_{m=0}^{M-1} \left[E\left(d_{k}^{i\,*} d_{n}^{i-m} \right) - \mu_{n}^{i-m} b_{k}^{i\,*} \right] \hat{\mathbf{H}}_{n} \mathbf{f}^{m} \tag{A.2}$$

where

$$\boldsymbol{\Upsilon}^i = \frac{1}{M}\sum_{n=1}^{N_t}\sum_{n'=1}^{N_t}\sum_{m=1}^{M-1}\sum_{m'=1}^{M-1} E\left(d_n^{i-m} d_{n'}^{i-m'*}\right)\hat{\mathbf{H}}_n \mathbf{f}^m \mathbf{f}^{m'H}\hat{\mathbf{H}}_{n'}^H + N_0\mathbf{I} \tag{A.3}$$

Substituting (A.1) and (A.3) into (A.2) obtains the linear weight vector $\mathbf{U}_k^i$ as

$$\mathbf{U}_k^i = v_k^i \boldsymbol{\Omega}^{i-1}\hat{\mathbf{H}}_k \mathbf{f}^0 \tag{A.4}$$

where $\mathbf{f}^i$ is defined in (3.33).

Substituting (A.1) and (A.4) into (3.29), the equaliser output signal $\tilde{d}_k^i$ is given by

$$\tilde{d}_k^i = \mu_k^i + \frac{1}{M}\mathbf{U}_k^{iH}\mathbf{X}\mathbf{f}^i - \frac{1}{M}\mathbf{U}_k^{iH}\sum_{n=1}^{N_t}\sum_{m=0}^{M-1}\mu_n^{i-m}\hat{\mathbf{H}}_n\mathbf{f}^m \tag{A.5}$$

To guarantee the perfect convergence behavior of Turbo equalisation [43, 47], $L^I\left(c_{k,q}^i\right) = 0$ for all q, leading to $\mu_k^i = 0$ and $v_k^i = 1$. Thus, $\mathbf{U}_k^i$ can be redefined in (3.32) by using the matrix inversion lemma [48], and (A.5) becomes

$$\tilde{d}_k^i = 0 + \frac{1}{M}\mathbf{U}_k^{iH}\mathbf{X}\mathbf{f}^i - \frac{1}{M}\mathbf{U}_k^{iH}\left(\sum_{n=1}^{N_t}\sum_{m=0}^{M-1}\mu_n^{i-m}\hat{\mathbf{H}}_n\mathbf{f}^m - \mu_k^{i-m}\hat{\mathbf{H}}_k\mathbf{f}^0\right) \tag{A.6}$$

By substituting $\sum_{n=1}^{N_t}\sum_{m=0}^{M-1}\mu_n^{i-m}\hat{\mathbf{H}}_n\mathbf{f}^m$ in (A.1) and (A.6) by $\sum_{n=1}^{N_t}\hat{\mathbf{H}}_n E(\mathbf{D}_n)\mathbf{f}^i$, where $E(\mathbf{D}_n)$ is defined in (3.35), the feedback coefficient b_k^i in (3.34) as well as the resulting equaliser output signal $\tilde{d}_k^i$ in (3.36) is obtained.

Appendix B

Derivation of The Recursive Parameter $\omega_{l,k}^{(q)}$ in (4.76)

From (4.57), (4.58) and (4.60), $\omega_{l,k}^{(q)}$ can be easily expressed as:

$$\omega_{l,k}^{(q)} = \sum_{i=0}^{M-1} E_L \left[\frac{\left|\mu^{s}_{\lceil k/(N+1)\rceil}{}^{(q)}\right|^2}{\left|\mu^{s}_{\lceil k/(N+1)\rceil}{}^{(q)}\right|^2 E_L\left(\left[\mathbf{p}_l^{(q|q-1)}\right]_{k,k}\right) + E_L\left(\eta_l^{i(q)}\right) + E_L\left(r_l^{i(q)}\right)} \right] \quad (s = (k-1)\%(N+1) + i - N) \text{(B.1)}$$

where $\eta_l^{i(q)} = \underbrace{\sum_{n=1}^{N_t}\sum_{k'=0}^{N}}_{s' \neq k} \left|\mu_n^{i-N+k'(q)}\right|^2 E_L\left(\left[\mathbf{p}_l^{(q|q-1)}\right]_{s',s'}\right) (s' = (n-1)(N+1) + k' + 1; i = 0, \cdots, M-1)$.

Thus, $E_L\left(\eta_l^{i(q)}\right) = \underbrace{\sum_{n=1}^{N_t}\sum_{k'=0}^{N}}_{s' \neq k} E_L\left(\left|\mu_n^{i-N+k'(q)}\right|^2\right) E_L\left(\left[\mathbf{p}_l^{(q|q-1)}\right]_{s',s'}\right) (s' = (n-1)(N+1) + k' + 1; i = 0, \cdots, M-1)$, where $E_L\left(\left|\mu_n^{i\,(q)}\right|^2\right)$ can be obtained using

$$E_L\left(\left|\mu_n^{i\,(q)}\right|^2\right) = \int_{-\infty}^{\infty}\int_{-\infty}^{\infty} \frac{1}{2}\left[tanh\left(\frac{y}{2}\right)^2 + tanh\left(\frac{z}{2}\right)^2\right] f_L(y) f_L(z) dy dz \quad \text{(B.2)}$$

with y and z denoting the integral variables replacing the two LLR components (*i.e.*, the real part and imaginary part) of a QPSK symbol. Similarly, $E_L\left(\mu_n^{i\,(q)}\right)(i=0,\cdots,M-1)$ can be expressed as

$$E_L\left(\mu_n^{i\,(q)}\right)=\int_{-\infty}^{\infty}\int_{-\infty}^{\infty}\frac{\sqrt{2}}{2}\left[tanh\left(\frac{y}{2}\right)+tanh\left(\frac{z}{2}\right)\cdot j\right]f_L(y)f_L(z)dydz \tag{B.3}$$

With $E_L\left(\left|\mu_n^{i\,(q)}\right|^2\right)$ and $E_L\left(\mu_n^{i\,(q)}\right)$, $E_L\left(v_n^{i\,(q)}\right)=E_L\left(\left|\mu_n^{i\,(q)}\right|^2\right)-\left|E_L\left(\mu_n^{i\,(q)}\right)\right|^2$, which leads to $E_L\left(r_l^{i(q)}\right)=tr\left[diag\left(E_L\left(v_1^{i-N(q)}\right)\cdots E_L\left(v_{N_t}^{i\,(q)}\right)\right)\mathbf{z}_l^{(q)}\right]+N_0$. Finally, $\omega_{l,k}^{(q)}$ is computed for the qth block as:

$$\omega_{l,k}^{(q)}=\sum_{i=0}^{M-1}\int_{-\infty}^{\infty}\int_{-\infty}^{\infty}\varrho_{l,k}^{i(q)}dydz \tag{B.4}$$

where

$$\varrho_{l,k}^{i(q)}=$$

$$\frac{\frac{1}{2}\left[tanh\left(\frac{y}{2}\right)^2+tanh\left(\frac{z}{2}\right)^2\right]f_L(y)f_L(z)}{\frac{1}{2}\left[tanh\left(\frac{y}{2}\right)^2+tanh\left(\frac{z}{2}\right)^2\right]E_L\left(\left[\mathbf{p}_l^{(q|q-1)}\right]_{k,k}\right)+E_L\left(\eta_l^{i(q)}\right)+E_L\left(r_l^{i(q)}\right)} \tag{B.5}$$

Appendix C

Derivation of The Recursive Parameter $\theta_{l,k}^{(q)}$ in (4.80)

From (4.69) and (4.71), The original expression $\theta_{l,k}^{(q)}$ is given by

$$\theta_{l,k}^{(q)} = \sum_{i=0}^{M-1} E_L \left[\frac{\left|\mu^s_{\lceil k/(N+1)\rceil}{}^{(q)}\right|^2}{\left|\mu^s_{\lceil k/(N+1)\rceil}{}^{(q)}\right|^2 E_L\left(\left[\mathbf{p}_l^{(q-1)}\right]_{k,k}\right) + E_L\left(\eta_l^{i(q)}\right) + \lambda E_L\left(r_l^{i(q)}\right)} \right] \quad (s = (k-1)\%(N+1) + i - N) \quad \text{(C.1)}$$

$E_L\left(\eta_l^{i(q)}\right)(i = 0, \cdots, M-1)$ is achieved in the same way as in Appendix A. As shown in (4.72), $\mathbf{z}_l^{(q)}$ depends on the channel observations for NRLS-SCE, which should be avoided while computing $E_L\left(r_l^{i(q)}\right)(i = 0, \cdots, M-1)$. To make $\mathbf{z}_l^{(q)}$ independent of the channel observations, the computation of $\mathbf{z}_l^{(q)}$ in (4.72) is revised as:

$$\mathbf{z}_l^{(q)} \approx \mathbf{z}_l^{(q-1)} + \mathbf{p}_l^{(q-1)} \quad \text{(C.2)}$$

and take $\mathbf{z}_l^{(1)} \approx \hat{\boldsymbol{\tau}}_l^{(0)^H} \hat{\boldsymbol{\tau}}_l^{(0)} + \mathbf{p}_l^{(0)}$. This revision is proven by the simulation to have little impact on the final result of the analytical MSE. The rest computation of

$E_L\left(r_l^{i(q)}\right)$ $(i = 0, \cdots, M-1)$ is the same as in Appendix A.

Then, following the same derivation procedure as $\omega_{l,k}^{(q)}$ in Appendix A, $\theta_{l,k}^{(q)}$ is computed for the qth block as:

$$\theta_{l,k}^{(q)} = \sum_{i=0}^{M-1} \int_{-\infty}^{\infty} \int_{-\infty}^{\infty} \varphi_{l,k}^{i(q)} dydz \tag{C.3}$$

where

$$\varphi_{l,k}^{i(q)} =$$

$$\frac{\frac{1}{2}\left[tanh\left(\frac{y}{2}\right)^2 + tanh\left(\frac{z}{2}\right)^2\right] f_L(y) f_L(z)}{\frac{1}{2}\left[tanh\left(\frac{y}{2}\right)^2 + tanh\left(\frac{z}{2}\right)^2\right] E_L\left(\left[\mathbf{p}_l^{(q-1)}\right]_{k,k}\right) + E_L\left(\eta_l^{i(q)}\right) + \lambda E_L\left(r_l^{i(q)}\right)} \tag{C.4}$$

Appendix D

Derivation of Turbo RLS Channel Estimation

Spreading $E\left\{\|\mathbf{X}_l^{(i)} - \hat{\boldsymbol{\tau}}_l^{(q)}\tilde{\mathbf{F}}\tilde{\mathbf{D}}^{(i)}\|^2\right\}$ in (4.28) yields

$$E\left\{\|\mathbf{X}_l^{(i)} - \hat{\boldsymbol{\tau}}_l^{(q)}\tilde{\mathbf{F}}\tilde{\mathbf{D}}^{(i)}\|^2\right\} = \hat{\boldsymbol{\tau}}_l^{(q)}\tilde{\mathbf{F}}E\left(\tilde{\mathbf{D}}^{(i)}\tilde{\mathbf{D}}^{(i)^H}\right)\tilde{\mathbf{F}}^H\hat{\boldsymbol{\tau}}_l^{(q)^H} + \mathbf{X}_l^{(i)}\mathbf{X}_l^{(i)^H} - 2Re\left[E\left(\hat{\boldsymbol{\tau}}_l^{(q)}\tilde{\mathbf{F}}\tilde{\mathbf{D}}^{(i)}\mathbf{X}_l^{(i)^H}\right)\right] \tag{D.1}$$

The transmitted symbols $d_n^{i\,(q)}(n = 1, \cdots, N_t; i = 0, \cdots, M-1)$ are regarded as the noisy observation of $\mu_n^{i\,(q)}$, *i.e.*,

$$d_n^{i\,(q)} = \mu_n^{i\,(q)} + \phi_n^{i\,(q)} \tag{D.2}$$

It yields

$$D_n^{m(q)} = E(D_n^{m(q)}) + \gamma_n^{m(q)} \tag{D.3}$$

where $\gamma_n^{m(q)}$ denotes the noise with a zero mean and a variance of $\sum_{i=0}^{M-1} v_n^{i\,(q)}$.

Thus, $\tilde{\mathbf{D}}^{(q)} = E\left(\tilde{\mathbf{D}}^{(q)}\right) + \tilde{\boldsymbol{\gamma}}^{(q)}$, where $\tilde{\boldsymbol{\gamma}}^{(q)} = mat(\boldsymbol{\gamma}^{0(q)} \cdots \boldsymbol{\gamma}^{N_s M-1(q)})$ with

$\boldsymbol{\gamma}^{m(q)} = \left[\gamma_1^{m(q)} \cdots \gamma_{N_t}^{m\,(q)}\right]^T$. Also let $cov\left(\tilde{\mathbf{D}}^{(q)}, \tilde{\mathbf{D}}^{(q)}\right) = diag(\boldsymbol{\chi}^{(q)}, \cdots, \boldsymbol{\chi}^{(q)})$, with $\boldsymbol{\chi}^{(q)} = diag\left(\sum_{i=0}^{M-1} v_1^{i\,(q)} \cdots \sum_{i=0}^{M-1} v_{N_t}^{i\ \ (q)}\right)$. Finally, the following is obtained.

$$E\left(\hat{\boldsymbol{\tau}}_l^{(q)}\tilde{\mathbf{F}}\tilde{\mathbf{D}}^{(i)}\mathbf{X}_l^{(i)H}\right) = \hat{\boldsymbol{\tau}}_l^{(q)}\tilde{\mathbf{F}}\left(E(\tilde{\mathbf{D}}^{(i)})\mathbf{X}_l^{(i)H} + cov\left(\tilde{\mathbf{D}}^{(i)}, \tilde{\mathbf{D}}^{(i)}\right)\tilde{\mathbf{F}}^H\boldsymbol{\tau}_l^{(i)H}\right) \quad \text{(D.4)}$$

Since $\boldsymbol{\tau}_l^{(i)}$ in (D.4) is unknown, it can be approximated by $\hat{\boldsymbol{\tau}}_l^{(i-1)}$. Thus, (D.1) becomes

$$E\left\{\|\mathbf{X}_l^{(i)} - \hat{\boldsymbol{\tau}}_l^{(q)}\tilde{\mathbf{F}}\tilde{\mathbf{D}}^{(i)}\|^2\right\} = \hat{\boldsymbol{\tau}}_l^{(q)}\tilde{\mathbf{F}}E\left(\tilde{\mathbf{D}}^{(i)}\tilde{\mathbf{D}}^{(i)H}\right)\tilde{\mathbf{F}}^H\hat{\boldsymbol{\tau}}_l^{(q)H}$$
$$+\mathbf{X}_l^{(i)}\mathbf{X}_l^{(i)H} - 2Re\left[\hat{\boldsymbol{\tau}}_l^{(q)}\tilde{\mathbf{F}}\left(E(\tilde{\mathbf{D}}^{(i)})\mathbf{X}_l^{(i)H} + cov\left(\tilde{\mathbf{D}}^{(i)}, \tilde{\mathbf{D}}^{(i)}\right)\tilde{\mathbf{F}}^H\hat{\boldsymbol{\tau}}_l^{(i-1)}\right)\right] \quad \text{(D.5)}$$

With (D.5) and (4.28), (4.25) can be obtained which minimises the cost function.

Bibliography

[1] J. Winters, "On the capacity of radio communication systems with diversity in a rayleigh fading environment," *IEEE J. Sel. Areas Commun.*, vol. 5, pp. 871–878, Jun. 1987.

[2] G. J. Foschini, "Layered space-time architecture for wireless communication in fading environments when using multi-element antennas," *Bell Labs Tech. J.*, pp. 41–59, 1996.

[3] E. Telatar, "Capacity of multi-antenna Gaussian channels," *Eur. Trans. Telecomm. ETT*, vol. 10, pp. 585–596, Nov. 1999.

[4] L. J. Cimini, Jr., "Analysis and simulation of a digital mobile channel using orthogonal frequency division multipexing," *IEEE Trans. Commun.*, vol. 33, pp. 665–675, Jul. 1985.

[5] D. Falconer, S. Ariyavisitakul, A. Benyamin-seeyar, and B. Eidson, "Frequency-domain equalization for single-carrier broadband wireless systems," *IEEE Commun. Mag.*, vol. 40, pp. 58–66, Apr. 2002.

[6] H. Sari, G. Karam, and I. Jeanclaude, "Transmission techniques for digital terrestrial TV broadcasting," *IEEE Commun. Mag.*, vol. 33, pp. 100–109, Feb. 1995.

[7] C. Berrou, A. Glavieux, and P. Thitimajshima, "Near shannon limit error-correcting coding and decoding: Turbo codes," in *Proc. IEEE Int. Conf. Commun.*, Geneva, Switzerland, May 1993.

[8] S. Song, A. Singer, and K. Sung, "Soft input channel estimation for Turbo equalization," *IEEE Trans. Signal Process.*, vol. 52, pp. 2885–2894, Oct. 2004.

[9] S. M. Alamouti, "A simple transmitter diveristy scheme for wireless communications," *IEEE J. Sel. Areas Commun.*, vol. 16, pp. 1451–1458, Oct. 1998.

[10] L. Greenstein, J. Andersen, H. Bertoni, S. Kozono, D. Michelson, and W. Tranter, "Channel and propagation models for wireless system design I and II," *IEEE J. Sel. Areas Commun.*, vol. 20, Apr./Aug. 2002.

[11] A. Abdi and M. Kaveh, "A space-time correlation model for multielement antenna systems in mobile fading channels," *IEEE J. Sel. Areas Commun.*, vol. 20, pp. 550–561, Apr. 2002.

[12] D. Shiu, G. Foschini, M. Gans, and J. Kahn, "Fading correlation and its effect on the capacity of multi-element antenna systems," *IEEE Trans. Commun.*, vol. 48, pp. 502–513, Mar. 2000.

[13] A. Goldsmith, S. A. Jafar, N. Jindal, and S. Vishwanath, "Capacity limits of MIMO channels," *IEEE J. Sel. Areas Commun.*, vol. 21, pp. 684–702, Jun. 2003.

[14] C.-N. Chuah, D. N. Tse, J. Kahn, and R. A. Valenzuela, "Capacity scaling in MIMO wireless systems under correlated fading," *IEEE Trans. Inform. Theory*, vol. 48, pp. 637–650, Mar. 2002.

[15] G. J. Foschini, D. Chizhik, M. Gans, C. Papadias, and R. A. Valenzuela, "Analysis and performance of some basic spacetime architectures," *IEEE J. Sel. Areas Commun.*, vol. 21, pp. 303–320, Apr. 2003.

[16] B. Hassibi and B. Hochwald, "Cayley differential unitary space-time codes," *IEEE Trans. Inform. Theory*, vol. 48, pp. 1485–1503, Jun. 2002.

[17] M. Hochwald, T. L. Marzetta, T. J. Richardson, W. Sweldens, and R. Urbanke, "Systematic design of unitary space-time constellations," *IEEE Trans. Inform. Theory*, vol. 46, pp. 1962–1973, Sep. 2000.

[18] S. Catreux, V. Erceg, D. Gesbert, and R. W. Heath, "Adaptive modulation and MIMO coding for broadband wireless data networks," *IEEE Commun. Mag.*, vol. 40, pp. 108–115, Jun. 2002.

[19] N. Al-Dhahir, "Overview and comparison of equalization schemes for space-time-coded signals with application to EDGE," *IEEE Trans. Signal Process.*, vol. 50, pp. 2477–2488, Oct. 2002.

[20] A. Lozano and C. Papadias, "Layered space-time receivers for frequency-selective wireless channels," *IEEE Trans. Commun.*, vol. 50, pp. 65–73, Jan. 2002.

[21] N. Al-Dhahir, C. Fragouli, A. Stamoulis, W. Younis, and R. Calderbank, "Space-time processing for broadband wireless access," *IEEE Commun. Mag.*, vol. 40, pp. 136–142, Sep. 2002.

[22] Chong and L. Milstein, "The performance of a space-time spreading CDMA system with channel estimation errors," in *Proc. IEEE ICC'02*, Apr. 2002, pp. 1793–1797.

[23] H. Huang, H.Viswanathan, and G. J. Foschini, "Multiple antennas in cellular CDMA systems: Transmission, detection and spectral efficiency," *IEEE Trans. Wireless Commun.*, vol. 1, pp. 383–392, Jul. 2002.

[24] Y. Li, J.Winters, and N. Sollenberger, "Mimo-ofdm for wireless communication: Signal detection with enhanced channel estimation," *IEEE Trans. Commun.*, pp. 1471–1477, Sep. 2002.

[25] B. Lu, X. Wang, and Y. Li, "Iterative receivers for space-time blockcoded OFDM systems in dispersive fading channels," *IEEE Trans. Wireless Commun.*, vol. 1, pp. 213–225, Apr. 2002.

[26] Y. Xin and G. Giannakis, "High-rate space-time layered OFDM," *IEEE Commun. Lett.*, pp. 187–189, May 2002.

[27] D. Gesbert, M. Shafi, D. S. Shiu, P. Smith, and A. Naguib, "From theory to practice: An overview of MIMO space-time coded wireless systems," *IEEE J. Sel. Areas Commun.*, vol. 21, pp. 281–302, Apr. 2003.

[28] T. Walzman and M.Shwartz, "Automatic equalization using the discrete Fourier domain," *IEEE Trans. Inform. Theory*, vol. IT-19, pp. 59–68, Jan. 1973.

[29] E. R. Ferrara, Jr., *Frequency-domain adaptive filtering.* NJ: Prentice Hall, 1985.

[30] "IEEE 802.16 a/b amendment to the 802.16 standard air interface for fixed broadband wireless access systems," Jun. 2001.

[31] J. M. Cioffi, G. P. Dudevoir, M. V. Eyuboglu, and G. D. Forney, "MMSE decision-feedback equalizers and coding. I. Equalization results," *IEEE Trans. Commun.*, vol. 43, pp. 2582–2594, Oct. 1995.

[32] G. D. Forney, "Maximum-likelihood sequence estimation of digital sequences in the presence of intersymbol interference," *IEEE Trans. Inform. Theory*, vol. IT-18, pp. 363–378, May 1972.

[33] M. V. Clark, "Adaptive frequency-domain equalization and diversity combining for broadband wireless communications," *IEEE J. Sel. Areas Commun.*, vol. 16, pp. 1385–1395, Oct. 1998.

[34] P. Vandenameele, L. V. der Perre, B. Gyselinckx, M. Engels, M. Moonen, and H. D. Man, "A single-carrier frequency-domain SDMA basestation," in *Proc. IEEE Int. Conf. Acoustics Speech and Signal Processing (ICASSP)*, vol. 6, Piscataway, NJ, May 2000, pp. 3714–3717.

[35] X. Zhu and R. D. Murch, "Layered space-frequency equalization in a single-carrier MIMO system for frequency-selective channels," *IEEE Trans. Wireless Commun.*, vol. 3, pp. 701–708, May 2004.

[36] J. Coon, S. Armour, M. Beach, and J. McGeehan, "Adaptive frequency-domain equalization for single-carrier MIMO systems," in *Proc. IEEE ICC'04*, vol. 4, Paris, France, Jun. 2004, pp. 2487–2491.

[37] M. Morelli, L. Sanguinetti, and U. Mengali, "Channel estimation for adaptive frequency-domain equalization," *IEEE Trans. Wireless Commun.*, vol. 4, pp. 2508–2518, Sep. 2005.

[38] Y. Wu, X. Zhu, and A. K. Nandi, "Adaptive layered space-frequency equalization for MIMO frequency selective channels," in *Proc. EUSIPCO'05*, Antalya, Turkey, Sep. 2005.

[39] R. Koetter, A. C. Singer, and M. Tüchler, "Turbo equalization," *IEEE Signal Process. Mag.*, vol. 21, pp. 67–80, Jan. 2004.

[40] C. Douillard, M. Jezequel, C. Berrou, A. Picart, P. Didier, and A. Glavieux, "Iterative correction of intersymbol interference: Turbo equalization," *Eur. Trans. Telecomm.*, vol. 6, pp. 507–511, Sep./Oct. 1995.

[41] A. Glavieux, C. Laot, and J. Labat, "Turbo equalization over a frequency selective channel," in *Proc. Intern. Symp. Turbo Codes*, Brest, France, Sep. 1997, pp. 96–102.

[42] X. Wang and H. Poor, "Iterative (turbo) soft interference cancellation and decoding for coded CDMA," *IEEE Trans. Commun.*, vol. 47, pp. 1046–1061, Jul. 1999.

[43] M. Tüchler, A. C. Singer, and R. Koetter, "Minimum mean squared error equalization using *a priori* information," *IEEE Trans. Signal Process.*, vol. 50, pp. 673–683, Mar. 2002.

[44] M. Tüchler, R. Koetter, and A. C. Singer, "Turbo equalization: Principles and new results," *IEEE Trans. Commun.*, vol. 50, pp. 754–767, May 2002.

[45] Y. Wu, X. Zhu, and A. K. Nandi, "Low complexity Turbo space-frequency equalization for single-carrier MIMO wireless communications," in *Proc. EUSIPCO'06*, Florence, Italy, Sep. 2006.

[46] A. Berthet, R. Visoz, and P. Tortelier, "Sub-optimal turbo-detection for coded 8-PSK signals over ISI channels with application to EDGE advanced mobile system," in *Proc. IEEE VTC'00 Fall*, Sep. 2000.

[47] M. S. Yee, M. Sandell, and Y. Sun, "Comparison study of single-carrier and multi-carrier modulation using iterative based receiver for MIMO system," in *Proc. IEEE VTC'04 Spring*, vol. 3, Milan, Itlay, May 2004, pp. 1275–1279.

[48] S. Haykin, *Adaptive Filter Theory.* NJ: Prentice Hall, 1996.

[49] M. Tüchler and J. Hagenauer, "Linear time and frequency domain Turbo equalization," in *Proc. IEEE VTC'01 Fall*, vol. 4, Oct. 2001, pp. 2773–2777.

[50] P. Frenger and A. Svensson, "Decision directed coherent detection in multicarrier systems on Rayleigh fading channels," *IEEE Trans. Veh. Technol.*, vol. 48, pp. 490–498, Mar. 1999.

[51] V. Mignone and A. Morello, "CD3-OFDM: A novel demodulation scheme for fixed and mobile receivers," *IEEE Trans. Commun.*, vol. 44, pp. 1144–1151, Sep. 1996.

[52] A. Anastasopoulos and K. M. Chugg, "Adaptive soft-input soft-output algorithms for iterative detection with parametric uncertainty," *IEEE Trans. Commun.*, vol. 48, pp. 1638–1649, Oct. 2000.

[53] J. Garcia-Frias and J. D. Villasenor, "Combined turbo detection and decoding for unknown ISI channels," *IEEE Trans. Commun.*, vol. 51, pp. 79–85, Jan. 2003.

[54] M. C. Valenti and B. D. Woerner, "Iterative channel estimation and decoding of pilot symbol assisted turbo codes over flat-fading channels," *IEEE Trans. Commun.*, vol. 19, pp. 1697–1705, Sep. 2001.

[55] J. Thomas and E. Geraniotis, "Soft iterative multisensor multiuser detection in coded dispersive CDMA wireless channels," *IEEE J. Sel. Areas Commun.*, vol. 10, pp. 1334–1351, Jul. 2001.

[56] V. Ramon, C. Herzet, X. Wautelet, and L. Vandendorpe, "Soft estimation of time-varying frequency selective channels using Kalman smoothing," in *Proc. IEEE ICC'07*, Glasgow, UK, Jun. 2007.

[57] R. Otnes and M. Tüchler, "Iterative channel estimation for Turbo equalization of time-varying frequency-selective channels," *IEEE Trans. Wireless Commun.*, vol. 3, pp. 1918–1923, Nov. 2004.

[58] Y. Wu, X. Zhu, and A. K. Nandi, "Low complexity adaptive Turbo frequency-domain channel estimation for single-carrier multi-user detection," *to appear in IEEE Trans. Wireless Commun.*

[59] B. Ng, C. Lam, and D. Falconer, "Turbo frequency domain equalization for single-carrier broadband wireless systems," *IEEE Trans. Wireless Commun.*, vol. 6, pp. 759–767, Feb. 2007.

[60] F. Pancaldi and G. M. Vitetta, "Block channel equalization in the frequency domain," *IEEE Trans. Commun.*, vol. 53, pp. 463–471, Mar. 2005.

[61] Y. Wu, X. Zhu, and A. K. Nandi, "Low complexity adaptive Turbo space-frequency equalization for single-carrier multi-input multi-output systems," *IEEE Trans. Wireless Commun.*, vol. 7, pp. 2050–2056, Jun. 2008.

[62] A. Gusmao, R. Dinis, and N. Esteves, "On frequency-domain equalization and diversity combining for broadband wireless communications," *IEEE Trans. Commun.*, vol. 51, pp. 1029–1033, Jul. 2003.

[63] J. Proakis, *Digital Communications.* New York: McGraw-Hill, 1995.

[64] P. Balaban and J. Salz, "Optimum diversity combining and equalization in digital data transmission with applications to cellular mobile radio. I. Theoretical considerations," *IEEE Trans. Commun.*, vol. 40, pp. 885–894, May 1992.

[65] X. Zhu and R. D. Murch, "Layered space-time equalization for wireless MIMO systems," *IEEE Trans. Wireless Commun.*, vol. 2, pp. 1189–1203, Nov. 2003.

[66] T. Zemen, F. Mecklenbräuker, J. Wehinger, and R. R. Müller, "Iterative joint time-variant channel estimation and multi-user detection for MC-CDMA," *IEEE Trans. Wireless Commun.*, vol. 5, pp. 1469–1478, Jun. 2006.

[67] P. A. Bello, "Characterization of randomly time-variant linear channels," *IEEE Trans. Commun. Syst.*, vol. CS-11, pp. 360–393, Dec. 1963.

[68] M. Tüchler, R. Otnes, and A. Schmidbauer, "Performance of soft iterative channel estimation in turbo equalization," in *Proc. IEEE ICC'02*, vol. 3, May 2002, pp. 1858–1862.

[69] Q. Dai and E. Shwedyk, "Detection of bandlimited signals over frequency selective Rayleigh fading channels," *IEEE Trans. Commun.*, vol. 42, pp. 941–950, Feb./Mar./Apr. 1994.

[70] W. N. Furman and J. W. Nieto, "Understanding HF channel simulator requirements in order to reduce HF modem performance measurement variability," in *Proc. 6th Nordic Shortwave Conf. HF*, vol. 3, Aug. 2001, pp. 6.4.1–6.4.13.

[71] H. Myung, J. Lim, and D. J. Goodman, "Single carrier FDMA for uplink wireless transmission," *IEEE Veh. Technol. Mag.*, vol. 1, pp. 30–38, Sep. 2006.

[72] R. Dinis, D. Falconer, C. T. Lam, and M. Sabbaghian, "A multiple access scheme for the uplink of broadband wireless systems," in *Proc. IEEE ICC'02*, vol. 6, Dec. 2004, pp. 3808–3812.

[73] *3rd Generation Partnership Project (3GPP); Technical specification group radio access network; Physical layer aspects for evolved UTRA (Release 7)*, Std.

[74] H. Myung, J. Lim, and D. J. Goodman, "Peak-to-average power ratio of single carrier FDMA signals with pulse shaping," in *Proc. IEEE PIMRC'06*, Sep. 2006, pp. 1–5.

[75] F. Horlin, A. Bourdoux, E. Lopez-Estraviz, and L. Perre, "Single-carrier FDMA versus cyclic-prefix CDMA," in *Proc. IEEE ICC'07*, Jun. 2007.

[76] H. Myung, "Single carrier orthogonal multiple access technique for broadband wireless communications," Ph.D. dissertation, Polytechnic Univ., Jan. 2007.

[77] T. Abe, S. Tomisato, and T. Matsumoto, "A MIMO turbo equalizer for frequency-selective channels with unknown interference," *IEEE Trans. Veh. Technol.*, vol. 52, pp. 476–482, May 2003.

[78] Q. Li, J. Zhu, X. Guo, and C. N. Georghiades, "Asynchronous co-channel interference suppression in MIMO OFDM systems," in *Proc. IEEE ICC'07*, Jun. 2007.

[79] T. A. Thomas and F. W. Vook, "Asynchronous interference suppression in broadband cyclic-prefix communication," in *Proc. IEEE WCNC*, Mar. 2003, pp. 568–572.

[80] Y. Wu, X. Zhu, and A. K. Nandi, "Low complexity adaptive Turbo frequency-domain channel estimation for single-carrier multi-user detection with unknown co-channel interference," in *Proc. IEEE ICC'07*, Glasgow, U.K., Jun. 2007.

[81] M. Pourahmadi, M. J. Daniels, and T. Park, "Simutaneous modelling of the cholesky decomposition of several covariance matrices," *accepted by Journal of Multivariate Analysis.*